Application of graphene in electrochemical sensing

Dissertation
Zur Erlangung des Doktorgrades der Naturwissenschaften
(Dr. rer. nat.)
der Fakultät für Physik
der Universität Regensburg

vorgelegt von
Masoumeh Sisakhti
aus
Shiraz, Iran

im Jahr 2016

Die Arbeit wurde von Prof. Dr. Christoph Strunk angeleitet.
Das Promotionsgesuch wurde am 25.10.2016 eingereicht.
Das Kolloquium fand statt am 09.12.2016

Prüfungsausschuss: Vorsitzender: Prof. Dr. Gunnar S. Bali
                      1. Gutachter: Prof. Dr. Christoph Strunk
                      2. Gutachterin: Prof. Dr. Antje J. Bäumner
                      weiterer Prüfer: Prof. Dr. Rupert Huber

To my best friend,

Ali

List of Publications

This thesis is based on the following publications:

1) Signal enhancement in amperometric peroxide detection by using graphene materials with low number of defects
A. Zöpfl, M. Sisakthi, J. Eroms F.M. Matysik, C. Strunk and T. Hirsch (Microchim. Acta, 183, (2016) 83–90)

2) Perforated graphene/NiO nanoparticle composites for high performance electrochemical sensors
M. Sisakhti et. al, (to be submitted)

Abstract

Graphene possesses distinctive properties such as chemical stability, wide potential window and large surface area, making it an ideal electrode material that could potentially yield significant benefits in many electrochemical applications. The quality of graphene has an enormous impact on its electrochemical performance. It is therefore necessary to study the influence of defects and impurities on the amperometric performance of graphene towards the sensing of a target analyte. This thesis studies the critical role of the fabrication routes of graphene materials on their efficiency and electrochemical performance, putting emphasis on the influence of defects and impurities on direct amperometric detection of hydrogen peroxide. It is found that the sensors based on graphene with lower number of defects lead to a higher sensitivity towards H_2O_2.

Furthermore, graphene's electrochemical and amperometric properties for non-enzymatic glucose determination based on electrodeposition of NiO nanoparticles have been investigated. To address this issue, CVD graphene was patterned with arrays of antidot lattices to provide artificial dangling positions for attachment of nanoparticles to the graphene surface. It is demonstrated that the nanopatterned graphene exhibited better performance in glucose sensing compared to pristine CVD graphene, and efficient tailoring of the size and lattice constant of the antidots on graphene surface can optimize electrodeposition of NiO nanoparticles and the amperometric response of graphene-based sensors towards glucose detection.

Contents

List of Figures

When nature finishes to produce its own species, man begins using natural things in harmony with this very nature to create an infinity of species.

the artist-scientist *Leonardo da Vinci*

1. Introduction

The key role of carbon atoms in all living organisms is unquestionable. However, for a long time only two main variants of carbon were known: diamond and graphite, both crystalline forms of the carbon element. Diamond possesses a covalent structure, with each carbon covalently bonded to four other carbon atoms in a tetrahedral arrangement to form a rigid, transparent, and insulating structure with a band gap of about 6eV. Unlike diamond, graphite is a soft and conducting structure, in which each carbon covalently bonds to three other carbon atoms in a hexagonal arrangement.

The first use of graphite can be traced back to the 4th millennium B.C. when Boian culture applied it as a ceramic paint to decorate pottery in southeastern Europe [Boa 82]. It consists of many sp^2 hybridized one-atom-thick sheets of carbon lattice stacked on top of each other, coupled via weak Van Der Waals forces. The band theory of graphite has been studied from 1947, when P. R. Wallace used the tight binding approximation method, which assumes conduction only happens in one layer which is graphene layer [Wal47]. Graphene, a two-dimensional (2D) monolayer of carbon atoms tightly packed into a honeycomb lattice, is basic building block for graphite and other graphitic materials of all dimensions (Figure 1.1) [Gei07].

Initially, it was believed for many years [All09] [Pei35] [Mer68] that strictly 2D crystals were thermodynamically unstable and could not exist. The experimental observations witnessed that a divergent contribution of thermal fluctuations in low-dimensional crystal lattices should lead to such displacements of atoms that they become comparable to interatomic distances at any finite temperature. For that reason, existence of such one-atom-thick graphene could not be reconciled with theory and graphene was just used for theoretical analysis until 2004, when Novoselov et al [Nov04] demonstrated the possibility to isolate it in a simple way. Since then many groups have undertaken the task of investigating graphene's electronic, mechanical and thermal properties both experimentally and theoretically [Cas09] [Sca09] [Bal08] [Bun08].

Graphene possesses many properties that make it an interesting candidate for researches and applications in various areas. Ballistic transport of electrons along the atomically thin layer, together with mobilities exceeding 300000 $cm^2V^{-1}S^{-1}$ and an ambipolar field effect make graphene an ideal material for the next generation of semiconductor devices [All09] [Guo12]. Although the lack of a bandgap limits the usage of two dimensional graphene for digital

switching, where high on/off ratios are necessary, the possibility of opening bandgaps lithographically by fabricating graphene nanoribbons enables graphene to be regarded as a possible candidate for electronic devices in the future [Mer08].

Beside these promising properties, other extraordinary features of graphene are also discussed. For instance the large and planar surface area of a single sheet and low electrical noise of graphene field effect transistors make it possible to be considered in optoelectronic and sensor applications [Bao12] [Bon10] [Koc13].
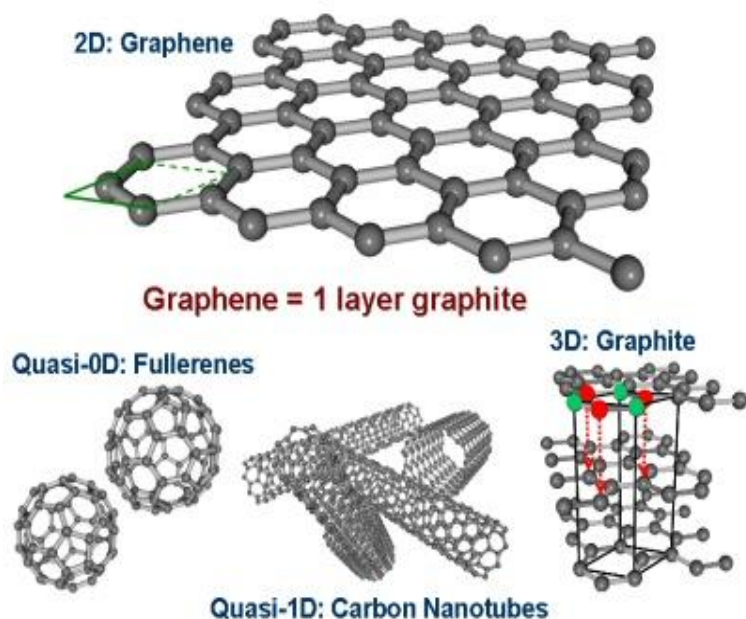
Figure 1.1. Graphene, a 2D building material for carbon materials of all dimensionalities. It can be wrapped up into 0D buckyballs, rolled into 1D nanotubes or stacked into 3D graphite. Image from [Gei07].

One area of particular interest where graphene has emerged as a rapidly rising star is electrochemistry, which has widely benefited from the application of graphene as an electrode material within a variety of sensing and energy storage devices [Xio14] [Amb14]. An essential characteristic of an electrode material is its surface area, which is important in applications such as energy storage, biocatalytic devices, and sensors. Exhibiting a theoretical surface area of 2630 m^2 g^{-1}, graphene materials have been considered to hold great promise for many applications, in particular as electrode material, claiming superior electrochemical performances when compared to traditional noble metals and various carbon based electrode materials, such as graphite and carbon nanotubes (CNTs) [Pum09] [Bro10].

Clearly, there are a variety of graphene materials with different properties. Some examples include mechanically exfoliated pristine graphene [Nov04], reduced graphene oxide [Eda08], chemical vapor deposited graphene [Kat14] and epitaxial graphene [Rie10]. The tremendous progress in the fabrication of graphene has provided the possibility to use them in a controllable and reproducible fashion in scientific experiments. Essential is the ability to fabricate individual single layer graphene sheets. This can be achieved by different means, for instance, micromechanical cleavage of graphite through which graphene sheets are directly deposited onto the substrate by mechanical cleavage. This approach, also known as the

"scotch-tape" method [Nov04], is widely used in many laboratories to obtain pristine perfect-structured graphene, but is restricted to small sample dimensions with incontrollable shape, size and location.

Chemical reduction of graphite oxide, usually based on Hummers method [Hum58] is considered to be the most economical way to produce reduced graphene oxide, with some advantages such as scalable, high volume production and ease of chemical modification. However, this approach does introduce some defects in graphene during the oxidation or reduction steps, and results in abundant structural damage of the graphene.

A more controllable process for synthesis of graphene is chemical vapor deposition (CVD). Recent development in the CVD process has led to the preparation of wafer-scale graphene film on metal substrates (Ru [Sut08] [Log09], Ni [Kim09] and [Rei09] and Cu [Hu12]) with single-layer yield as high as 95%. Although the CVD-graphene can only be produced on certain metallic substrates and it requires additional transfer steps, leading to some contaminations and destruction of graphene sheets, it still provides high conductivity and transparency, which allows electronic and electrochemical sensors to benefit from the high-yield and high-quality CVD graphene and enables the mass production of devices with high reproducibility.

The significance of knowing what sort of graphene with what properties we are utilizing, especially becomes noticeable when it comes to the fundamental issue of the electrochemical performance of graphene, where the role of defects and impurities can be considerable towards the sensing of a target analyte [Kum13] [Lin11]. In particular, as we learn from the plethora of different properties attributed to the graphene, the presence and role of such defects and impurities must be recognized and characterized. Raman spectroscopy, as will be discussed in section 5.2, can be used to determine the number of graphene layers and stacking order as well as density of defects and impurities. The critical role of the characterization of graphene materials fabricated by different methods is particularly important for a comparison between the efficiency and electrochemical performance of different graphene materials.

However, regardless of the preparation methods, graphene-based electrodes have demonstrated their utility in electrochemical sensors for detection of different biomolecules, as addressed in plenty of works [Pum11] [Wan11]. Extensively, biosensors based on enzymes have been researched [Sha10], where enzyme immobilization of modified graphene has been employed in order to construct efficient biosensors, suitable for selective and rapid analysis of various biological species in vivo and in vitro. However, the performance of enzyme-based sensors is greatly limited by enzyme immobilization techniques and detection environments (pH, temperature, etc.). In addition, natural enzymes are both expensive and unstable due to the intrinsic nature of the enzymes. Therefore, enzyme-free sensing is highly desirable and has the advantage of high stability, simplicity, good reproducibility, and low cost.

The present work aims at application of graphene for electrochemical sensing, investigating methods for graphene modification and functionalization, in order to improve the sensitivity and stability of the electrochemical sensors based on graphene.

This dissertation is divided into eight chapters, following the line of concepts indicated in the introduction section. In chapter 2 we will provide a thorough introduction to the electronic properties of graphene materials, employing tight binding argumentation and then briefly review those aspects of graphene's properties most relevant to electrochemical applications.

Chapter 3 delivers an overview of the general concept of electrochemical sensors, following an introduction to enzymatic and nonenzymatic approaches for electrochemical detection of glucose.

In chapter 4 an introduction is given on the electrochemical instrumentation and detection techniques utilized in this project, which is beneficial for understanding and interpretation of the performed experiments and achieved results.

Chapter 5 begins with an overview of the sample preparation steps of different graphene materials and focuses on the influence of the structural defects and device fabrication routs on the signal enhancement in non-enzymatic detection of hydrogen peroxide.

The main results of our efforts for fabrication of a graphene-based electrochemical glucose sensor will be presented in chapter 6, which mainly deals with the introduction of antidot lattices on graphene surface and their role on non-enzymatic sensing of glucose.

At the end of this work, chapter 7 summarizes the main findings of this thesis, presenting a brief outlook onto possible future experiments to employ graphene as an electrode material for fabricating an array biosensor and thereby detecting numerous target analytes simultaneously. This chapter is followed by an appendix (chapter 8), which mainly deals with the many additional experimental techniques used throughout this work to functionalize graphene surface through introduction of variable decorations both covalently and noncovalently. This chapter is particularly beneficial for those readers who are interested in studying enzymatic detection of glucose based on CVD graphene.

2. Properties of Graphene Materials

This chapter summarizes the most important structural and electrochemical characteristics of graphene materials. In the first part of this chapter we introduce the band structure of graphene and explain how the band structure calculated through tight binding model will cause the charge carriers in graphene to be viewed as massless Dirac fermions.

The remainder of this chapter is dedicated to electrochemistry of graphene and sensing and biosensing applications of graphene, which will be the focus of the next chapters of the work.

2.1 Structural properties of graphene

The carbon atoms in a graphene layer are sp^2-hybridized (one s-orbital and two p-orbitals hybridize together), forming three in-plane σ-bonds per atom which in turn leads to the formation of a hexagonal planar layer with a honeycomb-like atomic arrangement. The hexagonal graphene lattice is displayed in a top view model in Figure 2.1 (A) and exhibits a basis with two carbon atoms, A and B, per unit cell. These two atoms make up two non-equivalent sublattices in graphene, with an interatomic nearest neighbor separation of $a =$ 1.42 Å. The A atoms are connected only to B atoms and vice versa, this is called a bipartite lattice.

The real space unit vectors of the hexagonal lattice forming the basis of the unit cell are expressed as: $\vec{a_1} = a(3, \sqrt{3})/2$ and $\vec{a_2} = a(3, -\sqrt{3})/2$ [Cas09], while the corresponding reciprocal lattice vectors $\vec{b_1}$, $\vec{b_2}$ can be written as: $\vec{b_1} = 2\pi(1, \sqrt{3})/3a$ and $\vec{b_2} = 2\pi(1, -\sqrt{3})/3a$, defined by the condition $\vec{a_i} \cdot \vec{b_j} = 2\pi\delta_{ij}$, i.e. the direction of the unit vectors $\vec{b_1}$ and $\vec{b_2}$ of the reciprocal lattice are related by 90° from the unit vectors $\vec{a_1}$ and $\vec{a_2}$ of the hexagonal lattice in real space. The three nearest-neighbor vectors in real space are given by $\vec{\delta_1} = a(1, \sqrt{3})/2, \vec{\delta_2} = a(1, -\sqrt{3})/2, \vec{\delta_3} = a(1,0)$. We define the first Brillouian zone (FBZ) of the reciprocal lattice in the standard way, as bounded by the planes bisecting the vectors to the nearest reciprocal lattice points, illustrated in Figure 2.1 (B). This gives an FBZ of the same form as the original hexagons of the honeycomb lattice, but rotated with respect to them by $\pi/2$.
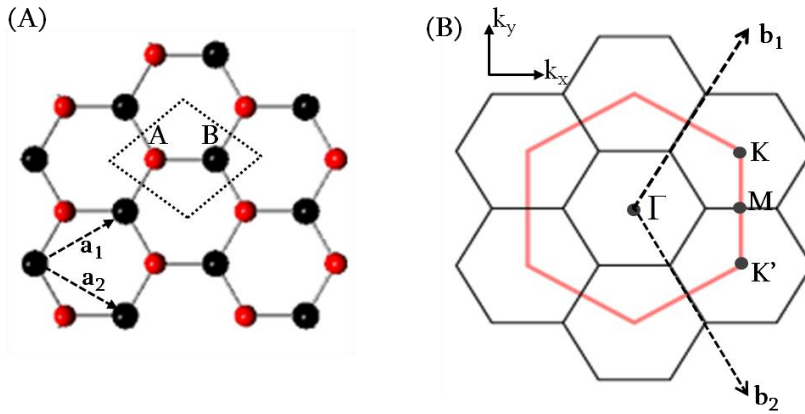
Figure 2.1. Lattice structure of graphene (A) The honeycomb lattice structure of graphene showing the unit cell in real space, which contains two sublattices marked A and B. The 2D-real space unit vectors $\overrightarrow{a_1}$ and $\overrightarrow{a_2}$ are also indicated. (B) the first Brillouin zone of graphene with the reciprocal unit vectors, $\overrightarrow{b_1}$ and $\overrightarrow{b_2}$, and high symmetry points Γ, M, K and K′.

Of particular importance for the physics of graphene are the three high symmetry points Γ, K and M at the center, corner and center of the edge in the BZ respectively. In graphene, most of the interesting physics occur near the two inequivalent BZ corners K and K′, where the bands cross the Fermi energy E_F . These are named Dirac points and their positions in momentum space are given by $\vec{K} = (2\pi/3a\,, 2\pi/3\sqrt{3}\,a)$ and $\overrightarrow{K'} = (2\pi/3a\,, -2\pi/3\sqrt{3}\,a)$. If we change the role of $\vec{K}$ and $\overrightarrow{K'}$ lattice points we actually reverse our time (flipping a $\vec{K}$ vector gives a $\overrightarrow{K'}$ vector). The time reversal is also connected to the chirality of particles: reversing time changes the roles of particles and antiparticles (electron and holes in our case). So the $\vec{K}$ and $\overrightarrow{K'}$ states are not equivalent (e.g. an electronic state in $\vec{K}$ forces the $\overrightarrow{K'}$ state to be positronic). The electronic band structure of graphene shows a very interesting conic point at the $\vec{K}$ and $\overrightarrow{K'}$ points in the Brillouin zone. The linear bands cross exactly at the Fermi energy, so that there is only one state, which can be treated as a hole or as an electron. Since there are no conducting states at the Fermi level, graphene behaves like a gapless semiconductor (also called semi-metal).

2.2 Electronic Structure of graphene in the tight binding model

As mentioned before, each non-equivalent carbon atom in the unit cell has four valence electrons, three out of which form strong σ covalent bonds at high binding energy, giving graphene exceptional mechanical strength and structural rigidity within its layers.

The σ bonding sp^2 orbitals are formed by the superposition of the s, p_x and p_y orbitals of atomic carbon leaving the p_z orbital unhybridized. The p_z-orbitals of neighboring carbon atoms overlap and form the distributed π-bonds that reside above and below each sheet and cross the Fermi energy E_F at the BZ corners K and K′ (Figure 2.2). These delocalized π orbitals are responsible for the excellent conductivity in graphene and all the intriguing physics.
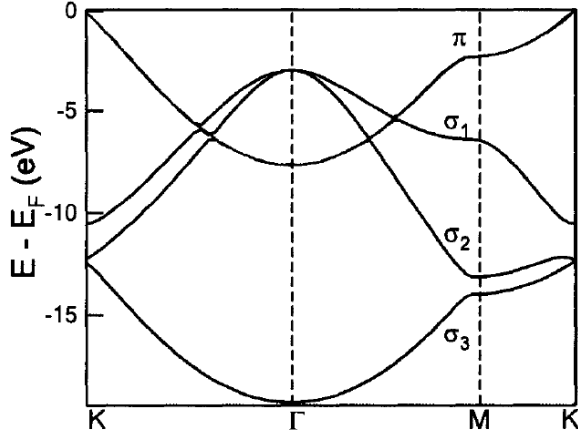
Figure 2.2. Band structure plot for graphene. Image from [Li10].

One of the simplest evaluations of the band structure and therefore the electronic properties of graphene can be derived from the tight binding approximation for the band theory of graphite, which was developed by Wallace long before graphene existed [Wal47]. This model is valid when the overlap of the wave function is large enough so that corrections to the isolated atoms are needed while at the same time not too large to invalidate the atomic description. In this case, the wave function for electrons can be approximated by a linear combination of the atomic wave functions. Thus the tight binding model is also known as the linear combination of atomic orbitals (LCAO) approximation.

In the atomic description, the Hamiltonian for each carbon atom localized at $\vec{r}_1$ and $\vec{r}_2$ is [Zho07]:

$$H_{1,2} = \frac{\nabla^2}{2m} + V_a(\vec{r} - \vec{r}_{1,2}) \tag{2.1}$$

where V_a is the atomic potential on each carbon atom.

The atomic wave function centered on each carbon site $\phi(\vec{r} - \vec{r}_{1,2})$ satisfy

$$H_{1,2}\phi(\vec{r} - \vec{r}_{1,2}) = E_{1,2}\phi(\vec{r} - \vec{r}_{1,2}) \tag{2.2}$$

In graphene, the total Hamiltonian is:

$$H_{1,2} = \frac{\nabla^2}{2m} + \Sigma_{\vec{R}}(V(\vec{r} - \vec{r}_1 - \vec{R}) + V(\vec{r} - \vec{r}_2 - \vec{R})). \tag{2.3}$$

The total Hamiltonian can be rewritten as the Hamiltonian for atom 1 or 2 with some corrections (ΔH_1 and ΔH_2) which take care of the potential created by all other atoms.

$$H_{1,2} = H_1 + \Delta H_1 = H_2 + \Delta H_2 \tag{2.4}$$

The Bloch wave function is

$$\psi(r) = \Sigma_{\vec{R}} e^{i\vec{k}.\vec{r}} \phi(\vec{r} - \vec{R}) \tag{2.5}$$

where the wave function ϕ is a linear combination of the localized wave functions $\phi(\vec{r} - \vec{r}_{1,2})$

$$\phi(r) = c_1(\vec{r} - \vec{r}_1) + c_2(\vec{r} - \vec{r}_2) \tag{2.6}$$

Here c_1 and c_2 are constants and $c_1^2 + c_2^2 = 1$

The eigenenergies can be obtained by solving the Schrödinger equation

$$H\psi(\vec{R}) = E(\vec{k})\psi(\vec{R}) \tag{2.7}$$

yielding to

$$E(\vec{k}) = \beta \pm \gamma \left| f(\vec{k}) \right| =$$
$$\beta \pm \gamma \sqrt{1 + 4\cos(\frac{k_x a}{2})\cos(\frac{\sqrt{3}k_y a}{2}) + 4\cos^2(\frac{k_x a}{2})} \tag{2.8}$$

Here β is a small correction to the overall energy, defined as $\equiv \langle \phi(\vec{r} - \vec{r}_1) | \Delta H_1 | \phi(\vec{r} - \vec{r}_1) \rangle$, γ the next nearest neighbor hoping integral defined as $\gamma \equiv \langle \phi(\vec{r} - \vec{r}_1) | \Delta H_1 | \phi(\vec{r} - \vec{r}_2) \rangle$, $f(\vec{k}) \equiv 1 + e^{i\vec{k}.\vec{a}_1} + e^{i\vec{k}.\vec{a}_2}$ and $a = \sqrt{3}a_0$. Figure 2.3 shows the π band dispersion of graphene. The valence and conduction bands touch only at the six corners of the BZ. Since each carbon atom contributes one electron, the valence band is completely filled up to the Fermi level, where the valence and conduction bands merge. Because of this, graphene is known as a semi-metal or zero-gap semiconductor.
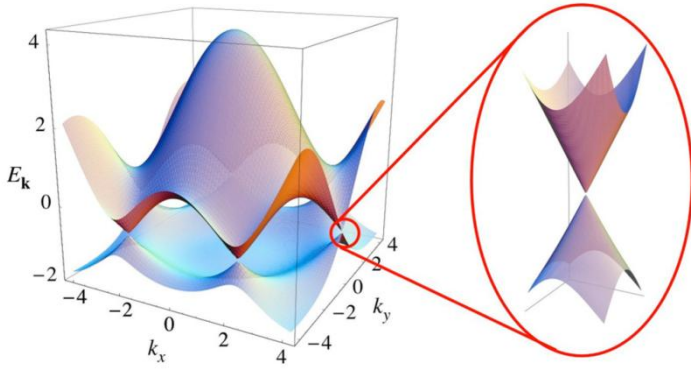
Figure 2.3. Energy dispersion as a function of the wave-vector components k_x and k_y. The lower and the upper surfaces denote the valence and the conduction energy bands, respectively. Image from [Cas09].

2.2.1 Massless Dirac fermions and massive quasiparticles

The low energy electronic structure of graphene near the corners of the BZ is extremely important since it determines the transport properties as well as various exotic phenomena observed in graphene.

To obtain the low energy electronic structure near the zone corners K (K'), we expand $f(\vec{k})$ to the first order around the Brillouin zone corners K, $\vec{k} = \vec{K} + \vec{\kappa}$:

$$f(\vec{k}) = 1 + 2e^{i\vec{\kappa}_x \frac{\sqrt{3}a}{2}}\cos(\frac{\kappa_x a}{2} + \frac{2\pi}{3}) = -\frac{\sqrt{3}a}{2}(\vec{\kappa}_x - i\vec{\kappa}_y) \tag{2.9}$$

Eq. 2.16 reduces to

$$-\frac{\sqrt{3}a}{2}\gamma \begin{pmatrix} 0 & \vec{\kappa}_x - i\vec{\kappa}_y \\ \vec{\kappa}_x + i\vec{\kappa}_y & 0 \end{pmatrix} \begin{pmatrix} c_1 \\ c_2 \end{pmatrix} = E(\vec{k}) \begin{pmatrix} c_1 \\ c_2 \end{pmatrix}. \tag{2.10}$$

Thus the Hamiltonian is

$$H = -\frac{\sqrt{3}a}{2} + \gamma(\kappa_x \sigma_x + \kappa_y \sigma_y) = -\hbar v_F \vec{\kappa}.\vec{\sigma} \tag{2.11}$$

where σ_x and σ_y are the Pauli matrices and $v_F = \sqrt{3}a\gamma/2\hbar$. The dispersion relation in Eq. 2.11 becomes $E(\vec{k}) = \pm\sqrt{3}a\gamma \left|\vec{k}\right|/2 = -\hbar v_F \vec{k}$. This is analogous to the dispersion relation formulated in Einstein's relativistic theory $E = \pm\sqrt{(m^2 c^4 + c^2 p^2)}$, with zero effective mass

m=0 and the speed of light c replaced by the Fermi velocity, v_F, which is ≈300 times smaller. This suggests that electrons in graphene are governed by a two-dimensional version of the relativistic quantum theory introduced by Dirac, which holds for massless relativistic Fermions (e.g. neutrinos). Because of this, the low energy quasiparticles in graphene are also described as "Dirac fermions" and the points where the valence and conduction bands merge are called "Dirac points". This Dirac physics of the charge carriers is the root cause of a lot of interesting physics observed in graphene. Starting from the very first observation of an anomalous, so called half integer, quantum Hall effect in graphene [Nov07] [Zha05] where the sequence of steps in the Hall conductivity is shifted with $1/2$, with respect to the classical quantum Hall effect. Another consequence of the gapless linear bands is the peculiar scattering properties of the charge carriers, which for certain incidence angles on electrostatic potential barriers can have a transmission probability of 1 [Bee08]. This, so called Klein tunneling causes the charge carriers in graphene to be unhindered by electrostatic potentials [Rob12].

Perhaps the most interesting aspect of graphene physics is that the band structure and physical properties of this material may be influenced by nanostructuring, functionalizing, mechanically straining, etc., yielding rich new physics to be studied and exploited [Fuh10] [Gei07] [Bar09].

Figure 2.4 shows a schematic drawing of the low energy dispersion near E_F. The peculiar linear dispersion for the valence and conduction bands results in many intriguing properties. First of all, the "Fermi surface" in graphene contains only six points, rather than a true Fermi surface. Because of the finite number of points at the Fermi surface, the density of states is vanishingly small at E_F.

Moreover, the linear dispersion also gives rise to many properties in graphene that are different from those in two dimensional semiconductors.
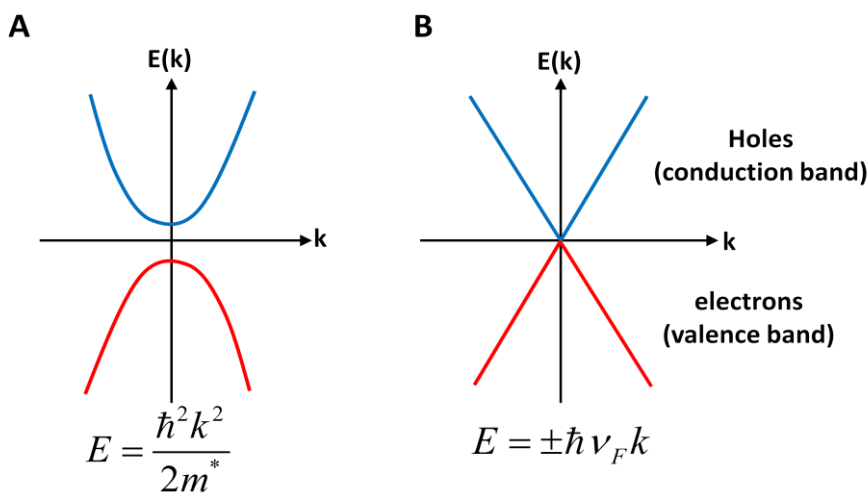
Figure 2.4. Energy gap in a conventional semiconductor vs graphene: Energy dispersion of (a) a typical two-dimensional semiconductor and (b) that of graphene, which is a zero-gap semiconductor.

In semiconductors, the typical band dispersions show a quadratic behavior (Figure 2.4), and the electrons can be described by nonrelativistic theory formulated in Schrödinger equation. An electron in these systems is modeled as a quasi-particle with a finite ("massive" compared to zero) effective mass $m^* = \hbar^2 (d^2E/dk^2)^{-1}$. The mass is usually different from the non-interacting electron mass and this mass renormalization is used to take into account the effects of electron-electron interaction and electron-phonon interaction. The velocity of electrons $v = (1/\hbar)(\partial E/\partial k)$ changes as a function of electron binding energy. The electron in graphene, however, shows a linear dispersion relation $\pm E(k) = \pm \hbar v_F k$ and travels with a constant velocity.

2.3 Basic electrochemistry of graphene

One area which has considerably benefited from carbon based materials is the field of electrochemistry, where carbon materials are at the forefront of innovation and widely utilized both analytically and industrially. As indicated in many studies, carbon materials have the potential to outperform the traditional noble metals in many areas [Bro11]. In particular, graphene has been reported to be advantageous in various electrochemical applications ranging from sensing through to energy storage and generation [Bro11] [Rac15]. This diversity and success stems largely from the often-cited advantages of graphene, including chemical stability, low cost, wide potential window, relatively inert electrochemistry, rich surface chemistry and electro-catalytic activity for a variety of redox reactions [Bro14] [Mcc08].

It has been shown that graphene exhibits high electrochemical capacitance with excellent cycle performance and hence has potential application in ultracapacitors [Sto08] [Mis11]. Shao et al. reported that graphene shows much higher electrochemical capacitance and cycling durability than CNTs. The specific capacitance was found to be ~165 and ~86 F/g for rGO and CNTs, respectively [Sha10c].

The electrochemical properties of graphene as electrode materials have been highly explored recently. It is well established that the choice of electrode material has a significant effect on the observed electrochemical signature in terms of the electrode's geometry, choice of composition and surface structure [Bro14]. When reviewing the essential characteristics of an electrode material for widespread applicability within electrochemistry, graphene's advantages become apparent. Due to its favorable electron mobility and unique surface properties, such as one-atom thickness and high specific surface area, graphene can accommodate the active species and facilitate their electron transfer at electrode surfaces. Furthermore, the high surface area of graphene facilitates large amounts of electroactive sites, which is favorable for loading high amount of biological species on the electrodes employed in electrochemical sensing applications.

Graphene's conductivity remains stable over a vast range of temperature, encompassing stability at temperatures as low as liquid Helium, where such stability is essential for reliability within many electrochemical applications [Bro10].

Considering the arguments already mentioned, graphene holds inimitable properties that are superior in comparison to other carbon allotropes of various dimensions and from any other electrode material, thus suggesting that graphene is a more favorable electrode material that could potentially yield significant benefits in many electrochemical applications.

2.4 Graphene for sensing applications

The beneficial implementation of graphene as a sensor substrate has been widely reported for the detection of a diverse range of analytes including numerous bio-molecules, gases and miscellaneous organic and inorganic compounds.

Graphene-oriented sensors can be expected to be highly sensitive for detecting individual molecules on and off its surface. The high sensitivity of graphene emerges due to two primary reasons: 1) the 2D nature of graphene allows total exposure of all of its atoms to the adsorbed target molecule, providing the high surface area per unit volume, and 2) it is inherently a low-noise material due to the quality of its crystal lattice, which leads to screen charge fluctuations more than one dimensional systems such as CNTs [Ali16].

Furthermore, graphene is an excellent conductor of electrical charge. Heterogeneous electron transfer (the transfer of electrons between graphene and the molecule in the solution necessary for the oxidation/reduction of electroactive species) occurs at the edges of the graphene or at plane defects, rather than the basal plane-the latter is sometimes referred to as being inert-due to the oxygen-containing groups present at the graphene edges.

The realization of devices employing such properties has been tried in various graphene-based systems over the last few years. For instance, a graphene-based gas sensor has been demonstrated to be one of the promising materials allowing the ultimate sensitivity, detecting the adsorption of individual gas molecules with fast response time at room temperature [Sch07].

The working principle of graphene devices as gas sensors is based on the changes of their electrical conductivity induced by surface adsorbates, which act as either donors or acceptors associated with their chemical natures, preferential adsorption sites and the surrounding atmospheres [Sch07] [Col00] [Ao08]. By monitoring changes in resistivity, minute concentrations of certain gases present in the environment can be well sensed. Till now, a number of groups have demonstrated good sensitivity for the detection of NO_2, NH_3, and other gaseous molecules under ambient conditions by using chemically derived graphene-based sensors [Ao08] [Hua08] [Fow09]. Some reports have also confirmed high sensitivity of sensors based on graphene nanocomposites decorated with metals and metal oxides for hydrogen [Alm10] [Lan11], carbon monoxide [Say15] and ethanol [Jia11] in the gas phase.

Another enticing scope is the use of graphene in biological devices for biosensing, where the excellent electrochemical and structural properties of graphene open up possibilities for designing and preparing graphene-oriented electrodes for a wide range of biosensing applications. Although CNTs offer many advantages in fabricating electrochemical devices,

graphene with favorable properties compared to CNTs, has opened a new horizon in the field of electrochemical sensing and biosensing applications. The primary distinguishing characteristics of graphene in comparison to CNTs are graphene's high biocompatibility, ease of processing, low cost and facile chemical functionalization, which offer a better alternative for high performance chemical and biological sensors [Vam06].

Additionally, graphene's high surface area to volume ratio provides more uniform distribution of electrochemically active sites than electrodes made from graphite and CNTs [Pum09]. This is advantageous for higher enzyme loading, thereby increasing the sensitivity of graphene-based biosensors [All10], since the whole surface area can be activated and even small changes in the charge environment caused by the adsorption of molecules can give measurable changes in their electrical properties [Yan10].

Graphene-based materials are considered to provide a suitable microenvironment for biomolecules immobilization, facilitating electron transfer between the immobilized biomolecules and electrode substrates. Novel graphene-based biosensors have been made regarding the fact that graphene oxide possess reactive functional groups that can easily bind with the free $-NH_2$ terminals of the enzyme or protein to result in a strong amide covalent linkage [Sha09] [Alw09] [Kan09].

Graphene materials have also been employed for sensitive and selective electrochemical detection of nucleobases, nucleotides, single stranded DNAs (ssDNA), and double stranded DNAs (dsDNA), where the existence of π-rich conjugation domains gives graphene the ability to interact with DNA molecules via π-π stacking interactions. Such electrochemical DNA sensors may provide a simple alternative approach for DNA analysis and sequencing [Liu12]. Stacked graphene nanofibers have been reported to be used to distinguish the four nucleobases, resulting in a sensitivity two to four folds higher than CNT-based electrodes, due to numerous open edges of individual graphene nanosheets which are much more electrochemically active compared to the basal carbon plane [Amb10b].

Graphene has also proved to be an ideal platform for rapid and sensitive detection of DNA hybridization and polymorphism, correlated to the development of Alzheimer's disease. Investigating the influence of various same-sized graphene platforms with different layer numbers on the impediometric detection of DNA polymorphism, single layered graphene provided the best sensitivity, as Bonnni et. al. reported [Bon11].

3. Electrochemical Biosensors

The modern concept of biosensors owes much to L. Clark and C. Lyons due to their first report about a glucose sensor at the New York Academy of Sciences Symposium in 1962 [Cla62], in which they showed that glucose in whole blood could be monitored by measuring the amount of oxygen consumed through the use of an amperometric electrode. Clark's work and the subsequent transfer of his technology to Yellow Springs Instrument Company led to the successful commercial launch of the first dedicated glucose biosensor in 1975 [Wil00]. Since then, various forms of electrochemical biosensors have been developed due to their high sensitivity, selectivity, ability to operate in turbid solutions, and amenability to miniaturization.

But what exactly is a biosensor? In its broadest sense, a biosensor is defined as an analytic device comprising three structural elements: a recognition element, a transducer, and an amplifier [Gri08]. The recognition component, which is any element sensitive to the analyte of interest, includes biological elements, ranging from tissues and cells to antibodies, enzymes, receptors, and nucleic acids, etc. Although biosensing devices employ a variety of recognition elements, electrochemical detection techniques have so far used predominantly enzymes. This is mostly due to their specific binding capabilities and biocatalytic activity [Egg02], [Dor03] and [Sch02]. It is important to note that the biological recognition element is either integrated within or in close proximity to the transducer.

The transducer acts as an interface between the biological element and the amplifier, thereby performing a detector function. The main role of the transducer is to transform the signal originating from the interaction between the analyte and the recognition element into a recognizable and/or quantifiable physical output, for example, a current in an amperometric biosensor. Major types of transducers include electrochemical, optical, piezoelectric, and calorimetric transducers, which measure the changes in electric distribution, optical properties, mass, and thermal properties, respectively. Finally, the amplifier amplifies the transducer signal, which is displayed in a user-friendly way. Examples of these components along with a schematic view of a biosensor are illustrated in Figure 3.1.

The compilation given in Figure 3.1 helps one to understand which parameters change during a biological recognition event in a biosensor. This knowledge is fundamental for developing and optimizing biosensors. The choice of the transduction process and transduction material is dependent on this knowledge as well as the chemical approach to construct the sensing layer on the transducer surface.

The choice of the biological recognition element is the crucial decision that is taken when developing a novel biosensor design. Among the various recognition elements listed, enzymes are the most common and well developed, because they combine high chemical specificity and inherent biocatalytic signal amplification [Alk13].

(A)

(B)
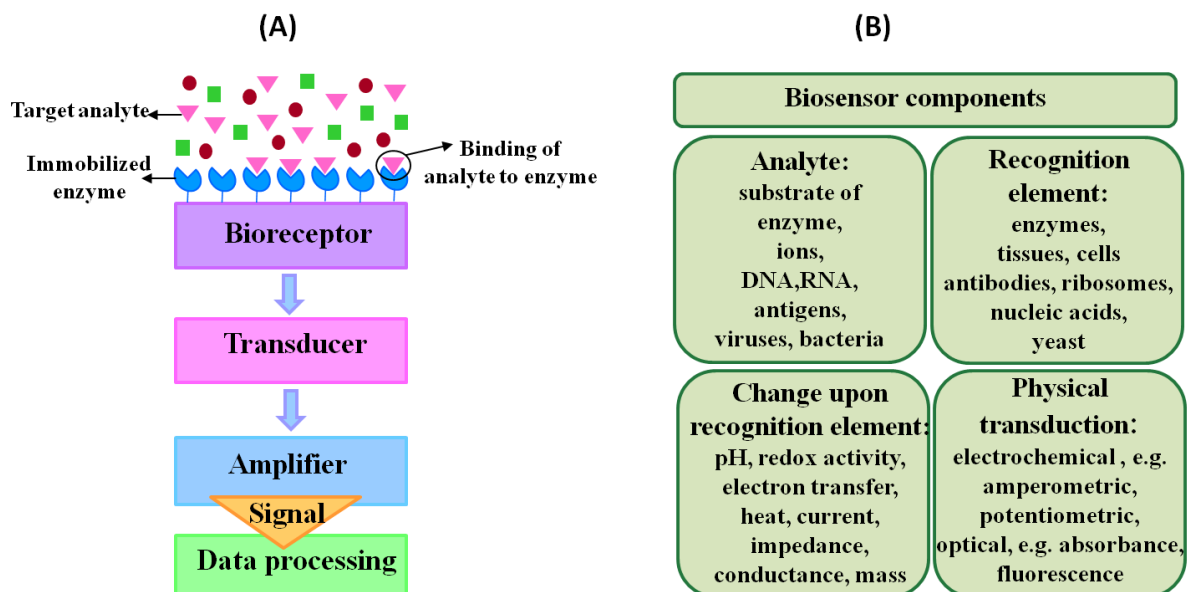
Figure 3.1. Biosensor components : (A) Schematics of a biosensor set-up. (B) Examples for biosensor components.

Most biosensors use electrochemical detection for the transducer because of the low cost, ease of use, portability, and simplicity of construction. The reaction being monitored electrochemically, typically generates a measurable current, a measurable charge accumulation or potential, or alters the conductive properties of the medium between electrodes.

Depending upon the electrochemical property to be measured by a detector system, electrochemical biosensors may further be divided into conductometric, potentiometric and amperometric biosensors.

Conductometric devices are based on the measurement of changes in conductance between two metal electrodes as a result of a biochemical reaction, whereas potentiometric biosensors measure the potential difference between the anode and the cathode as a function of analyte concentration. Finally, amperometric biosensors measure the current change resulted by chemical reaction of electroactive materials while a constant potential is being applied. The amperometric biosensors are known to be more reliable, inexpensive and highly sensitive for the clinical, environmental and industrial purposes [Cha02].

The biosensor's performance is usually experimentally evaluated based on its sensitivity, limit of detection (LOD), linear and dynamic ranges, reproducibility or precision of the response, selectivity and its response to interferences. Other parameters that are often compared include the sensor's response time (i.e. the time after adding the analyte for the sensor response to reach 95% of its final value), operational and storage stability, ease of use and portability. Figure 3.2 summarizes the key features of typical biosensors as well as several factors that are of additional importance for commercial devices.

```
┌─────────────────────────────────────────────┐
│     Key parameters of a biosensor performance │
└─────────────────────────────────────────────┘
```

- Analyte
- Employed biocomponent as recognition element
- Selectivity
- Sensitivity
- Dynamic range
- Limit of dietction
- Reproducibility
- Repeatability
- Stability
- Response time
- Duration to reach baseline
- Duration of measurement
- Measuring temperature
- Cost per measurement
- Sample volume

Figure 3.2. List of key characters of a biosensor

Ideally, the sensing surface should be regenerable in order for several consecutive measurements to be made. For many clinical, food, environmental, and national defense applications, the sensor should be capable of continuously monitoring the analyte on-line. However, disposable, single-use biosensors are satisfactory for some important applications such as personal blood glucose monitoring by diabetics.

3.1 Glucose sensors

The metabolic disorder of diabetes mellitus results in the deficiency of insulin and hyperglycemia and is reflected by blood glucose concentration higher or lower than the normal range of 80–120 mg dL^{-1} (4.4–6.6 mM). The complications of battling diabetes are numerous, including higher risks of heart disease, kidney failure, or blindness. The World Health Organization (WHO) estimated the prevalence of diabetes worldwide to be approximately 9% of adults aged 18+ in 2014, announcing the disease as a leading cause of death and disability. Diagnosis and management of diabetes mellitus requires a tight monitoring of blood glucose levels, stimulating scientists to develop novel techniques through which patients can easily monitor their blood glucose levels. In particular, electrochemical glucose sensors have played a leading role in the move to efficient and easy-to-use blood sugar testing, alerting a person if their blood glucose levels are out of the normal range.

Electrochemical methods may be broadly grouped into two main categories: enzymatic and non-enzymatic approaches. While the former group is glucose specific, the latter is broadly adaptable and may be used to detect not only glucose, but also an assortment of other carbohydrates.

3.1.1 Enzymatic glucose biosensors

Glucose oxidase (GOD) is the most frequently employed enzyme for the development of electrochemical glucose biosensors [Pri03]. It possesses relatively higher selectivity for glucose and is able to withstand a wider range of pH, ionic strength and temperature, compared with any other enzymes, thus allowing less stringent conditions during the manufacturing process and relatively relaxed storage norms for use [Hel08].

The first glucose enzyme electrode introduced by Clark and Lyons of the Cincinnati Children's Hospital [Cla62], relied on a thin layer of GOD entrapped over an oxygen electrode through the following reaction:

$$\text{glucose} + O_2 \xrightarrow{\text{GOD}} \text{gluconicacide} + H_2O \tag{3.1}$$
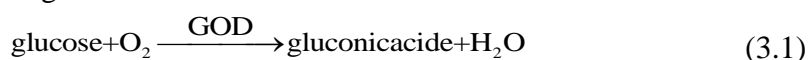
A negative potential was applied to the platinum cathode for a reductive detection of the oxygen consumption

$$O_2 + 4H^+ + 4e^- \rightarrow 2H_2O \tag{3.2}$$

The first product based on the above technology was commercialized by the Yellow Spring Instrument company (YSI) using only 25 µL whole blood samples.

The entire glucose sensor market has grown rapidly since then, leading to the development of three generations of glucose biosensors. The differences among the generations are mainly concerned with the mode of electron communication between the redox centers of the employed enzyme and the electrode.

3.1.1.1 First-Generation biosensors

The first-generation glucose biosensors rely on the use of the natural oxygen and generation and detection of hydrogen peroxide (Eqs. 3.3 and 3.4) [Wan08]. The biocatalytic reaction involves the reduction of the flavin adenine dincleotide (FAD) in the enzyme by reaction with glucose which results in the reduced form of the enzyme ($FADH_2$)

$$\text{GOD (FAD)} + \text{glucose} \rightarrow \text{GOD (FADH}_2) + \text{gluconolactone} \tag{3.3}$$

The reoxidation of the cofactor of GOD enzyme occurs in the presence of molecular oxygen, resulting in the formation of hydrogen peroxide (H_2O_2) as

$$\text{GOD (FADH}_2) + O_2 \rightarrow \text{GOD(FAD)} + H_2O_2 \tag{3.4}$$

Thus, the rate of reduction of oxygen is directly proportional to the glucose concentration that is enumerated by either measuring the reduced oxygen concentration or increased concentration of hydrogen peroxide. Hydrogen peroxide thus produced as a byproduct is oxidized at a platinum (Pt) anode. The electric current is measured and correspondingly, the number of electrons transferred is directly proportional to the number of glucose molecules present.

$$H_2O_2 \rightarrow O_2 + 2H^+ + 2e^- \tag{3.5}$$

Measurements of peroxide formation have the advantage of being simpler, especially when miniaturized devices are concerned. However, the main problem with the first generation is electroactive interference, since a relatively high electric potential was needed to measure the H_2O_2. The high potential leads to endogenous reducing species, such as ascorbic and uric acids and some drugs, like acetaminophen [Wan08]. Another drawback is the oxygen dependence. As shown in Equation (3.4), the oxygen amount is a limiting factor (oxygen deficit) that controls the changes in sensor response and the upper limit of linearity.

3.1.1.2 Second-Generation bioensors

The abovementioned limitations of the first-generation glucose biosensors were overcome by using mediated glucose biosensors, i.e., second-generation glucose sensors.
Since the FAD redox center of the GOD is surrounded by a thick protein layer, the direct electron transfer from GOD to traditional electrodes is blocked. Various strategies have been employed to facilitate electron transfer between the GOD redox center and the electrode surface, such as employing nanomaterials, like gold nanoparticles (NPs) [Hol11] or CNTs [Woo14] as electrical connectors between the electrode and the FAD center. Covalent bonding of redox polymers is another approach to reduce the distance between the redox center of the polymers and the FAD center of the enzymes, which leads to a high current output and fast sensing response [Deg89].

The sensor performance was further improved by replacing oxygen with a nonphysiological electron acceptor (called redox mediators), that was able to shuttle electrons from the enzyme to the surface of the working electrode. The reduced mediator is formed instead of hydrogen peroxide and then reoxidized at the electrode, providing an amperometric signal and regenerating the oxidized form of the mediator. The reaction can be described as follows [Tog10]:

$$\text{Glucose} + \text{GOD}_{(ox)} \rightarrow \text{gluconic acid} + \text{GOD}_{(red)} \tag{3.6}$$

$$\text{GOD}_{(red)} + 2\text{M}_{(ox)} \rightarrow \text{GOD}_{(ox)} + 2\,\text{M}_{(red)} + 2\,\text{H}^+ \tag{3.7}$$

$$2\text{M}_{(red)} \rightarrow 2\text{M}_{(ox)} + 2\text{e}^- \tag{3.8}$$
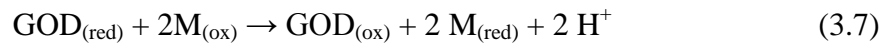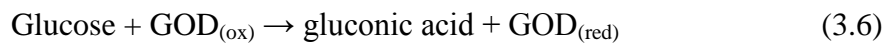
where $\text{M}_{(ox)}$ and $\text{M}_{(red)}$ are the oxidized and reduced forms of the mediator. Artificial electron-carrying mediators, like ferrocene derivatives, ferricyanide, transition-metal complexes, etc. are of particular interest, fitting the criteria for a good mediator, such as (i) reacting rapidly with the reduced enzyme while not reacting with oxygen, (ii) good electrochemical properties, like low operational potential, (iii) low solubility in aqueous medium, (iv) chemical stability in both reduced and oxidized forms [Bor12].

3.1.1.3 Third-Generation bioensors

In order to avoid complications offered by synthetic or natural mediators in second generation biosensors, new strategies for direct electron transfer between the electrode and active center of enzyme have been researched [Bar14] [Tas11], with the aim of developing highly selective and sensitive third-generation biosensors. The absence of mediators is the main advantage of such third-generation biosensors, leading to a very high selectivity (owing to the very low operating potential). However, as discussed earlier, critical challenges must be overcome for the successful realization of this direct electron-transfer route, owing to the globular structure of GOD with the active site, containing $FAD/FADH_2$ redox cofactor, buried deep inside a cavity of ~13A°, which is a major hinderance for direct electron flow.

Figure 3.3 summarizes various generations of amperometric glucose biosensors based on different mechanisms of electron transfer, including the use of natural secondary substrates, artificial redox mediators, or direct electron transfer.
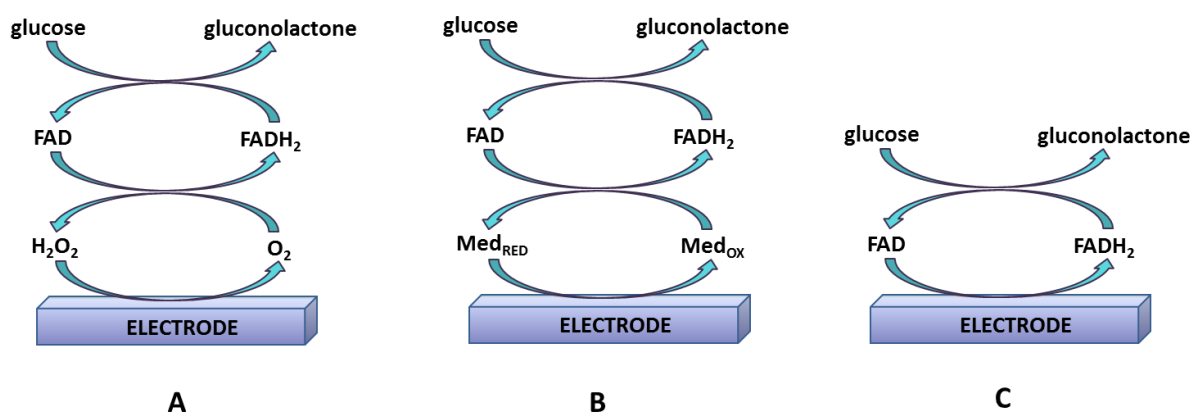
Figure 3.3. Summary of enzymatic glucose oxidation mechanisms , presented as (a) first, (b) second and (c) third generation sensors.

Although enzyme electrodes have witnessed massive progress and commercially available glucosemeters have opened broad opportunities for monitoring glucose level in real time [Gal15], notable drawbacks and disadvantages have been extensively interrogated, which originate mainly from the nature of GOD. Principally, the activity of enzyme is prone to be affected by temperature, acidity, and toxic chemicals, resulting in poor reproducibility and stability. Furthermore, laborious and complex protocols are required to immobilize enzyme on electrode, complicating the fabrication procedures and thus affecting their final performance [Urb15]. Because of the mentioned flaws, fabrication of enzyme-free glucose sensors has been continuously motivating research interests.

3.1.2 Electrochemical non-enzymatic glucose sensors

Various studies have been conducted to alleviate the drawbacks of enzymatic glucose sensors. A non-enzymatic amperometric sensor for direct determination of glucose is an attractive

alternative technique to solve the disadvantages of enzymatic biosensors, especially because of their higher repeatability and stability. Instead of facilitating the needs of a fragile and relatively difficult enzyme, non-enzymatic electrodes strive to directly oxidise glucose in the sample. This is an ideal system which was first investigated a century ago by Walther Löb [Tog10], who electrochemically oxidised glucose in sulphuric acid at a lead anode. This occurred long before the fabrication of the Clark oxygen electrode, though extensive research on the non-enzymatic approach actually coincided with enzymatic development.

The performance of non-enzymatic glucose sensors relies mostly on two factors: the efficient electron transfer rate and an excellent catalytic material. A number of catalytic materials such as noble metals (Au, Pt) [Bad14] and their alloys (Pt–Pb, Pt–Ru, Pt–Au, Ni–Pt) [Sun15], transition metals and their oxides (Ni, Cu, CuO, NiO, CoO, MnO_2, Co_3O_4) [Rei08] [Saf09] [Su16], CNTs [Ler13] and graphene [Teh15] have been explored to fabricate enzyme-free glucose sensors.

The development of non-enzymatic glucose sensors has risen over the past decade at a considerable rate. In addition, the fabrication of a wide variety of nanomaterials has introduced a plethora of selective and highly responsive glucose sensors. Research into this area of sensing is therefore evidently in full force.

Before we discuss the experimental techniques that we used throughout this work in order to fabricate an enzymatic, as well as non-enzymatic graphene based glucose sensor, a fundamental introduction of the experimental electrochemical methods and a general description of the setups is needed, which is provided in the next chapter.

4. Experimental Techniques and Instrumentations

This chapter focuses primarily on the introduction of electrochemical instrumentation and detection techniques utilized in this project. The aim of this chapter is to enable the reader to understand the experiments as well as the interpretations of the results presented in the next chapters. Therefore, in the first section of this chapter an introduction on the electrochemical cell and its components is presented. The second section deals with a short summary on the most commonly used techniques for the electrochemical detection, including cyclic voltammetry, amperometry and electrochemical impedance spectroscopy (EIS).

4.1 Electrochemical cell

An electrochemical cell is used to generate voltage and current from chemical reactions or induce chemical reactions by the input of electrochemical signals [Li13]. It can be formed by two or three electrode systems. The two electrode system is the simplest approach to the study of current/voltage characteristics, but often has far more complex results and corresponding analysis. Two-electrode setups are used in the experiments where measurement of the whole cell voltage is significant, for example electrochemical energy storage or conversion devices like batteries, fuel cells, photovoltaic panels, etc. [Bar02]. The three-electrode cell setup is the most common electrochemical cell setup used in electrochemistry and consists of the working electrode, auxiliary or counter electrode and reference electrode, employing a potentiostat as the measuring and control device. Three-electrode setups have a distinct experimental advantage over two electrode setups: they measure only one half of the cell. That is, the potential changes of the working electrode are measured independent of changes that may occur at the counter electrode.

A brief description of the components of a three-electrode setup is presented in the following.

4.1.1 Potentiostat

Potentiostat is an electronic instrument fundamental to modern electrochemical studies, which is utilized along with a three-electrode cell, for investigations of reaction mechanisms related to redox chemistry and other chemical phenomena.

A potentiostat is mainly used for two reasons:

1) To accurately control the voltage between the working and the reference electrode,

2) For measuring the current flow between the working and the counter electrode.

The working electrode (WE) is the electrode in an electrochemical system which makes contact with the analyte. Its surface is the place where the reaction of interest occurs. After the WE is applied with a certain potential, the transfer of electrons between electrode and analyte

takes place. Common WEs can be made of inert materials such as Au, Ag, Pt and carbon materials.

The reference electrode (RE) is an electrode which maintains a stable voltage and is used as a point of reference in the electrochemical cell for the potential control and measurement. The high stability of the RE potential is usually reached by employing a redox system with constant (buffered or saturated) concentrations of each participants of the redox reaction.
There are two common and commercially available RE types:
1) Ag/AgCl Electrode: There is a silver (Ag) wire coated with silver chloride (AgCl) and dipped into sodium chloride (NaCl) solution at $E^0 = +0.22V$

$$AgCl + e^- \rightarrow Ag + Cl^- \tag{4.1}$$

2) Saturated-Calomel Electrode (SEC): It consists of mercury, which is in contact with a paste of Calomel (other name of mercurous chloride (Hg_2Cl_2)), dipped into a saturated solution of potassium chloride (KCl) at $E^0 = +0.24V$

$$Hg_2Cl_2 + 2e^- \rightarrow 2Hg + 2Cl^2 \tag{4.2}$$
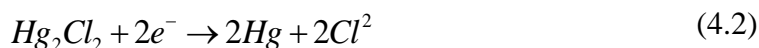
As soon as a current passes a RE, it is polarised, that means its potential varies with the current. Hence, to maintain a stable potential, no current is allowed to pass the RE. Now, how can we achieve to maintain a constant potential difference between the reference electrode and the working electrode? We are forced to introduce a third electrode, which is called counter electrode.

The counter electrode (CE), also known as auxiliary electrode, is an electrode which is used to close the current circuit in the electrochemical cell. It is often fabricated from electrochemically inert materials such as gold, platinum or carbon, and usually does not participate in the electrochemical reaction. The current flows between the WE and the CE, high enough and in proper polarity to keep the WE potential at a constant value with respect to the RE. The total surface area of the CE must be larger than the area of the WE so that it will not be a limiting factor in the kinetics of the electrochemical process under investigation. The potential of the CE is not measured against the RE but adjusted to balance the reaction occurring at the WE. This configuration allows the potential of the WE to be measured against the RE.

The potentiostat must have a bipolar operational amplifier (OPA) with two inputs: an inverting input and a non-inverting one, which has following qualities: By introducing a voltage into the non-inverting input of an operational amplifier, it will produce an amplified voltage (or current) of the same sign. By introducing the voltage into the inverting input, the result will be a signal of the same magnitude, but of opposite sign. To close the loop, the working electrode must be connected to the non-inverting input (+), the reference electrode to the inverting input (-), and the counter electrode to the output. The difference between WE and RE will be amplified and inverted by the OPA. A matching current is fed to the CE. The control circuit is closed by the cell, where the current passes the electrolyte from the CE to the WE. This polarises the WE exactly so that the difference between the RE input and the WE input is set to zero. Doing so, you can keep the potential of the working electrode exactly on the potential of the reference electrode. If you want to shift the potential of the WE to some

other value referring to RE, you only must insert a voltage in series between reference electrode input and the reference electrode.

To measure the current through the CE, the system needs a resistor (R) in the CE wiring, across which a voltage can be measured, proportional to the current flowing.

The RE input is commonly protected by an input resistor (RS), which prevents the potential amplifier from being destroyed by static high voltage shocks, when the input is open.

Schematic illustration of the three-electrode system has been shown in Figure 4.1
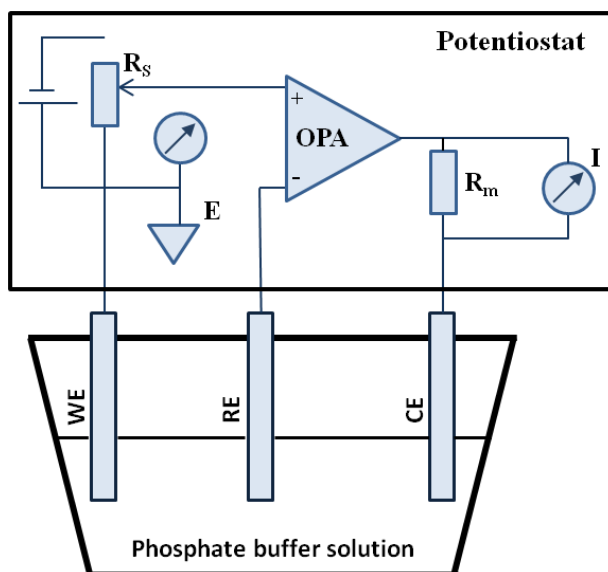
Figure 4.1. Basic diagram of a potentiostat and a three-electrode cell

The three electrode set-up illustrated in this section can be used for different electrochemical measurements. Next sections will describe in detail some of the most common electrochemical analytical techniques and their applications in the field of electrochemical sensing.

4.2 Cyclic voltammetry

Cyclic voltammetry (CV) is a type of electroanalytical technique which provides information on the thermodynamics of redox processes, adsorption processes and the kinetics of electron transfer reactions. It is the most widely used measuring technique in electrochemical analysis. In a typical cyclic voltammetry, the potential is ramped linearly versus time and a pair of well-defined redox peaks are observed. Single or multiple cycles can be performed depending on the requirements of specific analysis. In a CV experiment, the voltage is measured between the reference and the working electrode, and the current is measured through the working and the counter electrode.

Using an electrochemical set-up along with a potentiostat, a current–voltage curve can be recorded. When current I flows in an electrochemical cell, a potential drop between the

reference electrode and the working electrode occurs, determined by i×R, where R is the resistance owing to the electrolyte between the working and the reference electrode, known in this case as uncompensated resistance. This resistance causes a drop in potential in the solution during current flow owing to Ohm's law. This drop increases with solution resistivity and with the distance between the working electrode and the reference point. Therefore, it is always advisable to place the reference electrode outside the path of ion migration between the working and the counter electrode. When this is not possible because of the setup configuration, one should try to place the reference electrode as close as possible to the working electrode to avoid large potential drops between the working and the reference electrode, which are responsible for incorrect potential measurement or control.

Figure 4.2 shows the principles for the generation of a cyclic voltammetric curve. A linearly dependent potential (in relation to the reference electrode) is imposed on the working electrode, being switched between two potential values (E_1 and E_2) at a fixed rate. A CV scan begins at the initial potential, E_1 , and proceeds to the final (or reverse) potential (E_2). After reaching the set potential (E_2), the scan is reversed and the voltage is switched back to E_1 . The inversion of scanning can happen multiple times during a single experiment. The scan rate (v) is the change of potential as function of time ($v = dE/dt$) and can be deduced from the gradient of the curve (Figure 4.2 A). The scan rate is a critical factor, since the duration of scan should provide sufficient time to allow the chemical reaction to be complete. During the scan, the flowing current is recorded. Because potential and current are both functions of time, they can be easily interrelated and the current flow can be plotted as a function of the applied electrode voltage. Figure 4.2 B shows the result of a CV experiment: a cyclic voltammetric curve, or voltammogram.

As illustrated by the CV curve, when the voltage is increased from E_1 to E_2 with scan rate v, at first almost no current flows.
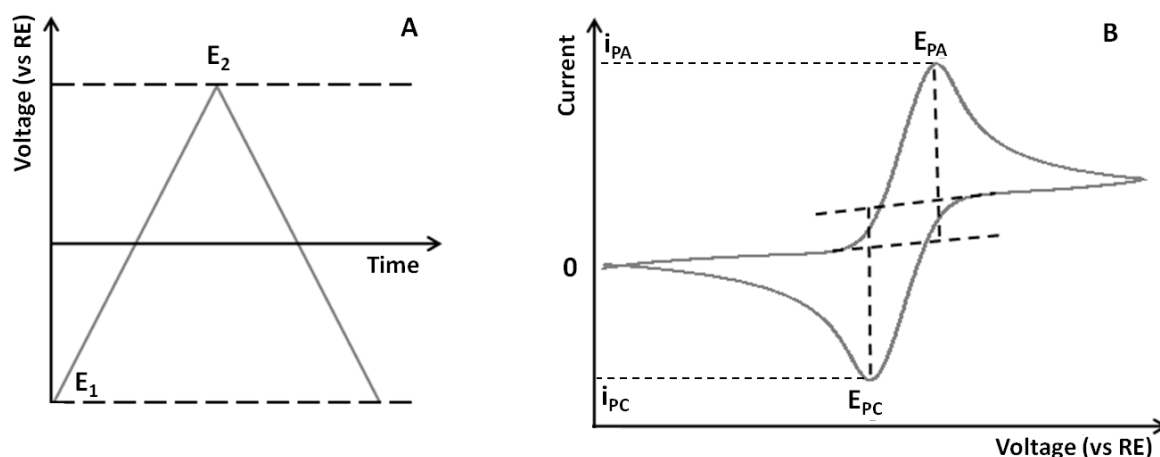
Figure 4.2. Principles for the generation of a CV curve. During CV, a potential (in relation to the used reference electrode) is applied to the working electrode (A). A CV scan starts at the initial potential, E_1, proceeds to the final potential (reverse potential), E_2, and then proceeds back to E_1 with a certain scan rate, v; thus, the flowing current is recorded. The spectrum show the applied potential. The derived spectrum (B), which shows the current as a function of potential, is called a cyclic voltammetric curve.

From a certain potential, the current begins to increase up to a maximum value owing to an electrochemical oxidation reaction on the electrode surface, and then decreases afterwards. This maximum current is called the peak current, for the anodic oxidation process (i_{pA}). The respective potential where the maximum current occurs is called peak potential, here anodic peak potential (E_{pA}). After reaching E_2 and decreasing the potential back to E_1, the respective reduction reaction starts to proceed and the peak cathodic current (i_{pC}) and the associated peak potential (E_{pC}) can be identified.

4.3 Amperometry

The principle of amperometry is based on the continuous measurement of the current between the working and counter electrode. In amperometric electrochemical sensors, the current generated by redox reaction of an analyte at the WE is measured as the sensor signal while a fixed potential is being applied between the WE and the RE. The measured current is directly proportional to the concentration of a redox active species in the analyte solution. The electrical potential of the WE versus the measured solution is achieved by a separate RE and is controlled by a potentiostat electronic system. The relationship between current and concentration is linear, typically over 3 orders of magnitude, and measurements with high sensitivity (ppm and ppb) are possible with excellent measurement accuracy under constant potential conditions.

4.4 Chronocoulometry

Chronocoulometry is an electrochemical technique to evaluate the electrodeposition behaviors and belongs to the family of step techniques. As its name implies, chronocoulometry is the measurement of charge (coulombs) as a function of time (chrono) [Sko07]. Applications of this technique include measurement of electrode surface area, diffusion coefficients, concentration, kinetics of both heterogeneous electron transfer reactions and chemical reactions coupled to electron transfer, adsorption, and the effective time window of an electrochemical cell. In this technique the experiment starts at a potential where no reaction is occurring. The potential is then changed instantaneously (stepped) to a potential where either the oxidation or reduction occurs. The current vs. time plot for during this potential step can be described by the Cottrell equation, the most useful equation in chronoamperometry

$$i_d = (2nFAD^{1/2}C_0 t^{1/2}) / \pi^{1/2} \qquad (4.3)$$

that is, the current decreases as a function of $t^{-1/2}$.

Here, n, F, C_0, and D are the number of electrons transferred, Faraday constant (in Coulombs/mole), concentration of analyte in solution (in moles/cm^3) and diffusion constant of the analyte (in cm^2/s^{-1}) [Bar01].

The response for the chronoamperometry experiment, charge (Q) vs. time curve is then obtained by integrating the Cottrell equation,

$$Q_d = (2nFAD^{1/2}C_0t^{1/2}) / \pi^{1/2} \qquad (4.4)$$

From this data the surface area of the electrode as well as the effective time window of an electrochemical cell can be determined (See sec. 5.3.1).

4.5 Electrochemical impedance spectroscopy

Electrochemical Impedance Spectroscopy (EIS) has been known as a powerful technique for the characterization of electrochemical systems. In the majority of EIS experiments [Bar05], a sinusoidally varying voltage, U, is applied by a potentiostat across the WE and RE in a three-electrode cell containing a solution of electrolyte harboring the molecule under investigation. The magnitude of the voltage of the fixed sinusoidal voltage is dependent upon the type of molecular system under investigation [Hir08]. Biological molecules tend to be subject to smaller voltages than non-biological ones as the structures of the biological molecules are easily denatured this way [Ran13]. Through the application of this potential, one measures the resulting current response, I [Kat03], [Wil 05]. By varying the excitation frequency, ω, of the applied potential over a range of frequencies, one can determine the complex impedance, sum of the real and imaginary impedance components, of the system as a function of the frequency (i.e. angular frequency ω). Therefore, EIS combines the analysis of both real and imaginary components of impedance denoted by $Z^{'}(\omega)$ and $Z^{''}(\omega)$ respectively, as shown in Equation 4.4 [Pat99] [Tli06]

$$Z(j\omega) = \frac{U(j\omega)}{I(j\omega)} = Z^{'}(\omega) + jZ^{''}(\omega); \quad \omega = 2\pi f \qquad (4.5)$$

Using the calculated (processed) data, the real and imaginary impedances are determined and plotted against each other for different perturbation frequencies in what are called Nyquist impedance spectra (Figure 4.3). Another representation called Bode diagram, which shows the logarithm of the impedance modulus (log|Z|) and the phase displacement as function of the logarithm of frequency, is also a common way of analysing impedance data providing explicit information on the frequency dependence of the impedance.

The impedance can be approximated by the solution resistance (R_s), double layer charging at the electrode surface (C_{dl}), charge transfer resistance (R_{ct}), and the so-called Warburg Element (Z_w), as depicted in the inset of Figure 4.3. The combination of these elements is known as a Randles circuit [Ran13]; such circuits are habitually used to simulate EIS experiments.

The Warburg Element accounts for the diffusion of the ions in solution in an electrochemical reaction. For instance at high frequencies, Warburg impedance is not observed as migration

occurs over much longer time periods than the operational frequency and thus the relatively slow movement of molecules in solution renders impedance contributions to be obsolete. Hence, Warburg contributions are generally seen in the low frequency region.
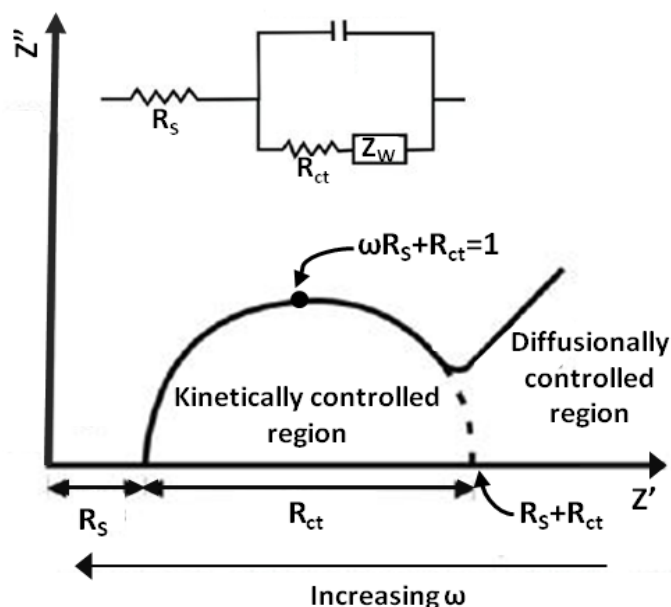
Figure 4.3. Simple Randles equivalent circuit for an electrochemical cell. Inset: the equivalent circuit for the Naquist plot. Image from [Ran13].

The right hand side of Figure 4.3 illustrates the diffusionally controlled region of a Nyquist plot obtained using EIS. The solution resistance is independent of the frequency and is observed in Figure 4.3 at the highest frequency where the real axis is intersected (R_s). The charge transfer resistance (R_{ct}) is the opposition experienced to electron movement and is a real quantity. R_{ct} is observed in Figure 4.3 at the second extrapolated intersection with the real axis in the mid- to low-frequency region; this region is marked as the kinetically controlled region of the Nyquist plot in Figure 4.3. The double layer capacitance (C_{dl}) can be roughly estimated from Figure 4.3 by the Z' at the maximum of the semi-circle.

Next chapter deals with graphene application in electrochemical detection of hydrogen peroxide (H_2O_2), presenting a detailed study on the influence of the choice of graphene materials with different qualities on the amperometric detection of H_2O_2. The results provided by this chapter help us determine which graphene material satisfy our needs for fabrication of a more efficient sensor device.

5. Signal Enhancement in Amperometric Peroxide Detection by Using Graphene Materials with Low Number of Defects

The detection of H_2O_2 has been a widely researched topic, owing to its vital role in biological systems, pharmaceutical and biochemical industries. Besides these applications, it is an enzymatic product of many biochemical processes, e.g. in enzyme-based biosensors, where H_2O_2 produced from analyte oxidation induces increase in conductance of the measuring electrode and as a result, the quantification of the analyte is achieved via electrochemical detection of the enzymatically liberated H_2O_2.

Graphene sheets for amperometric detection of H_2O_2 have been addressed in plenty of works. Many of these investigations have focused on the enzyme immobilization of modified graphene in order to enhance electron transfer rates and catalytic activity [Yu15], while others have found the application of nonenzymatic modified graphene more beneficial [Par15], due to the lack of a simple and stable enzymes/proteins immobilization approach and the denaturation of immobilized enzymes/proteins.

The present chapter, as well as figures 5.6 - 5.12, are based on a jointly authored paper that has been published previously [Zöp16].

The aim of this chapter is to investigate the influence of the choice of the graphene materials on the amperometric properties in direct hydrogen peroxide detection and study the effect of the synthesis routes of graphene materials on the sensing performance of graphene-based H_2O_2 sensors. In contrast to the other literatures which have mainly studied functionalization of graphene with an enzyme Layer [Yu15] or its modification by nanostructured materials [Leo14] for fabricating H_2O_2 sensors, our work in this chapter focuses on identifying the most efficient graphene material for the fabrication of an electrochemical sensor, using no complex modifications or functionalization steps to graphene.

The graphene materials were prepared by three different approaches, comprising a different degree of defects. All types of carbon materials have been characterized with Raman spectroscopy, and their electrochemical behavior has been investigated by cyclic voltammetry (CV), electrochemical impedance spectroscopy (EIS), chronocoulometry and amperometry. The sensing performance and catalytic properties of the sensors will be investigated in detail.

5.1 Sample preparation and experimental methods

Graphene can be generated by a number of different methods including micromechanical exfoliation of graphite (scotch tape method) [Nov04], direct chemical reduction of graphene

oxide (GO) [Chu14] [Hum58], chemical vapor deposition (CVD) [Zha13] [Str15], and epitaxial growth on silicon carbide [Nov12] [War13].

In the present work, three kinds of graphene materials, have been utilized, i.e. graphene synthesized through CVD, mechanical exfoliation and reduction of graphene oxide.
A detailed description of the mentioned methods for the production of graphene will be provided through the next sections. The advantages and disadvantages of each method will be discussed afterwards.

5.1.1 Micromechanical exfoliation

The starting point for the sample preparation is the selection of an appropriate wafer material. For the present case a highly doped silicon wafer with an insulating silicon oxide top layer (typical thickness of 300nm) is used. The insulating layer was generated via thermal oxidation. We patterned coordinate systems lithographically onto the aforementioned substrates, which allow us in later processes to orientate on the sample and localize and recover the graphene flakes. The spacing between the Cr/Au (5 nm/50 nm) alignment markers is 50 μm. The material is then cut into pieces of typically 4.5mm × 9mm.

Through micromechanical exfoliation method [Nov04], thin sheets of graphite are detached from a bulk graphite sample using adhesive tape (Figure 5.1 A). After peeling it off the graphite, multiple-layer graphene remains on the tape. By subsequent tape-to-tape peeling, the multiple-layer graphene is cleaved into various flakes of few-layer graphene. Graphene is ready to peel onto the substrate when it becomes semi-transparent and dispersed onto the tape in many smaller crystals, some of which are single-layer. To transfer it onto the SiO_2/Si substrate, the tape is attached to the substrate, pressed slightly and then removed, leaving various flakes on different spots of the substrate. This peeling process works because the carbon layers of graphite are weakly bonded and the van der Waals force between them is not as strong as the force between the graphite/graphene and the SiO_2. So, once the graphite pieces on the tape are applied to the substrate, it is likely that when the tape is lifted the interlayer bonds will break, leaving some amount of graphite/graphene flakes on the substrate. The obtained flakes differ considerably in size and thickness, where the sizes range from nanometers to several tens of micrometers for single-layer graphene. Subsequently the single graphene flakes are detected under an optical microscope and their position with respect to the alignment marks is taken. Due to the grayscale contrast of the graphene flakes with respect to the background, the layer thickness of the flakes can be determined very fast and easily. Consequently one knows if it is single, bi-, tri- or multi-layer graphene. In order to perform further measurements, subsequently Ti/Au (5nm/60nm) contacts were patterned to the graphene samples by EBL and thermal evaporation. In Figure 5.1 B a typical sample is illustrated.
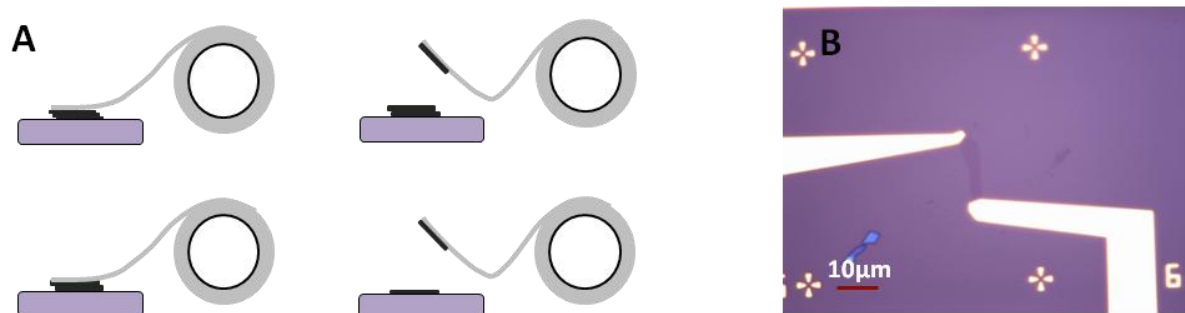
Figure 5.1. Micromechanical exfoliation of graphene. (A) Schematics of graphene exfoliation process. (B) Microscopic image of a typical sample with two Ti/Au (5nm/60nm) contacts.

The quality of the obtained graphene is very high with almost no defects (detailed discussion will be presented in section 5.2). The complexity of this method is basically low, nevertheless the graphene flakes need to be found on the substrate surface, which is labour intensive. Moreover, the size of the flakes acquired through this method is limited to tens of micron and it is difficult to obtain larger amounts of graphene by this method, hence the yield of devices based on exfoliated single-layer graphene (SG) is extremely low.

5.1.2 The reduction of graphene oxide

This method involves initial oxidation of bulk graphite to hydrophilic graphite oxide. Graphite oxide has a similar layered structure to graphite, but the plane of carbon atoms in graphite oxide is heavily decorated by oxygen-containing groups, which not only expand the interlayer distance but also make the atomic-thick layers hydrophilic. As a result, these oxidized layers can be exfoliated in water under moderate ultrasonication. If the exfoliated sheets contain only one or few layers of carbon atoms like graphene, these sheets are named graphene oxide (GO). The most attractive property of GO is that it can be (partly) reduced to graphene-like sheets by removing the oxygen-containing groups with the recovery of a conjugated structure. The reduced GO (rGO) sheets are usually considered as one kind of chemically derived graphene. Currently, GO is prepared mostly based on a route involving the steps of graphite oxidation, exfoliation, and chemical reduction proposed by Hummers and Offeman in 1958 [Hum58], where the oxidation of graphite to graphite oxide is accomplished by treating graphite with a water-free mixture of concentrated sulfuric acid, sodium nitrate and potassium permanganate. Though some modification has been proposed [Xia15] [Kum15a] [Gao09], the main strategy is unchanged. As a result, these methods are usually named modified Hummers methods. The widely accepted GO model proposed by Lerf and Klinowski [Ler98] is a nonstoichiometric model (shown in Figure 5.2), wherein the carbon plane is decorated with hydroxyl and epoxy (1,2-ether) functional groups.

Carbonyl groups (CO) are also present, most likely as carboxylic acids (COOH) along the sheet edge but also as organic carbonyl defects within the sheet. In summary, GO can be described as a random distribution of oxidized areas with oxygen-containing functional

groups, combined with non-oxidized regions where most of the carbon atoms preserve sp^2 hybridization.
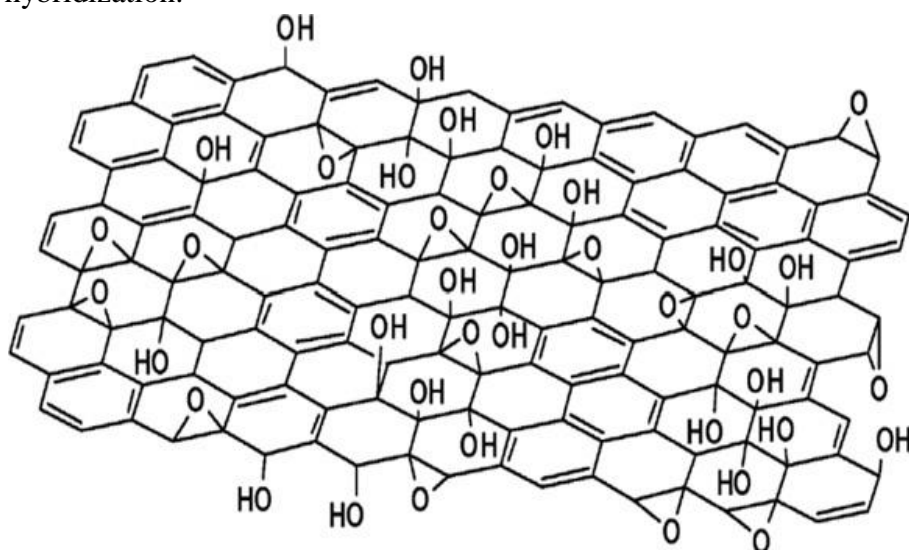
Figure 5.2. Proposed structure of graphite oxide (GO) based on the Lerf–Klinowski model with the omission of minor groups (carboxyl, carbonyl, ester, etc.) on the periphery of the carbon plane of the graphitic platelets of GO. Image from [Dre11].

To derive graphene from GO, chemical [Sta07] [Sta06] or thermal [Sch06] [Mca07] reduction is the final step to remove the functional groups. Reduction of GO to graphene can be carried out chemically by using reducing chemical agents such as hydroquinone, dimethyl hydrazine and hydrazine hydrate or thermally, by high temperature annealing.

Theoretically, a simple reduction of GO should remove the oxygen groups and rehybridize the effected sp^3 C atoms to sp^2 C, thereby leaving it aromatic and defect free. However experimentally, after any reductive treatment of GO a substantial number of oxygen groups and defects remain. These defects affect the properties of the reduced GO (RGO), e.g. provide reaction centers for catalytic activity or reduce the electric conductivity of rGO.

The rGO utilized in this work has been prepared at the department of Analytical Chemistry, at the University of Regensburg, using a slightly modified Hummers method [Hum58]. Briefly, 1 g graphite (China flake graphite, K. W. Thielmann & Cie KG) was mixed with 75 mg $NaNO_3$, 7.5 mL conc. H_2SO_4 and 450 mg $KMnO_4$ was added in small portions under vigorous stirring and cooling in an ice bath. The mixture was sonicated for 3 h and stirred for 3 days at room temperature. Subsequently, 7.5 mL of 5% H_2SO_4 was added and the mixture was stirred for 2 h at 100 C, followed by the addition of 1.5 mL of 30% H_2O_2 under constant stirring for 1 h at room temperature. For purification the obtained GO was washed with the following solutions: four times in 3% H_2SO_4 with 0.5% H_2O_2; two times in 3% HCl; and three times in water. The product was dialyzed against water (14 kDa cut-off) for 10 days, changing the water three times.

To obtain chemically reduced GO, 7mL of a GO suspension (0.5 mg mL^{-1}) was mixed with 31 mL NH_3 (32% in water) [Li08]. After adding 5 mL of 98% hydrazine hydrate the reaction mixture was refluxed for 1 h at 100 C. Finally the resulting black suspension was washed with water and isolated by centrifugation.

Chemically reduced GO was deposited on photolithographically prepared gold microelectrodes with interdigitated structure of thin gold layers (Figure 5.3) via drop casting of 1 µL of an aqueous rGO suspension (0.25 g·L^{-1}). Afterwards the electrodes were dried at room temperature, followed by a final annealing step of 230 °C for 30 seconds on a hot plate.
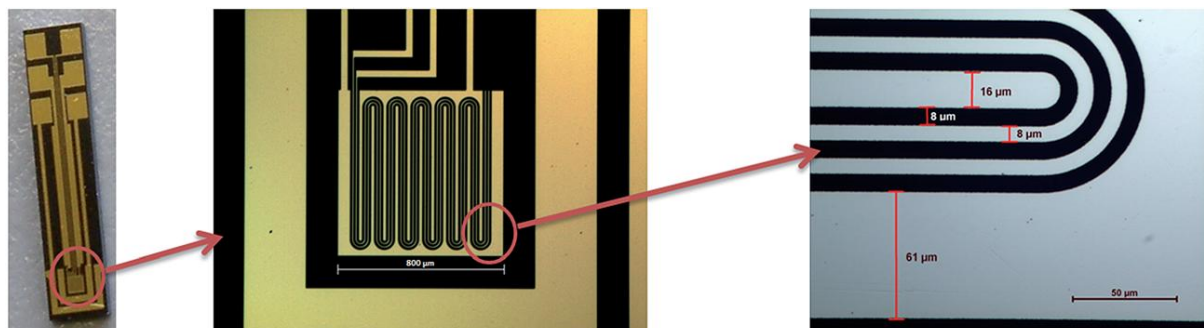
Figure 5.3. rGO deposited microelectrodes with an interdigital structure consisting of gold conducting paths on a Si/SiO$_2$ wafer substrate. The sample and the image were the courtesy of Dr. A. Zöpfl from the department of Analytical Chemistry, Regensburg University.

Chemical reduction of GO is a very scalable method, but unfortunately the rGO produced has often resulted in relatively poor yields in terms of surface area, electronic conductivity and electrical mobility [Nav07]. During thermal annealing, unfortunately, the heating process damages the structure of the graphene platelets as pressure between builds up and carbon dioxide is released. This also causes a substantial reduction in the mass of the GO, creating imperfections and vacancies, and potentially also having an effect on the mechanical strength of the rGO produced [Fue14]. Nevertheless, rGO is the material most commonly used for electrochemical applications (68% of all publications), probably because of its easy access, scalable synthesis, low cost and simple functionalization [Koc12].

5.1.3 Chemical vapor deposition

Chemical vapor deposition (CVD) is a technique of thin solid film deposition on substrates from the vapor species through chemical reactions. The chemical reaction is the characteristic feature that distinguishes CVD from other film deposition techniques such as physical vapor deposition (PVD). Graphene CVD was first reported in 2008 and 2009, using Ni and Cu substrates, [Arc09] [Rei09] [kim09] which was followed by an explosion of research activities and publications using a variety of transition metal substrates [Sea14] [Pol15] [Cus15].

A typical tube-furnace CVD system is composed of a gas delivery system, a reactor (with heaters surrounding it to provide high temperatures for the reaction) and a gas removal system [Mia11]. During the CVD process, reactive gas species are fed into the reactor by the gas delivery system and pass through the hot zone, where hydrocarbon precursors decompose to carbon radicals at the metal substrate surface and then, form single-layer and few-layers graphene. Eventually the by-products of the reaction and non-reacted gases are removed by the gas delivery system. During the reaction, the metal substrate not only works as a catalyst

to lower the energy barrier of the reaction, but also determines the graphene deposition mechanism, which ultimately affects the quality of graphene.

The role of a substrate is substantial in the graphene CVD, as it catalyzes the reactions that define the quality and morphology of graphene. Two major substrates used for reliable fabrication of large area CVD graphene are copper (Cu) and Nickel (Ni). The first successful graphene deposition via CVD was conducted using Ni as catalyst with the inspiration coming from the CNT growth [Eiz79]. The CVD of graphene on the Ni catalyst has been described as a two-step mechanism including a first stage of carbon atoms incorporation into the Ni substrate, followed by outdiffusion onto the Ni surface to form graphene layers when rapid cooling of the substrate occurs [Li09]. Conversely, growth on polycrystalline Cu substrates has been regarded more viable to obtain monolayer graphene mainly by a surface controlled process [Luo11]. Even first modeling of graphene growth on different metals shows that the Cu catalyzed process differs from the growth on other metals [Che10]. Primarily the difference in the growth kinetics and mechanism between Ni and Cu has been ascribed to a very low carbon solubility (<0.001 atomic%) in Cu compared to the higher solubility of carbon in Ni (>0.1 atomic%). The advantages of Cu as an excellent candidate for making large-area, uniform thickness (95%), single-layer graphene films have been widely reported [Mat11] [Wir14].

To facilitate graphene for electrochemical and electronic applications, we need to remove the catalytic metal substrates from graphene and transfer graphene onto arbitrary substrates. To do so, graphene needs to be coated by a thin layer of a polymeric support, e.g. polymethyl methacrylate (PMMA) and subsequently baked to evaporate the solvent. The metal layer should be then removed by Ni or Cu etchant, leaving only the PMMA/ graphene film, which is strong enough to be transferred to another substrate without damaging the material. The metal etching step represents a key step in the transfer process since an incomplete etching and a poor removal of the etching solution could cause significant contamination of the graphene film with metallic species.

The next step is cleaning the film by deionized (DI) water and then transferring it onto a targeting substrate. After evaporating water vapor away, PMMA is to be removed by acetone, leaving a graphene film on top of the targeting substrate [Woo15] [Suk11].

In the present work, single-layer CVD graphene on Si/SiO_2 substrates were purchased from Graphenea Company in Spain, later processed in the clean room of the Regensburg University as follows:
After cutting the substrates to favorable sizes, a predesigned photomask (Figure 5.4 A) was used to expose patterns on the graphene film, preparing it for the subsequent oxygen plasma etching step, in order to remove graphene, leaving only some 0.04 mm^2 channel areas of graphene. These well-defined graphene areas will later serve as the working electrode in our electrochemical experiments.

Another photolithography step (pertaining photomask illustrated in Figure 5.4 B) was employed afterwards for patterning the contact lines, which connect each piece of graphene to

at least two metal leads, followed by a thermal evaporation step for creating Ti/Au (5nm/60nm) contacts.
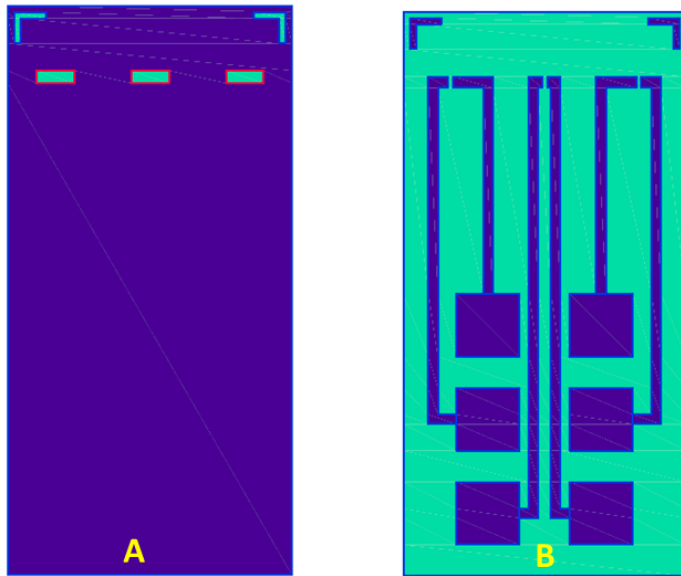
Figure 5.4. Two-step photolithography for preparation of the CVD graphene electrodes : (A) Photomask used to remove CVD graphene from the Si/SiO$_2$ substrate, leaving rectangular 0.04 mm^2 sized areas of graphene (B) Photomak used to pattern the contact line.

Although the additional transfer steps during a CVD process may lead to contaminations and destruction of graphene sheets [Amb14] [Cel13] [Kat14], preparation of wafer-scale graphene film with single-layer yield as high as 95% enables the mass production of devices with high reproducibility, which, along with the high conductivity and excellent quality of the graphene sheets, make the CVD-graphene perfect for flexible electrodes used in sensor applications.

5.2 Characterization of graphene materials through Raman spectroscopy

Raman spectroscopy has historically played an important role in the structural characterization of graphitic materials [Dre05] [Pim07] [Fer07], and has also become a powerful, noninvasive tool for understanding the behavior of electrons and phonons in graphene [Fer06] [Mal09] [Fer13]. A large amount of information such as disorder, edge and grain boundaries, thickness, doping, and strain of graphene can be learned from the Raman spectrum and its behavior under varying physical conditions.

The most prominent Raman feature in graphene is the so-called G peak at about 1580 cm^{-1} in electrically neutral single layer graphene. It stems from a single-phonon process involving an optical Γ-point phonon.

Another Raman feature in graphene is the D peak [Eck13], whose position is sensitive to the excitation wavelength and is found around 1345 cm^{-1} when an excitation wavelength of 532 nm is used [Hey14]. The D peak is only found at edges or other defect sites and is frequently

used to determine the quality of a graphene flake (D for defect or disorder). The intensity of the D-band is directly proportional to the level of defects in the sample and the nature of this defect is also crucial to a successful Raman process. It has been suggested that not every defect contributes to the D peak; a perfect zigzag edge cannot activate the D peak due to momentum conservation. That is to say, the D peak is forbidden at pure zigzag edges [Hey14].

The second overtone of the D peak at about 2700 cm^{-1}, called 2D peak was reported by Nemanich and Solin [Nem77]. It is, like the D peak, caused by a double-resonant intervalley scattering process and its position is sensitive to the excitation wavelength. In single layer graphene, the 2D peak appears as a single, sharp Lorentzian. In bi- and multilayer graphene, it changes shape and position, allowing for certain distinction of single- and bilayer graphene.

Because of added forces from the interactions between layers of AB-stacked graphene, as the number of graphene layers increases, the spectrum will change from that of single-layer graphene, namely a splitting of the 2D peak into an increasing number of modes that can combine to give a wider, shorter, higher frequency peak [Gra07]. The G peak also experiences a smaller shift from increased number of layers [Jan13]. Thus, for AB-stacked graphene, the number of layers can be derived from the ratio of peak intensities, I_{2D}/I_G, as well as the position and shape of these peaks [Jan13]. A comparison of the Raman spectra of single-layer graphene and bulk graphite (A-B stacked) can be seen in Figure 5.5. The Raman measurements were done by Dr. F. Yaghobian from the department of Physics, Regensburg University.

For a review of all Raman modes in graphene and graphite, see e.g. [Fer13] [Mal09] [Rei04].
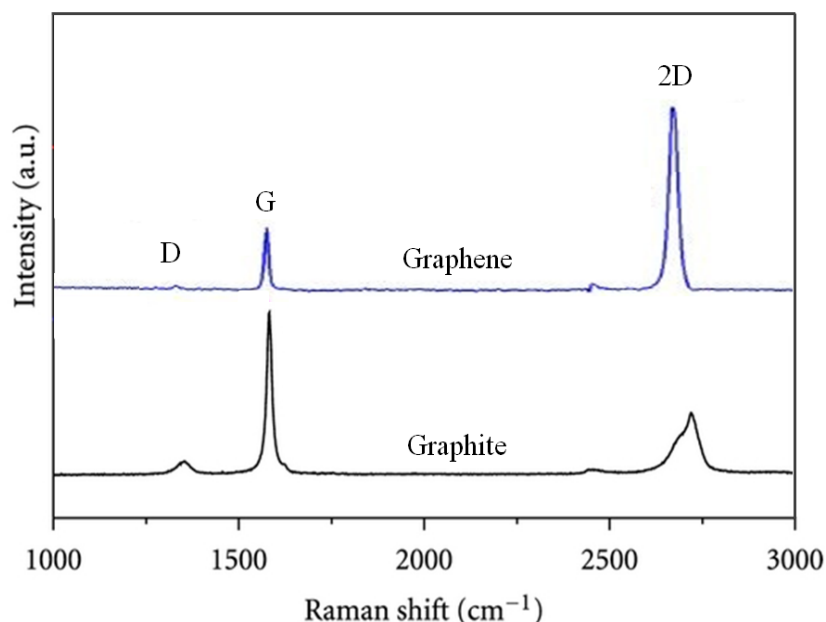
Figure 5.5. Typical Raman spectra for a single-layer graphene and bulk graphite using a 532 nm excitation laser. The spectra are offset vertically for clarity. Graphene can be identified by the position and shape of its G (1580 cm^{-1}) and 2D (2690 cm^{-1}). The image was a courtesy of Dr. F. Yaghobian from the department of Physics, Regensburg University.

After introducing the different modes in Raman spectra of graphene materials, we will focus on the characterization of the three different graphene materials we have used, discussing the changes in electronic properties and atomic structure upon varying the fabrication methods of graphene.

Unless otherwise stated, all Raman spectra shown in this work were recorded by a Thermo Fisher Scientific DXR Raman microscope, with a 532 nm laser excitation and a laser power of 10 mW at room temperature under ambient conditions. All spectra have been measured 10 times with an integration of 1 s, and a spot size of 2.1 μm in diameter.

As can be seen in Figure 5.6 the map of the integrated D line signal of the different graphene flakes reveals that no observable D peak is evident in the spectrum pertaining the mechanically SG, which proves the high structural perfection for this type of graphene. However, the appearance of a small D peak in Raman spectrum of CVD graphene (around 1342 cm^{-1}) and a distinguishable D peak in the spectrum of rGO (around 1352 cm^{-1}), indicate that the graphene sheet produced by these methods have a more disordered structure. Especially for rGO the D band becomes more dominant and broader, indicating a higher level of lattice disorder compared to CVDG.
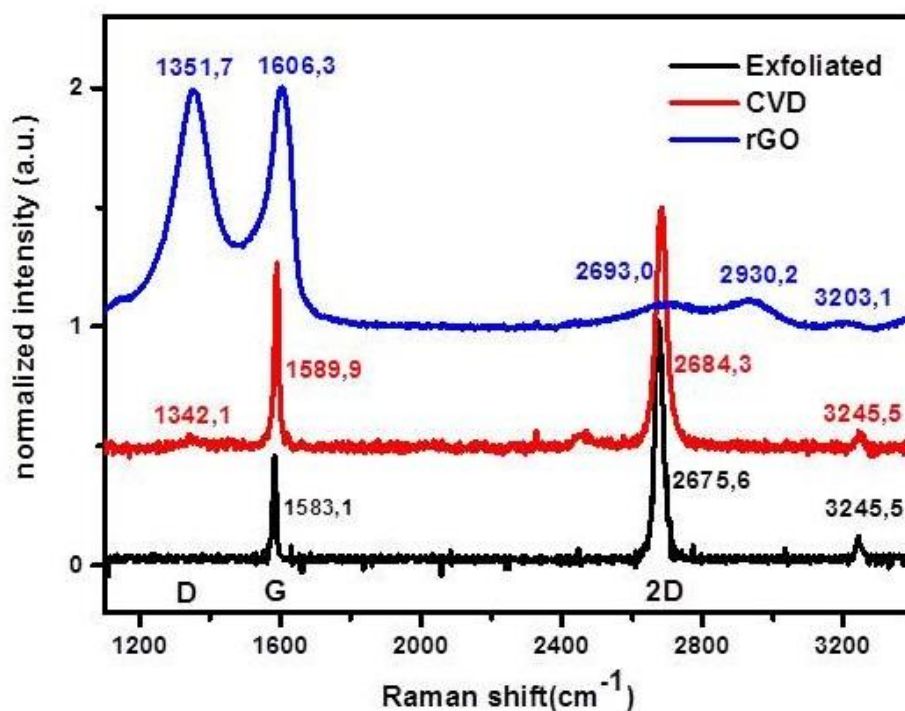
Figure 5.6. Raman spectra of graphene produced via exfoliation, CVD and reduction of GO

A symmetric single 2D peak can be found in the spectra of SG and CVDG at 2676 and 2684 cm^{-1} respectively. Furthermore, the significant higher intensity compared to the G band at 1583 and 1590 cm^{-1} indicates that these materials consist of high quality single layer graphene. In contrast, the noticeable changes in shape and intensity of the G and 2D peaks in rGO confirm the presence of multiple layers and inhomogeneities in this type of graphene compared with CVDG and SG.

5.3 Electrochemical characterization of different graphene electrode materials

All Electrochemical characterizations and measurement methods including CV, amperometry, EIS and chronocoulometry were conducted using a CH Instrument electrochemical workstation Model 602a, with a conventional three-electrode setup consisting of a Pt wire as counter electrode and a saturated calomel electrode (SCE) as reference electrode. The differently prepared graphene materials (SG, CVDG, and rGO) assembled on a silicon wafer substrate electrically contacted by gold leads were used as working electrode. In order to prevent current leakage from ionic conduction, all gold leads in contact with the electrolyte need to be insulated and shielded by dipping the electrode into a solution of 100 μM 1-mercaptooctadecane in ethanol, to form a self-assembled monolayer. The successful shielding of the gold contacts exposed to the electrolyte was proven by cyclic voltammetry (Figure 5.7), done by Dr. A. Zöpfl.
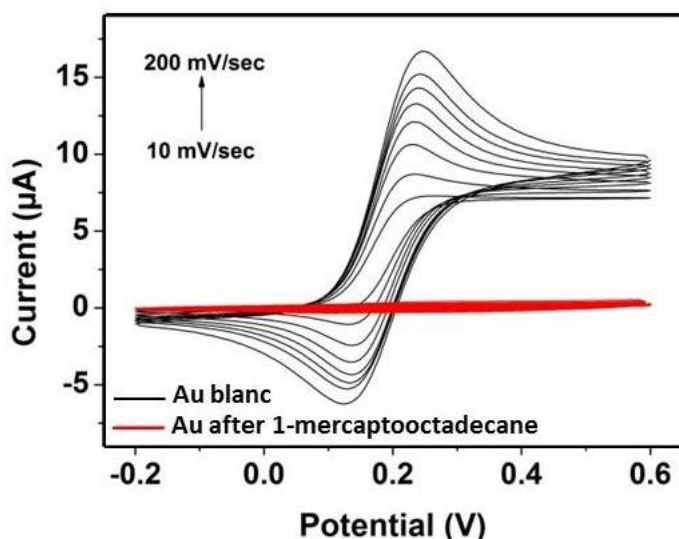
Figure 5.7. CV performed to prove the successful shielding of the gold contacts. Cyclic voltammograms of 5 mM $K_4[Fe(CN)_6]$ recorded in 0.1 M KCl at different scan rates with a bare gold electrode before and after passivation with 100 μM 1-mercaptooctadecane (Aeff/AGeo ≈ 2.1%).

In order to have a better comparison between the efficiency of graphene materials and their near counterparts, electrochemical measurement approaches were conducted, under the same defined circumstances on one of the most commonly utilized electrodes, a custom-built carbon disc electrode, comprising a carbon fiber composite (www.conrad.de, Regensburg, Germany) with 2 mm diameter encased in Teflon.

For electrochemical experiments, the supporting electrolytes were 0.1 M KCl or 10 mM phosphate buffer with 140mM NaCl (pH 7.4). Before each measurement argon was bubbled through the solutions to remove dissolved oxygen (since oxygen is electroactive and can be

reduced quite easily, it must be removed from the solution. Oxygen is typically removed by bubbling an inert gas (e.g., nitrogen or argon) through the solution for about 10 minutes).

All experiments were performed at room temperature. The amperometric response towards H_2O_2 was investigated in a magnetically stirred electrolyte solution (10 mM phosphate buffer, 140 mM NaCl, pH 7.4) by doubling the concentration of peroxide after each injection, to obtain a step-by-step increase of analyte concentration, covering a range from 25 to 25.6 mM.

5.3.1 Determination of the real electroactive area of the electrodes by chronocoulometry

Due to the different nature of the various types of graphene one cannot prepare electrodes of the same size. But size has huge influence on the sensitivity of the modified electrodes. The geometric area calculated based on microscopic images, gives only a rough estimation, therefore chronocoulometric measurements in the presence of 0.1 mM $K_3[Fe(CN)_6]$ were performed in order to estimate the total electroactive area (A_{el}) of each electrode. The charge at any time can be calculated by simply integrating the Cottrell equation as follows

$$Q = Q_{dl} + Q_{ads} + \frac{2nFAcD^{1/2}t^{1/2}}{\pi^{1/2}} \qquad (5.1)$$

where Q is the electron transfer charge, Q_{dl} the double layer charge which is eliminated by background subtraction, Q_{ads} the Faradaic charge consumed by adsorbed species, F the Faraday constant, n the number of transferred electrons, c (in mol cm^{-3}) the concentration of the redox probe, A the electroactive area (cm^2) and D the diffusion coefficient of 0.1 mM $K_3[Fe(CN)_6]$ ($7.6 \cdot 10^{-6}$ cm$^2 \cdot$s^{-1}) [Zöp16]. If Q is plotted versus $t^{1/2}$ the result is the Anson plot [Ans83] shown in Figure 5.8, where, assuming that no adsorption occurs, the slope of the line is

$$\frac{2nFAcD^{1/2}t^{1/2}}{\pi^{1/2}} \cdot \qquad (5.2)$$
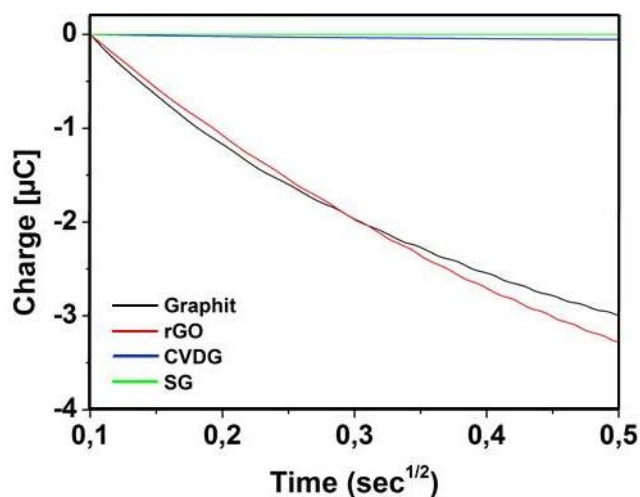
Figure 5.8. Chronocoulometric measurements for different electrodes

According to equation 5.1 and the results obtained from chronocoulometric measurements which were done by Dr. A. Zöpfl, (see Figure 5.8), A_{el} was calculated to be $2.9 \cdot 10^6$ µm^2 for graphite electrode, which constitutes 92.2% of the geometric area (A_{geo}). The calculated values of A_{el} for rGO, CVDG and SG were respectively $2.6 \cdot 10^6$ µm^2 (85.3% of A_{geo}), $3.9 \cdot 10^4$ µm^2 (88.1% of A_{geo}), and 51 µm^2 (92.8% of A_{geo}). These values will be further used for the calculation of current densities.

5.3.2 Electrochemical impedance spectroscopy of different modified electrodes

As mentioned before (see sec. 4.5), EIS is a technique commonly utilized for providing information on the interfacial properties of the electrodes.

Figure 5.9 illustrates the Nyquist and Bode plots of the three types of graphene electrodes and the carbon disc electrode in presence of 5 mM K$_4$[Fe(CN)$_6$], containing 0.1 M KCl at 0.2 V vs SCE. The experiment was done by Dr. A. Zöpfl from the department of analytical chemistry, Regensburg University. Electrodes modified with SG, CVDG and rGO cannot be fully described by a Randles equivalent circuit (See sec. 4.4, consisting of the electrolyte resistance R_s in series with a parallel combination of double-layer capacitance (C_{dl}), an impedance representing the charge transfer resistance (R_{ct}) and the Warburg element (Z_w) taking diffusion into account.
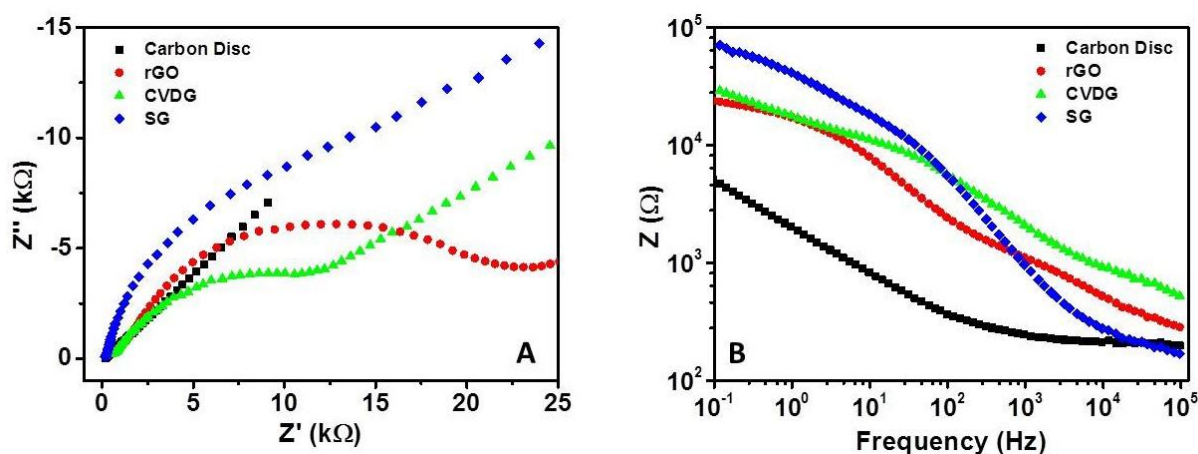
Figure 5.9. EIS spectroscopy for graphite, rGO, CVDG and SG : (A) Nyquist plot and (B) Bode plot, recorded in 0.1 M KCl and 5 mM K$_4$[Fe(CN)$_6$] for (at 0.2 V vs SCE with an amplitude of 5 mV).

For high frequencies the impedance (Z) for all materials is approaching the electrolyte resistance. For small frequencies the charge transfer resistance increases for the different electrodes in the order of carbon disc, rGO, CVDG to SG. The behavior of the CVDG can be explained by impurities adsorbed on the graphene. These impurities may be introduced during the transfer process, which causes the polymer residues to remain on the surface. The Nyquist

plot in Figure 5.9 suggests that additional impedance for adsorbates need to be applied to the equivalent circuit. For the rGO system, which consists of multilayers and comprises many defects, it is expected that the impedance spectrum is not in accordance to the simple model described by the Randles equivalent circuit. The SG as well as the carbon disc electrode show a diffusion process for the redox species at low frequencies.

The higher double-layer capacitance of SG in contrast to the carbon disc electrode as can be seen from the imaginary part in the Nyquist plot ($Z^{"}$) can be attributed to the hydrophobic character of the aromatic system which is repelling the redox species. After normalization of the total impedance (Z) to the electroactive surface area, the charge transfer resistance (R_{ct}) of carbon disc electrode is approximately $1.2 \cdot 10^6$ times higher than that of the SG, for CVDG R_{ct} per area is $1.7 \cdot 10^3$ times and for rGO $1.3 \cdot 10^5$ times higher. This shows that all graphene types enhance the electron transfer of the ferro/ferricyanide redox system compared to a plain carbon disc electrode. The variation of the R_{ct} between the three different types of graphene materials is in accordance to the increase of the number of defects of the two-dimensional carbon nanomaterial.

5.3.3 Study of reaction kinetics of electrodes through cyclic voltammetry and amperometry

The reduction of H_2O_2 on the various graphene electrodes was studied by CV (Figure 5.10) in the absence and presence of H_2O_2 in a freshly prepared phosphate buffered saline (PBS) at pH 7.4. Comparison of the recorded cyclic voltammograms before and after introduction of 10 mM H_2O_2 demonstrates that once 10mM H_2O_2 was added into the PBS, the cathodic current increased, compared to the time there was no H_2O_2 in the solution, confirming the efficient catalytic effect of the graphene films towards the electrochemical reduction of H_2O_2. The comparatively weaker cyclic response of the graphite electrode, however, does not seem to be as noticeable as that of the graphene materials.

Moreover, the current increase for electrodes modified with CVDG and SG is already more observable at low potentials of -0.1 V vs SCE. This is a lower potential compared to the case for rGO and carbon disc electrode, which can be attributed to an electrocatalytic effect of the carbon nanomaterials.
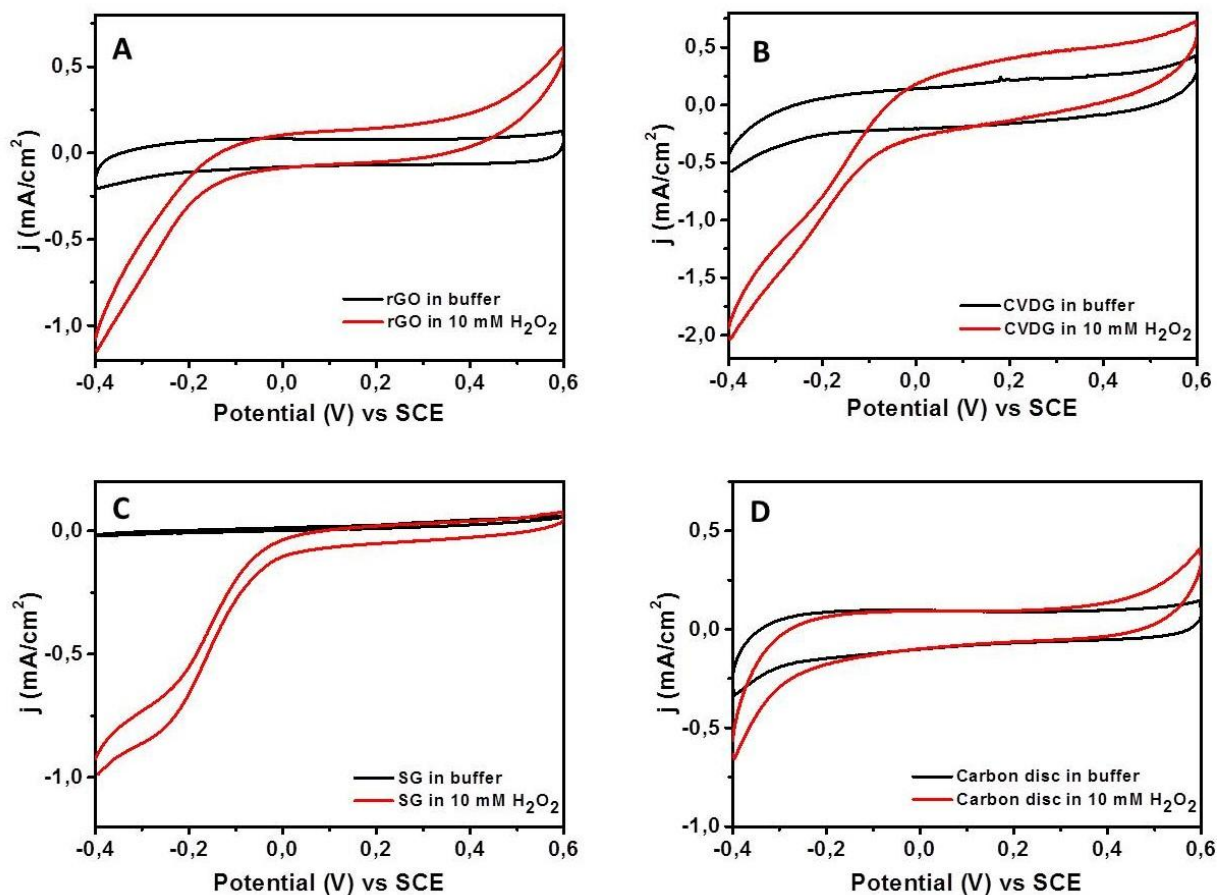
Figure 5.10. Steady state current density/voltage cycles for different electrodes : (A) rGO, (B) CVDG, (C) SG, and (D) graphite electrodes in phosphate buffered saline pH 7.4 before and after addition of 10 mM H_2O_2 vs SCE (scan rate 0.1 Vs^{-1}).

Figure 5.11 also confirms that the change in the current density under exactly the same conditions is significantly higher for the graphene materials than for the carbon disc electrode. At a working potential of -0.3 V vs SCE the current flow is enhanced about 4 times for rGO, 5 times for SG and 8 times for CVDG. Especially CVDG electrodes provide maximum response, perhaps due to the best ratio of pristine graphene lattice to defects and edges.
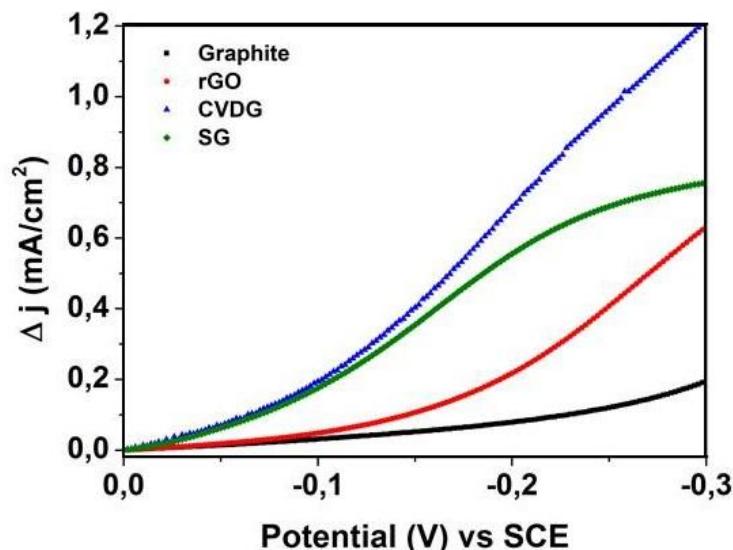
Figure 5.11. Change in current density for H_2O_2 reduction during the cyclic voltammetry in phosphate buffered saline pH7.4 with 10 mM H_2O_2 vs SCE (scan rate 0.1 Vs^{-1}).

In order to get high selectivity in real sample analysis it is desired to determine the analytes at potentials close to 0 V. We found that at very low potentials graphene with low number of defects, here CVDG and SG, show nearly the same enhancement in the signal whereas rGO as very defective material shows a behavior more like the carbon disc electrode (Figure 5.11). For more negative electrochemical potentials all four types of carbon materials give an individual signal enhancement. From this result one can conclude that for working potentials lower than -0.1 V vs SCE it is mandatory to use high quality graphene with low number of defects in order to get any benefit in using a two dimensional carbon nanomaterial as electrode in amperometric detection of H_2O_2.

All three types of graphene-modified electrodes have been tested in an amperometric setup to detect peroxide (Figure 5.12). A constant potential of -0.3 V vs SCE was applied in order to get the maximum sensitivity. Every 100 seconds, certain aliquots of H_2O_2 were successively added into the supporting solution.

Figure 5.12 (B) and (C) present dynamic amperometric responses of the three graphene types as well as graphite, to growing concentration of H_2O_2. It can be observed that the steady-state reductive current response of all sensor devices increase obviously with the increase of H_2O_2 concentration. The reduction current signals start from the very initial injections of H_2O_2 at rGO, graphite and CVD grown graphene, and increase after each addition of H_2O_2. For low concentrations of the analyte one can see that low-defect graphene (SG) does not exhibit notable changes in the current. One reason is that the size of these flakes is very small and therefore the total signal is very small. However, after normalization of all signals to the total electroactive surface area, the situation changed and the resulted graphs (Figure 5.12 C) reveal contradiction to our previous findings.
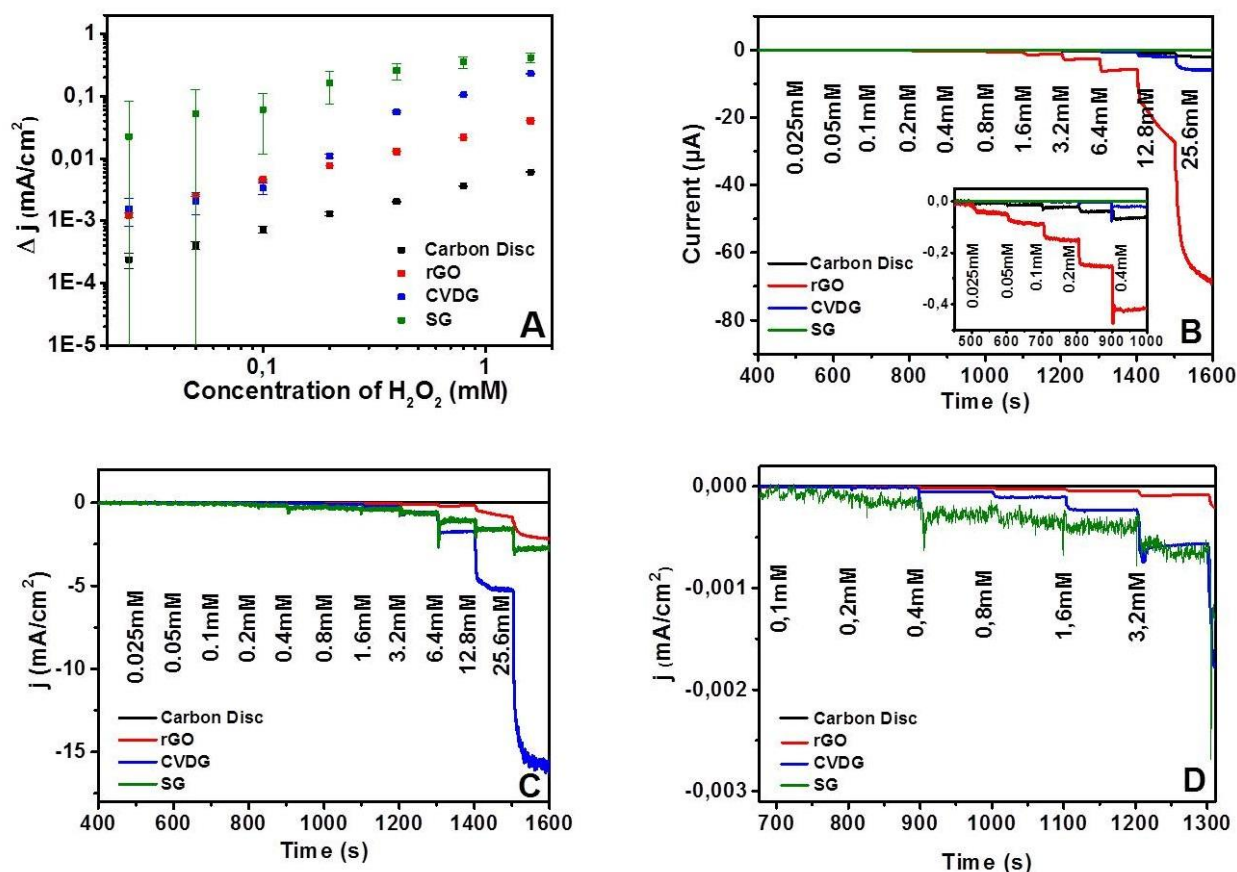
Figure 5.12. Electrochemical behavior of different electrodes toward growing concentration of H_2O_2 (A) Concentration dependency of the amperometric response at -0.3 V vs SCE upon successive addition of 0.025-25.6 mM H_2O_2 into continuously stirred phosphate buffered saline pH 7.4. (B) Amperometric response at -0.3 V (vs SCE) and upon successive step injection of 0.025- 25.6 mM H_2O_2 into continuously stirred phosphate buffered saline pH7.4. Inset: response to the first five additions. (C) Normalized amperometric response referring to the electrodes size. (D) The magnified view of the current density/ [H_2O_2] plot for the first five analyte injections.

Opposed to the displayed amperometric plots in Figure 5.12 (B), the primary current responses of the exfoliated and CVD-grown graphene toward the initial additions of H_2O_2 are more distinct compared to those of rGO and graphite. Furthermore, it can be deduced from Figure 5.12 (D) that all the three graphene materials are able to detect very low concentrations of H_2O_2 down to amounts smaller than 0.1 mM, whereas graphite doesn't show such a low detection limit.

To further illustrate the relationship between the electrocatalytic reduction current and the concentration of H_2O_2, the calibration curves between the amperometric current density of the fabricated graphene materials, as well as the graphite, were plotted versus the concentration of H_2O_2 (Figure 5.13). The linear electrocatalytic response towards the H_2O_2 concentration could be witnessed for the graphene materials in a wider range (between 0.4 mM and 4 mM), compared to that of graphite, indicating the superiority of the graphene materials over graphite for fabricating more reliable devices.
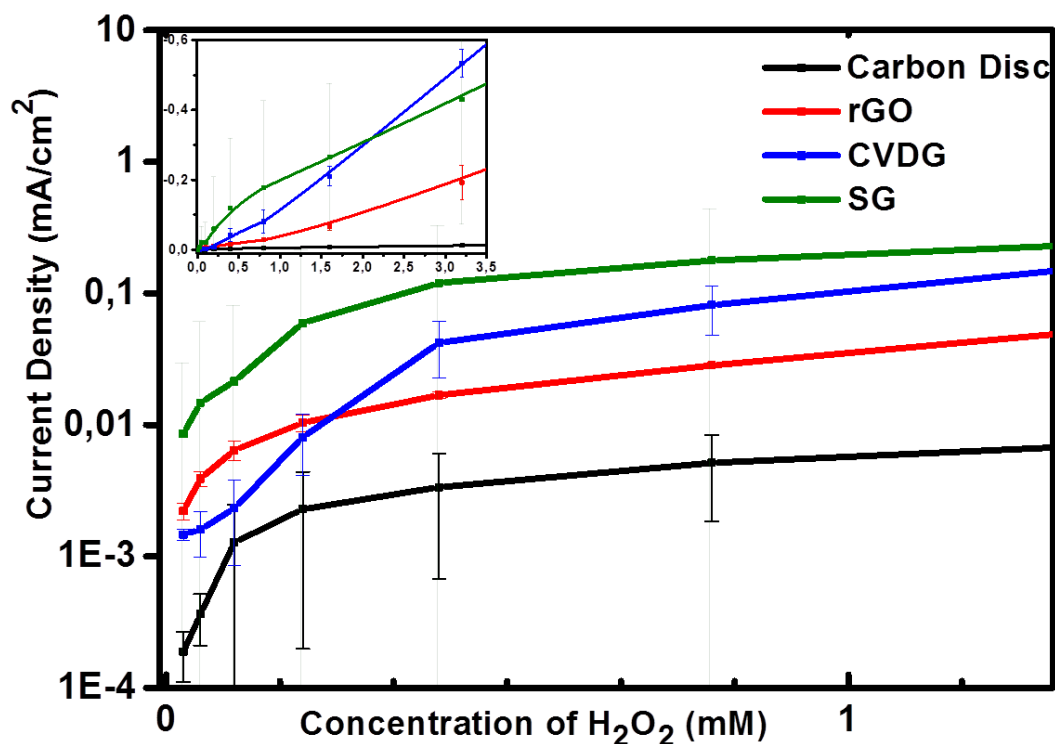
Figure 5.13. The magnified view of the current density/ [H_2O_2] for the first five analyte injections. Inset: The whole view of calibration curves between current density and the concentration of H_2O_2 has been shown

According to Figure 5.13, an increase of absolute sensitivity is observed, starting from carbon disc (3.2 mA $M^{-1}cm^{-2}$) to rGO (25 mA $M^{-1}cm^{-2}$) to CVDG (173 mA $M^{-1}cm^{-2}$), and SG modified electrodes (202 mA·M^{-1}·cm^{-2}). Again, a lower number of defects lead to a higher sensitivity towards H_2O_2. Nevertheless, the noise level of SG electrodes is higher than the other electrodes which can be attributed to the low absolute current values. Noise at an amperometric electrode is closely associated with the double layer capacitance (C_{dl}) and the surface of the WE. Calculating the limit of detection from a signal to noise ratio of three, values of 9.2 µM for rGO, 15.1 µM for CVDG and 651.5 µM for SG electrodes are obtained.

These findings indicate the great perspective of graphene in amperometric detection systems. It is evident that the exfoliated and CVD-grown graphene showed higher sensitivity and better performance than the rGO and graphite.

The H_2O_2 sensing performance and characteristics of the various utilized electrode materials in this work are compared with previous reports as displayed in table 1. All these works are based on chemically derived graphene (e.g. rGO), which has been further modified with metal or metal oxide nanomaterials to improve sensitivity. It is shown that hybrid nanomaterials lead to better sensitivities. From our study one can suggest that there could be further improvement by using graphene with low number of defects. For taking benefit from the electrocatalytic effect of graphene as well as from the signal enhancement, it is mandatory to use electrodes consisting of high quality graphene, which means, to use a 2D nanomaterial with as low number of defects and impurities as possible. Up to now it has been challenging to provide such a high quality graphene on an insulating material with electric contacts in

reasonable quantities and of adequate size for developing sensor applications operated with a low cost potentiostat.

Electrode material	Potential (V)	sensitivity(mA $M^{-1}cm^{-2}$)	LOD (μM)	Reference
PB/graphene	-0.05 (vs Pt)	196.6	1.9	[Jin10]
CoOxNPs/ERGO	0.75 (vs SCE)	148.6	0.2	[Li14a]
Nafion/GO/Co$_3$O$_4$	0.76 (vs Ag/AgCl)	560	0.3	[Ens13]
MnO$_2$NTs/rGO	0.4 (vs SCE)	194.5	4.29	[Mah14]
Polydopamine-rGO/Ag	-0.5 (vs Ag/AgCl)	355.8	2.1	[Fu15]
rGO-PMS/AuNPs	-0.7 (vs Ag/AgCl)	39.2	0.06	[Maj14]
rGO	-0.3 (vs SCE)	25	9.2	This work
CVDG	-0.3 (vs SCE)	173	15.1	This work
SG	−0.3 (vs SCE)	202	651.5	This work

Table 1. Comparison of analytical performance of various graphene and graphene composite materials used for the electrochemical detection of H$_2$O$_2$ (PB: Prussian Blue, CoOxNPs: Cobalt oxide nanoparticles, ERGO: Electrochemically reduced graphene oxide, AgNPs: Silver nanoparticles, PQ11: Poly [(2-ethyldimethylammonioethyl methacrylate ethyl sulfate)-co-(1- vinylpyrrolidone)], PMS Periodic mesopourous silica, AuNPs Gold nanoparticles, Ag/AgCl Saturated silver/ silver chloride reference electrode)

By taking a look at the relative signal changes obtained with the different types of electrodes used in this study, one can see that SG performs best, but accompanied by huge error bars ascribed to the decline in signals and increase of the noise. This could be overcome by using bigger graphene flakes or by better potentiostats. Good signal enhancement can also be obtained with CVDG. Nevertheless the fabrication of one of such electrodes is a time consuming complex process. This material is already commercially available. But the drawback in using this material for an application is that there is a lack of a technique for a clean and easy transfer of this material onto microelectrodes providing a good electrical contact. This material offers the possibility to be functionalized chemically [Kui12] or by plasma treatment [Hey10]. It is expected that with this technique selectivity can be introduced and functionalized graphene for amperometric detection systems will be designed. The rGO does not result in such great improvement in contrast to the carbon disc electrode, but here processing of the material as well as functionalization is easy. Therefore it offers a pathway to interesting composite materials for electrochemical sensors.

5.4 Conclusion/Summary

In summary, we have studied non-enzymatic detection of hydrogen peroxide using electrodes based on various types of graphene, without utilizing any functionalization or modification steps.

Low-defect graphene (SG) was obtained through mechanical exfoliation of natural graphite, while higher-defect graphenes were produced by CVD and by chemical oxidation of graphite and subsequent reduction. The carbonaceous materials were mainly characterized by Raman microscopy and their electrochemical properties and sensing applications were studied by chronocoulometry, CV, EIS and amperometry, and compared with a carbon disc electrode.

The effects of the device fabrication on the reductive amperometric determination of H_2O_2 were investigated. It is shown that the quality of the graphene has an enormous impact on its amperometric performance and the use of carbon materials with many defects (like rGO) does not result in a significant improvement in signal compared to a plain carbon disc electrode.

Further results reveal that all three graphene materials exhibit sensitivity to the catalytic reduction of H_2O_2 and are able to detect H_2O_2 to concentrations below 0.1 mM, showing fast amperometric response upon successive additions of H_2O_2. In comparison with carbon disc electrode, the application of graphene nanomaterials offers large perspectives in amperometric detection systems due to electrocatalytic effects that result in highly sensitive detection.

Moreover, it is clearly demonstrated that mechanically exfoliated graphene as well as graphene prepared by CVD are promising candidates for sensor applications, due to their efficiency in better detection of H_2O_2 with higher sensitivity compared to rGO. The sensitivities in case of using CVDG and SG are 173 and 202 mA $M^{-1}cm^{-2}$ respectively, which are about 7 to 8 times better than that of rGO. The calculations of LOD for H_2O_2 also prove the absolute advantage of SG and CVDG upon rGO according to table 1.

However, due to the laborious process needed for production of exfoliated graphene and its irregularity in shape, size and location, this type of graphene, being described as an 'academic' material, is more suitable for proof-of-concept demonstration.

In summary, the results support CVDG as the material of choice for commercial purposes and mass production, since it offers uniform continuous films at particular locations and with desired geometries, providing a superior candidate for fabrication of highly sensitive electrochemical- and biosensors, particularly by further functionalization and modification with enzymes or nanoparticles.

6. Graphene for Non-Enzymatic Glucose Detection

After the potential of graphene for fabricating highly sensitive sensors has been stressed already on plenty occasions during the previous parts of this work, chapter 6 provides a detailed description of the processes that led to the fabrication of a graphene-based electrochemical sensor for sensitive detection of glucose.

Based on the results obtained in chapter 5, CVDG presents superior advantages compared to other graphene materials and suits mass production of sensors, while offering high sensitivity at the same time. In order to modify CVDG to fabricate a sensor for glucose determination, a variety of approaches have been explored throughout this project, which may be divided into two main categories: efforts for immobilization of GOD on graphene surface and thereby fabricating an enzymatic biosensor for glucose detection, and attempts for fabrication of an enzymeless sensor based on modification of graphene surface mainly with metal oxide nanoparticles.

It is well established that edges and defects on graphene provide a high electron transfer rate [Amb10], so before we do any modifications on graphene, we introduce circular holes on its surface by plasma etching to provide the modifying groups artificial dangling positions for attachment to the graphene surface. To our knowledge, so far no experimental investigation of these artificial plasma-etched holes, which we call antidots, has been conducted. We will later investigate how graphene's electrochemical properties and amperometric response of the sensor to the glucose may be affected by the size and lattice distance of the antidots.

6.1 Modification of graphene surface with antidots

In order to increase the number of anchoring groups on the graphene surface for receptor immobilization, we created artificial defects in the form of periodic arrays of circular holes, so-called circular antidots, with a hole diameter of 70 nm. The arrays with periods of 500 and 600 nm were defined using electron beam lithography (EBL) and oxygen reactive ion etching as sketched in Figure 6.1.
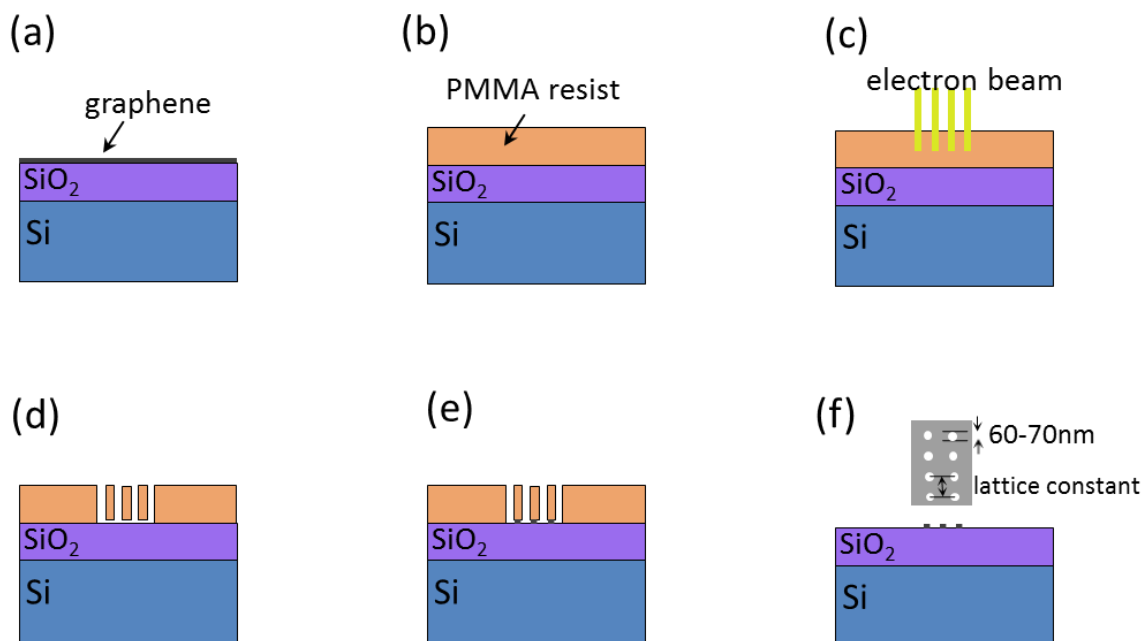
Figure 6.1. Schematics of EBL and RIE processes for creation of antidot lattices on graphene (a) CVDG-covered Si/SiO2 chip was cut into desired size. (b) Polymethylmethacrylate (PMMA) resist is deposited on the chip. (c) Electron beam is exposed to define square lattice arrays of circular dots. (d) Through a developing process, the resist is removed from the antidot lattices which were created by E-beam exposure. (e) Using RIE with O_2 plasma graphene is etched in the resist-free regions. (f) The final washing process removes the PMMA resist from the substrate and the antidot lattices are formed on the graphene surface.

In practice, Polymethylmethacrylate (PMMA) resist was first sputtered on the Si/SiO$_2$ substrate covered with CVDG. After baking the substrate on a hotplate of 150°C temperature for five minutes, the graphene sample was placed in a Scanning electron microscope (SEM), and a 200*100μm^2 area was continuously scanned by the electron beam in order to write array patterns of circular holes. The beam's kinetic energy was 30 keV, and the beam current was 370 pA. Afterwards the patterned dots were developed by Methyl isobutyl ketone (MIBK)/propanol for 90 seconds. The antidots were then etched by RIE with oxygen as reactive gas, for 15 seconds, leaving circular dots on the surface of graphene. In the last step, the samples were washed with acetone and propanol to remove the PMMA resist, followed by a 30-minute annealing process in order to completely clean the residual adsorbates caused by PMMA coating on the sample surface.

Visualizing the antidot lattices was accomplished using SEM as illustrated in Figure 6.2.
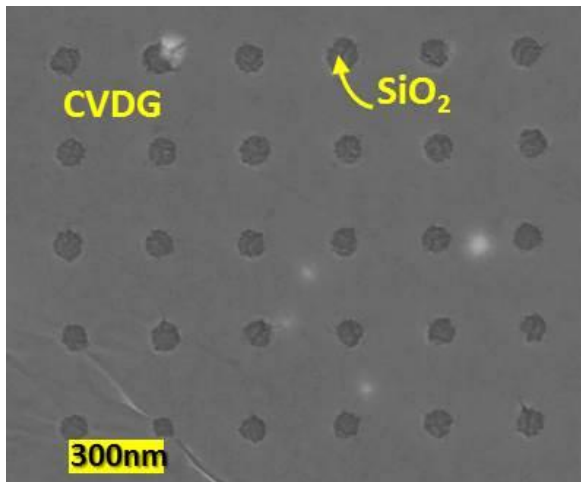
Figure 6.2. SEM image of the CVDG on Si/SiO$_2$ substrate structured with circular antidot lattices through EBL and RIE with O$_2$ plasma

Raman spectroscopy was also performed to characterize the prepared antidot lattices and locally investigate the structural quality of the nanopatterned graphene. As seen in Figure 6.3 the influence of circular antidots on the Raman spectra of single layer graphene is reflected in an increased D peak, which is interpreted to be dominantly caused by the introduction of additional edges into the sample due to the creation of the holes and not by additional defects or disorder, which might be caused by the preparation process [Hey10]. It can also be observed that in samples with smaller lattice constant (LC), i.e. more number of defects, the D' and D+D' peaks appear around 1620 and 2935 cm^{-1}, respectively. Furthermore, Figure 6.3 reveals that the continuous decrease of LC leads to the increase of D peak.
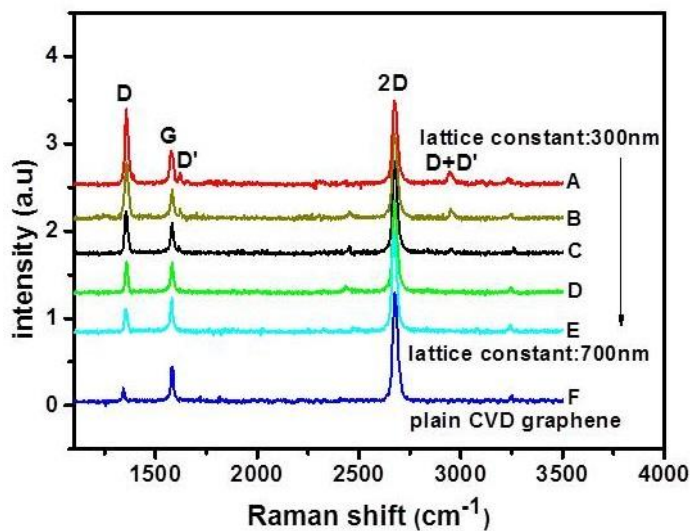
Figure 6.3. Raman spectra recorded on CVDG modified by antidots of 70nm diameter with different lattice constants of: (A) 300nm, (B) 400nm, (C) 500nm, (D) 600nm, (D) 700nm and (F) CVDG without antidots. The main Raman peaks are labeled. Increase of the lattice constant causes the defect-induced modes to decrease.

Nanoperforated graphene samples have been reported to have p-type doping [Kim12], despite special care to avoid contamination of the samples. Kim et al. employed a sacrificial polymer

buffer layer to protect the graphene during etching, but still found p-type doping, which they attributed to dangling oxygen bonds on the edges of the antidots. These functional groups can provide many active sites on the graphene surface, thereby turning out to be beneficial for accelerating electron transfer between the electrode and species in solution. To endow graphene with sensing capabilities, it is often necessary to modify it with recognition elements that bring the detection targets onto the graphene surface through specific interactions and sometimes also assist in signal transduction. Throughout this project, various strategies have been tried to functionalize graphene both covalently and non-covalently, which will be described in more detail in the appendix. In pursuit of fabricating a highly sensitive graphene-based glucose sensor, both enzymatic and nonenzymatic methods have been investigated; however, the enzymatic approach didn't satisfy the needs for fabrication of a sensitive and stable glucose biosensor with low detection limit (see the appendix), which urged us to develop nonenzymatic detection platforms for glucose determination.

6.2 Enzymeless detection of glucose via NiO electrodeposition

Enzymatic glucose sensors dominate the biosensing industry. This is understandable given the high selectivity of the enzyme towards glucose. However, due to the intrinsic instability of enzymes and loss of enzyme activity during the immobilization process, such enzyme-based sensors usually suffer from the low reproducibility and stability.

Despite numerous attributes with respect to relative stability, GOx is still constrained to pH ranges of 2-8, temperatures below 44ºC [Tog10], and ambient humidity levels [Li07]. Ensuring the stability of immobilized enzyme and mediator electrodes requires considerable attention, with elaborate fabrication processes of electropolymerisation [Li07], covalent cross-linking at a pretreated surface [Nen10], sol-gel entrapment at the electrode surface [Han05], or even the electrochemical 'wiring' of enzymes to mediated polymer chains [Hel10], ensuring greater fabrication costs, lower reproducibility and short-term stability.

Considering the mentioned disadvantages, we investigated the development of electrochemical non-enzymatic glucose biosensors.

6.2.1 Electrodeposition of nickel oxide nanoparticles on graphene

Combining graphene with different nanomaterials including noble metals [Gut12] [Pal15] [Shi15], metal oxides [Don12] [Joh14] and metal sulfides [Bai13] [Kum15b] has been considered as a versatile technique for sensor application.

Compared to the other materials, NiO benefits from some excellent properties such as large specific capacitance, good electrochemical stability and low cost, making it suitable for the fabrication of sensors in batch.

To deposit NiO nanoparticles on graphene surface, electrochemical approach was employed [Qia12]. In the first place, nickel hydroxide is formed on the electrode through electrodeposition from a nickel salt containing solution:

$$NiCl_2(aq) + 2NaOH(aq) \rightarrow Ni(OH)_2(s) + 2NaCl(aq) \tag{6.1}$$
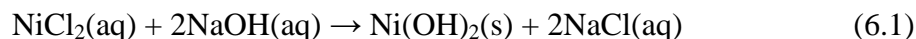
Nickel hydroxide is subsequently involved in the electrochemical redox reaction of equation (6.2) where the transition from $Ni(OH)_2$ to NiOOH after intercalation and deintercalation of OH^- ions causes charge transfer from Ni^{2+} to Ni^{3+}:

$$Ni^{2+}(OH)_2 + OH^- \rightleftarrows Ni^{3+}OOH + H_2O + e^- \tag{6.2}$$
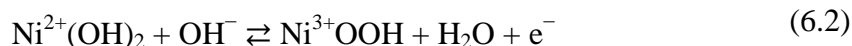
$Ni(OH)_2$/NiOOH redox system possesses excellent reversibility and the electrocatalytic oxidation mechanisms of Ni and its oxides toward small molecules in alkaline electrolyte are related to the Ni $(OH)_2$/NiOOH redox transition [Mia14].When glucose is added, a catalytic reaction is performed for the oxidation of glucose to glucolactone by the high valent NiOOH:

$$NiOOH + glucose \rightarrow Ni(OH)_2 + glucolactone \tag{6.1}$$
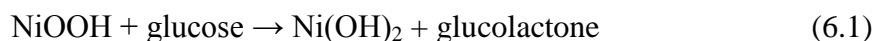
In experiment, the electrodeposition of metallic nickel was carried out in an aqueous solution containing 10 mM nickel chloride at a constant potential of 0.9 V for 10 seconds. Afterwards, the oxidization of metallic nickel was processed in 0.1M NaOH solution, performing CV (60 cycles) in the potential range of 0.2V to 0.6V at a scan rate of 100 mV.s^{-1}.

The prepared $Ni(OH)_2$-graphene modified electrode can be then used for the detection of glucose without further treatment.

6.3 Effect of the antidot lattice on the NiO deposition and glucose detection

Fabricating two different types of electrodes, one with perforated graphene (70nm hole diameter, 600nm lattice constant) and the other one with plain CVD graphene, the influence of the antidot lattices on the electrochemical deposition and on the electrocatalytic oxidation of glucose was investigated.

The morphology of NiO nanoparticles on perforated and nonperforated graphene was examined by the SEM, as illustrated in Figure 6.4. The comparison of Figure 6.4 (A) and (B) reveals that the deposition of NiO nanoparticles is site selective and occurs preferably on defective sites of the surface. The NiO nanoparticles have a more homogeneous grain size (of averagely 60 nm) on the sample modified with perforated graphene, compared to the one without perforation.
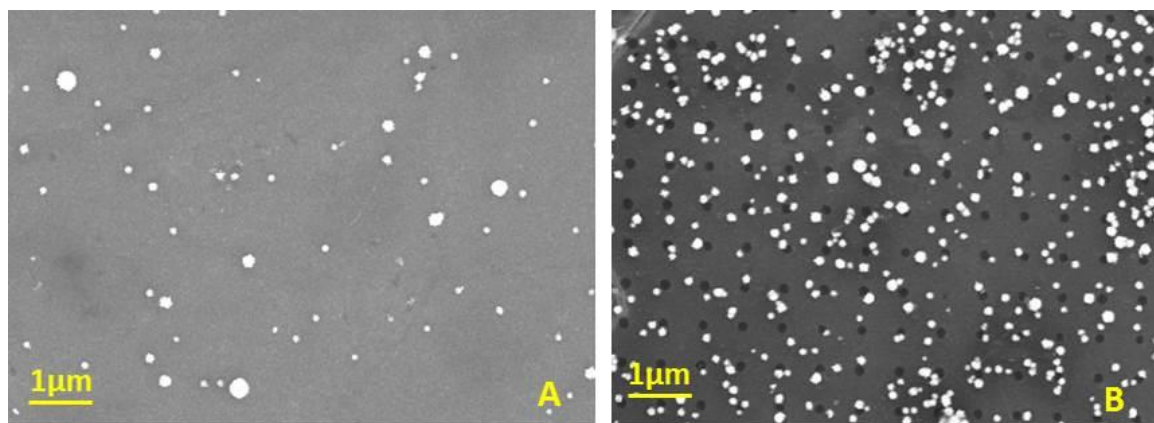
Figure 6.4. SEM image of electrodeposited NiO nanoparticles on graphene (A) without antidots, and (B) modified with antidot lattices. The deposition of NiO nanoparticles on the sample with antidots occurs site selective and at a higher density compared to the plain graphene.

Amperometric measurements were performed to investigate the impact of antidots on the electrocatalytic oxidation of glucose. Figure 6.5 (A) compares the current density (j) of the NiO modified perforated graphene with those of the NiO deposited plain graphene toward successive injection of 0.025-102.4 mM glucose concentration in 0.1M NaOH at the potential of 0.45V. The total electroactive area of each electrode was calculated by subtracting the total area of the antidots from the initial area of the graphene.

Compared to the plain graphene, the antidot-modified graphene exhibited a more rapid, more stable and more enhanced response toward glucose.
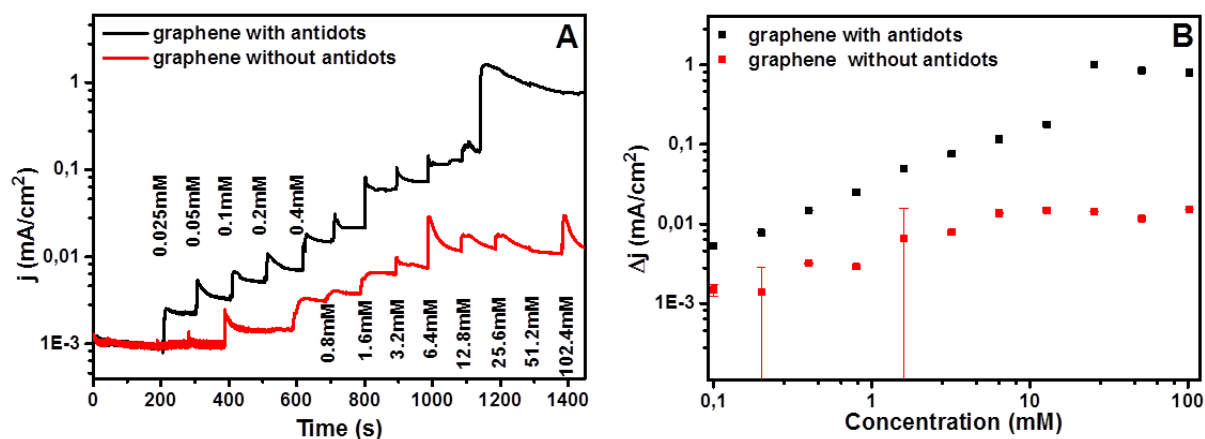
Figure 6.5. Electrochemical behavior of NiO/graphene electrodes toward glucose. (A) The amperometric response of the sensor electrode based on NiO/ antidot-modified-graphene vs graphene without antidots toward sequential increase of glucose concentration from 0.025 mM to 102.4 mM in gently stirred 0.1M NaOH solution at 0.45 V. (B) Calibration plots obtained for NiO/perforated graphene (black) and NiO/pure graphene electrode (red).

Also observed in Figure 6.5 (B), the sensor based on graphene with antidots displays a linear current response toward glucose in a wider range (0.1-12.8mM) with correlation coefficient of 0.899 and a higher sensitivity (54.47μA mM^{-1} mm^{-2}), while graphene without antidots shows linearity over a lower concentration range of 0.2-6.4mM with a slope of 8.48 μA mM^{-1} mm^{-2}

and correlation coefficient of 0.88. Thus, it can be concluded that the imposed array of antidots greatly enhances the catalytic current.

This is believed to be a result of the artificial attachment cites provided by the ordered nanopatterns that offered a condition for more deposition of nanoparticles on the dangling sites and thereby, enhancing the chemical reactivity of graphene.

6.4 Impact of antidots' size and lattice constant on the electrocatalytic oxidation of glucose

We prepared square antidot lattices with five different lattice constants of 300, 400, 500, 600 and 700 nm and four types of hole diameter: 50, 70, 150 and 200 nm in order to investigate the influence of array properties on electrochemical deposition of NiO nanoparticles on graphene and further electrochemical behavior of the sensor. Electrodeposition of NiO nanoparticles was carried out according to the approach mentioned in the previous section and the obtained materials were then characterized by SEM. As illustrated in Figure 6.6 and Figure 6.8 (A), the density of the nanoparticles can be manipulated by changing the lattice constants. A comparison of the images A-D shows that the density of NiO nanoparticles on the antidot-modified graphene increased with the increase of the lattice distance to 500nm. With the lattice constant further extended to 700 nm, a decrease in the amount of the deposited nanoparticles is again observed. When the lattice constant was 500 nm, the NiO nanoparticles deposited on the graphene film had the highest density. The average number of NiO nanoparticles on this sample showed an approximate 2.5-fold increase compared to the samples with 600 and 400 nm lattice constants. The results were obtained from ImageJ software, counting the number of nanoparticles for the same area for all the samples (see Figure 6.8). In comparison to samples with 700 nm and 300 nm lattice constants, the density of the NiO nanoparticles on sample with 500 nm lattice constant appeared to be respectively 5 and 10 times higher. We attribute the observed enhanced density of nanoparticles to the number of the antidots, whose edges provide safe positions for the NiO nanoparticles to get deposited on the substrate (as obvious from the image 6.6). Smaller lattice constant means more antidots and anchoring positions for the nanoparticles; however, as the lattice constant decreases to 400 and 300 nm, the graphene structure gets more and more distorted and defected by the many antidots that are imposed. This leads to deterioration of the physical and chemical properties of graphene and a decrease in the number of electrodeposited NiO nanoparticles on the substrate.

Moreover, the density of the deposited nanoparticles can be modulated by simply changing the diameter of the antidots. As depicted in Figure 6.7 and Figure 6.8 (B), the antidots with diameter of 70 nm provided the best substrate for the most density of nanoparticles in comparison to other diameters. Based on the results demonstrated in Figure 6.8 (B), the density of NiO nanoparticles on the sample with antidots of 70 nm diameter is 1.4 times, 3.5 times and 5 times more than the samples with antidots of 50 nm, 150 nm and 200 nm, respectively. By incresing the diameter of the antidots from 50 nm to 70 nm, the circumference of the imposed circular holes increase and more NiO nanoparticles find the oportunity to get deposited on the antidots edges. By further increasing the diameter however,

larger areas of graphene are etched and distorted, leading to decline in the density of deposited NiO nanoparticles on the substrate.

The influence of the size and lattice distance of the patterned antidot arrays on the density of the NiO NPs deposited on graphene has been further investigated by counting the number of nanoparticles per area, using the ImageJ software. Figure 6.8 displays the averaged density of NPs per area for different diameters (at the fixed lattice constant of 500nm) and for different lattice constants (where the antidots had a fixed diameter of 70 nm). The results obtained from the particle counting by ImageJ confirms the observations yielded from the SEM images (Figure 6.6 and Figure 6.7).
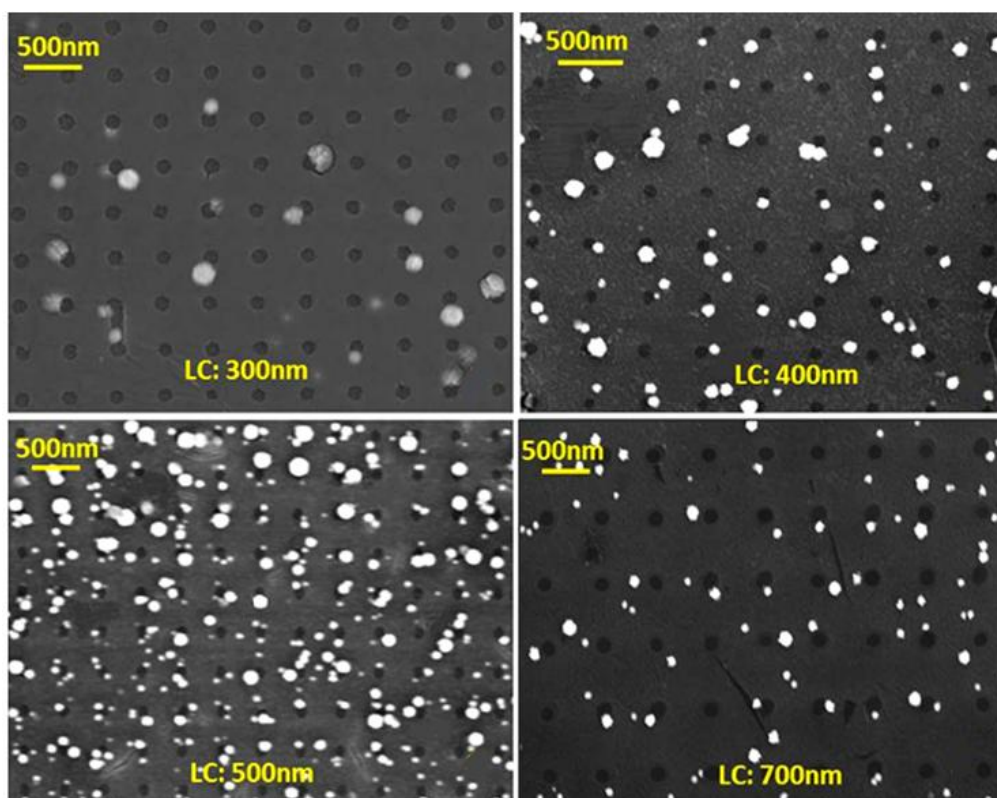
Figure 6.6. SEM images of the electrodeposited NiO nanoparticles on graphene modified with antidots of the same hole diameter (70nm) and different lattice constants : 300nm (A), 400 nm (B), 500 nm (C), and 700 nm (D). When the LC is 500 nm, the NiO nanoparticles deposited on the graphene film have the highest density.
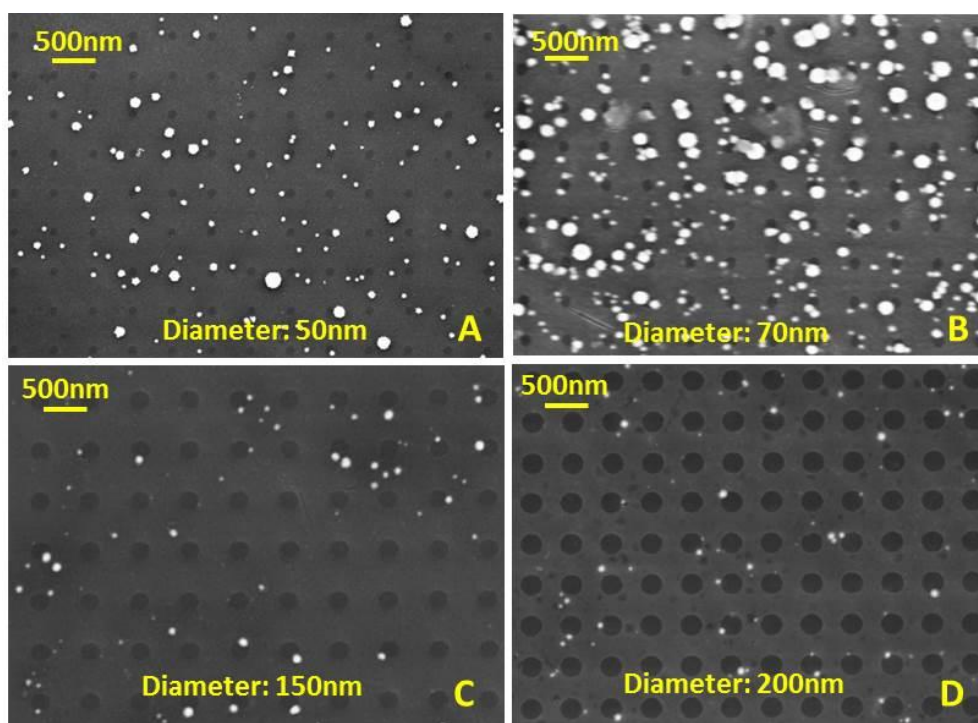
Figure 6.7. SEM images of the electrodeposited NiO nanoparticles on graphene modified with antidots of the same lattice constant (500nm) and different hole diameters **:** 50nm (A), 70 nm (B), 150 nm (C), and 200 nm (D). The density of the NiO nanoparticles deposited on the graphene film with antidots of 70 nm is the highest.
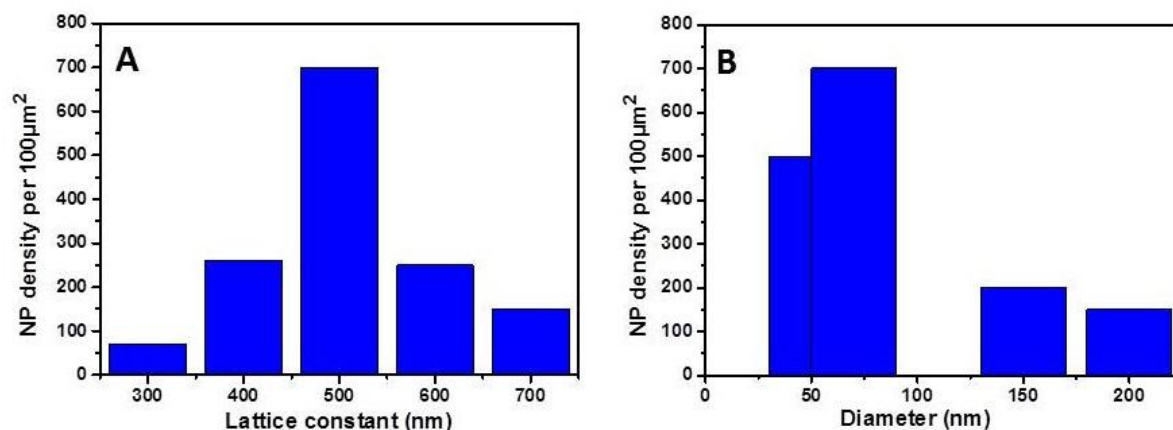
Figure 6.8. Density of electrodeposited NPs on graphene versus (A) lattice constant, and (B) diameter

6.5 Electrocatalytical performance of modified electrodes toward the oxidation of glucose

The electrochemical behavior of the array-modified electrodes with different lattice constants was studied using CV technique before and after the introduction of 102.4 mM glucose in 0.1 mM NaOH. Observed from Figure 6.9, a pair of redox peaks appears in the absence of glucose which are attributed to the oxidation of $Ni(OH)_2$ to NiOOH and successive reduction back. The redox signal increases further with the increase of potential scan cycle number from 1 to 60. It is observed that the first cycle needs higher potential for the nucleation of NiOOH. In the next cycles, the anodic and cathodic peaks shift to lower potentials and the peak currents shift to high values as the cycle numbers increase. This is due to the nucleation of

NiOOH and the following increase of activation sites (Ni^{2+} or Ni^{3+}). These Ni^{+2}/Ni^{+3} species on the electrode surface (embeded in $Ni(OH)_2$/NiOOH redox couple) act as a catalyst for the oxidation of glucose. When glucose diffuses to the electrode surface, it is rapidly oxidized to glucolactone by the Ni^{+3} species on the electrode, as indicated in Eq. 6.1.
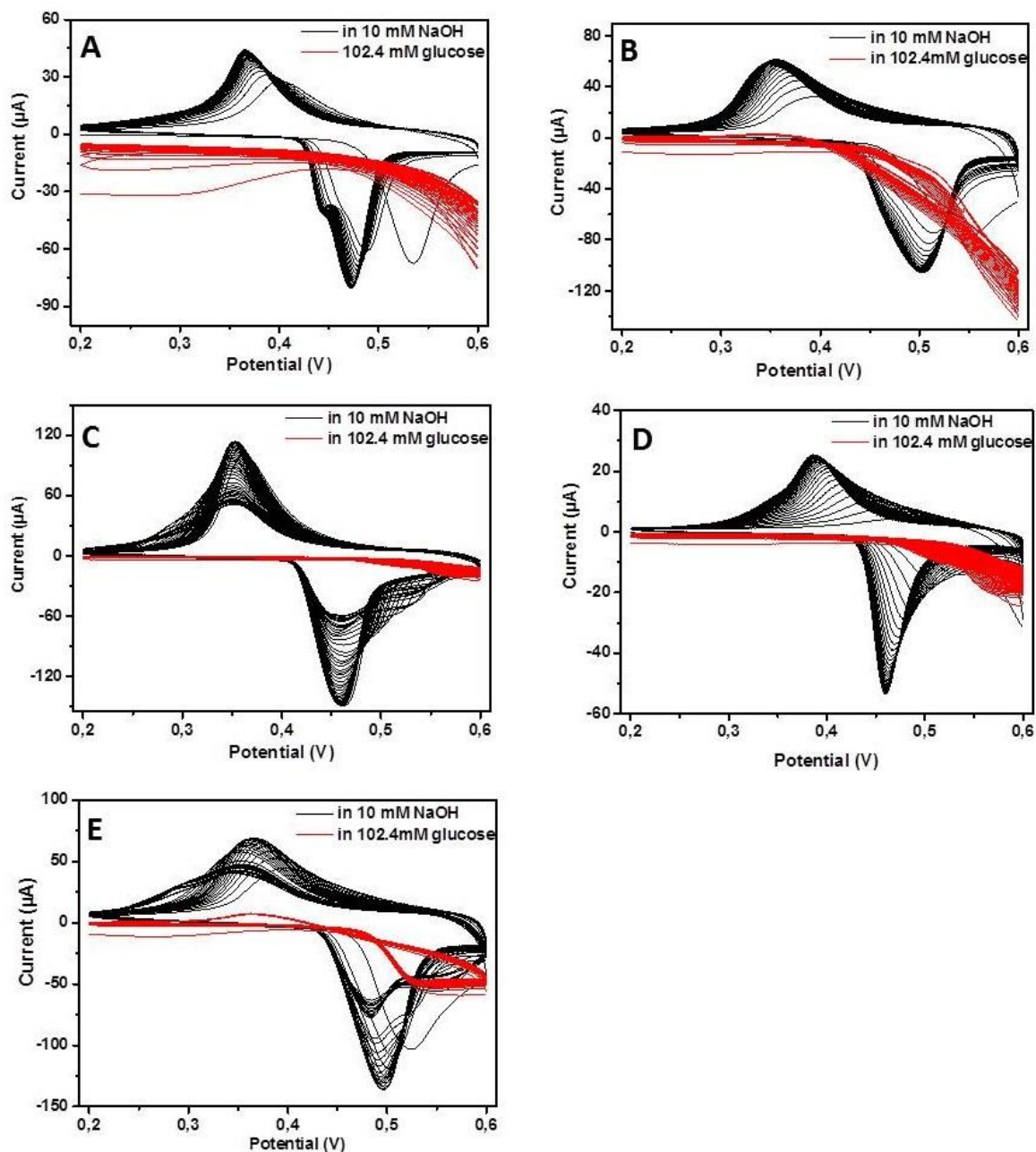
Figure 6.9. CV of the NiO/ antidot-modified-graphene electrodes in the absence and presence of glucose in 0.1 M NaOH solution, where graphene was modified with antidot lattices of 70nm diameter and LC of 300nm (A), 400nm (B), 500nm (C), 600nm (D) and 700nm (E).

Comparison of the recorded cyclic voltammograms before and after introduction of 102.4 mM glucose demonstrates that once glucose was added into the NaOH solution, the oxidation potential shifted to more positive values. This phenomenon is attributed to the catalytic

electrooxidation of glucose, since glucose molecules adsorbed on the surface of NiOOH can be oxidized at higher potentials [Jaf09] [Mar11].

In order to evaluate the amperometric behavior of the sensors, all five types of modified electrodes were tested in an amperometric setup to detect glucose.

It is well known that the applied potential strongly affects the amperometric response of a sensor [Zha13] [Sun15]. Therefore, in each measurement of Figure 6.10 the potential at which the maximum peak current occurred (ranging between 0.45 and 0.5 V) was chosen as the optimized sensing potential for amperometric measurements. Results plotted in Figure 6.10 indicate that graphene perforated with antidots of 500nm lattice constant is the optimal sensor for glucose detection, since compared to other sensors, it results in a higher step-like signal response upon the addition of glucose and shows the highest sensitivity towards the nonenzymatic detection of glucose, thus can be chosen as the working electrode for further experiments.
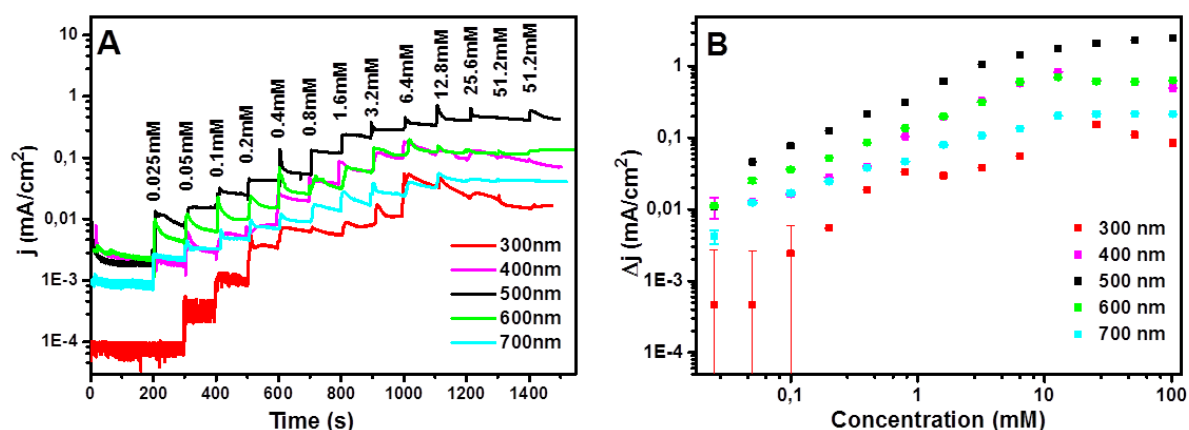
Figure 6.10. Electrochemical behavior of electrodes with different lattice constants toward growing concentration of glucose (A) amperometric responses of sensors with different lattice constants carried out in 10 mM NaOH, upon a step-wise increase of glucose concentration from 0.025mM to 102.4 mM while the solution was magnetically stirred. (B) Calibration plots of the mentioned sensors for glucose determination in a potential range of 0.45 – 0.5 V.

To evaluate the impact of the lattice constant on the performance of the sensors, the low limit of detection (LOD), linear calibration range and sensitivity for glucose determination at sensors with different lattice constants have been calculated and listed in Table 2.

Lattice constant (nm)	Linear range (mM)	Sensitivity($\mu A\ mM^{-1}mm^{-2}$)	LOD (μM)
No antidots	0.1-1.6	8.48	7.75
300	0.05-0.8	14.3	9.5
400	0.4-12.8	68.1	1.1
500	0.05-6.4	146.1	0.57
600	0.05-6.4	57.4	1.2
700	0.05-0.8	15.1	5.1

Table 2. Comparison of the performance of various glucose sensors where antidot arrays on graphene had different lattice constants.

It can be observed that the detection limit and linear calibration range for glucose determination at sensor with lattice constant of 500nm is better than other electrodes listed. In addition, the high sensitivity of this electrode is another advantage for this sensor.

6.6 Stability and reproducibility

The response reproducibility and stability were examined for the developed glucose sensor based on NiO decorated graphene electrode. Three independent graphene electrodes were modified with antidot lattices (hole diameter 70nm and lattice constant 500nm) and electrodeposited with NiO nanostructures under the similar conditions and their current response was measured in 10 mM NaOH at the applied potential of 0.46 V.

As illustrated in Figure 6.11, the three electrodes fabricated independently showed an acceptable similar current response in the presence of 102.4 mM glucose. All three sensors exhibit similar sensitivity ($\sim$146 μA mM^{-1}mm^{-2}) to the catalytic reduction of glucose and are able to detect glucose concentrations as low as 0.025 mM, showing fast and reproducible amperometric response upon successive additions of glucose.
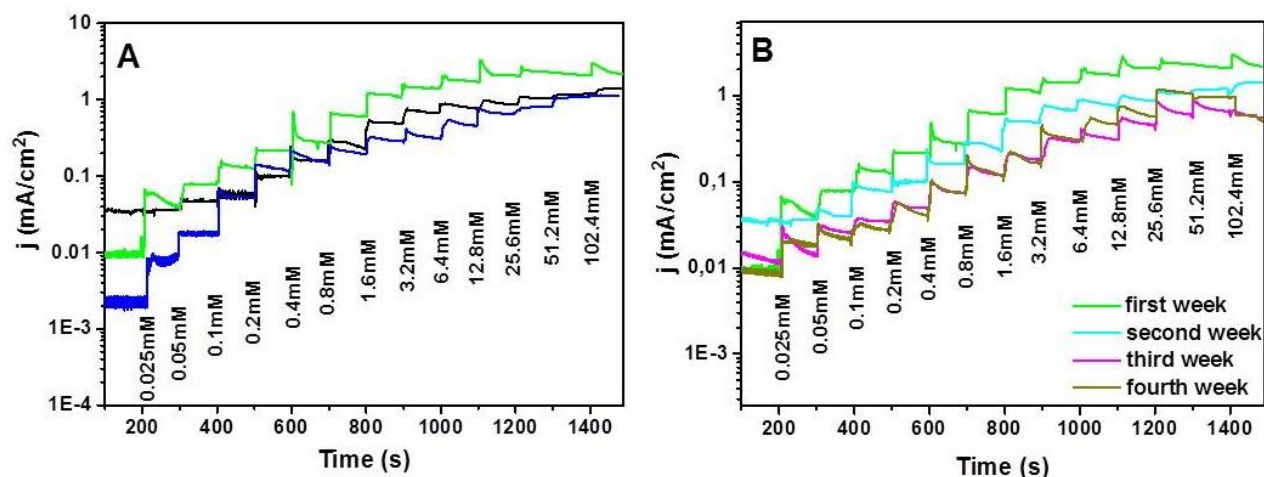
Figure 6.11. Study of response reproducibility and stability (A) Three different non-enzymatic glucose sensors, prepared independently, yielded a reproducible current response to a gradual increase of glucose concentration, from 0.025 to 102 mM. (B) During four series of amperometric measurements, no obvious current decline was observed, confirming long-term stability.

The stability of the sensor electrode was evaluated for four weeks. After stored at ambient conditions for one month, the sensor electrode maintained about 57% of its original activity, not undergoing poisoning through the formation of oxidation product (Figure 6.11 (B)). This experiment indicated that sensor electrode is stable and can be used repeatedly for the detection of glucose without a substantial change in the response of the sensor electrode.

6.7 Selectivity

In real samples, some possible interfering species such as ascorbic acid (AA) or carbohydrates such as fructose and sucrose might affect the detection of glucose. Therefore, the selectivity of the sensor was investigated. Figure 6.12 compares the amperometric responses of 0.4 mM glucose with 0.57 mM fuctose, 0.57 mM sucrose and 0.57 mM AA on the NiO/ antidot-modified-graphene glucose sensor in gently stirred 0.1M NaOH solution at a working potential of 0.45 V. As demonstrated, the sensor was able to selectively determine glucose in presence of other interfering species.
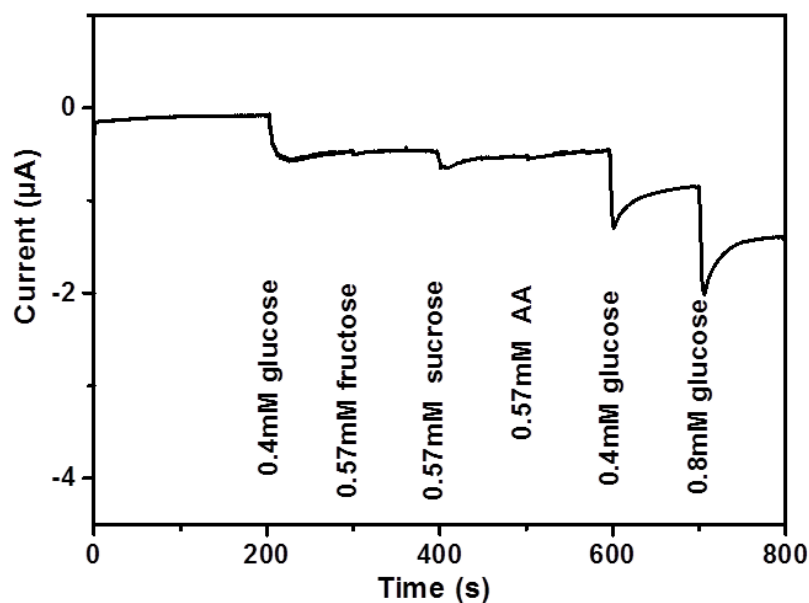
Figure 6.12. Investigation of the sensor's selectivity : Amperometric response of the NiO/antidot-modified-graphene electrode toward successive addition of glucose, sucrose, fructose, ascorbic acid (AA), and again glucose in 0.1 M NaOH solution at 0.45 V. Here, the labels denote the respective concentration increments in each step.

The addition of fructose and AA did not show any current response, and sucrose showed little current response which may not interfere with the detection of glucose. The results prove that the selectivity of the sensor for glucose detection was satisfactory. This is ascribed to the fact that the amperometric detection can be performed with a low detection potential (0.45 V), which can avoid interference of other species. The best potential for amperometric detection of fructose, sucrose and AA have been reported to be 0.5 V [Ike91] [Kin97], 0.59 V [Maj08] [Moh05] and 0.5 V [Tom05] respectively, which are out of the potential range we have determined for glucose detection.

6.8 Conclusion/Summary

The introduction of nano-scale defects in graphene can significantly modify its electrochemical properties. Previous theoretical studies shed light on enhanced chemical reactivity of 1D line defects, especially grain boundaries, in CVD graphene [Bri11] [Wan13] but the available experimental study on this subject is limited [Kim14].

Here, for the first time, we have studied the introduction of antidot lattices in graphene as an approach to modify the electrochemical properties of CVD graphene and its amperometric behavior towards glucose.

We demonstrated that electrodeposition of NiO nanoparticles at the antidot-modified graphene occur predominantly at the edges of the antidots due to the dangling positions provided by these defect sites. Images obtained from SEM directly confirm that most of the NiO deposition sites coincide with the circular defects created by antidot lattices on graphene. Moreover, amperometric measurements confirm high-performance glucose sensing using antidot-modified graphene and show its advantages over pristine CVD graphene in which NiO nanoparticles decorate the surface of graphene non-selectively.

These antidots allow us to selectively functionalize the graphene and systematically tune its electrochemical properties. As the number of antidots per area increases (i.e. the lattice constant decreases), NiO nanoparticles deposited along the defect sites grow in number, reaching their maximum density at lattice constant of 500 nm. With the lattice constant further shrinking to 400 and 300 nm, a decrease in the amount of the deposited nanoparticles is again observed, due to high distortion of graphene structure.

We demonstrate that the sensor based on graphene modified with antidots of 500 nm lattice constant and 70 nm diameter yields a superior platform for glucose sensing because it enhances the step-like signal response upon the addition of glucose and shows the highest sensitivity towards the non-enzymatic detection of glucose.

The glucose sensing performance and characteristics of the antidot-modified graphene utilized in this work are compared with previous reports as displayed in table 3.

Electrode material	Potential (V)	sensitivity($\mu A \cdot mM^{-1} \cdot cm^{-2}$)	LOD (μM)	Reference
NiO/Pt/ERGO	0.6	668.2	0.2	[Li14b]
rGO/Ni(OH)$_2$	0.6	11400	15	[Sub14]
rGO/NiO	0.4	1571	1	[Li14c]
Ni(OH)$_2$/ERGO/MWCNT	0.5	2042	2.7	[Gao14]
Pt-CuO/rGO	0.35	3577	0.01	[Dha14]
CuO/rGO	0.4	2221	0.1	[Wan14]
NiO/antidot-CVDG	0.4	14610	0.57	This work

Table 3. Comparison of analytical performance of various graphene-based nonenzymativ glucose sensors.

Compared with other sensors reported formerly, the glucose sensor we fabricated, exhibited a notably higher sensitivity and relatively lower detection limit.

All the sensors studied in the previous literatures are based on rGO, probably because of its easy access and low cost. However, during the chemical oxidation and reduction process toward rGO, a large number of defects are created, leading to poor structure quality, electronic conductivity and electrical mobility compared to CVD graphene. In our work, we propose a method which benefits from high quality CVD graphene and at the same time, allows us to selectively introduce controllable defects and dangling sites in order to optimize the electrochemical reactivity of graphene.

While some previously reported sensors are highly sensitive to glucose detection, they show rather poor stability and selectivity, owing to the high potential requirement for operation. Some other authors have investigated sensors able to operate at low enough potential, not producing interfering signals and stability problems, but their sensitivity is low. The sensor proposed in this work benefits from high sensitivity and stability, showing almost no interference due to the low operating potential.

Moreover, the NiO/ antidot-modified graphene electrode is capable of direct electrooxidation of glucose without enzyme immobilization, reducing the costs of the sensor fabrication and showing no loss of sensitivity due to denaturation of protein enzymes in the immobilization or detection procedures.

These remarkable features of the proposed sensor, as well as its high reproducibility and ease of operation provide enough potential for the sensor to be applicable as a high-performance non-enzymatic glucose sensor.

7. Summary and outlook

The focus of this work has been the experimental application of graphene in electrochemical sensing and exploring the effect of synthesis routes and artificial edges on the sensing properties of graphene.

We investigated the influence of the choice of the graphene material on the amperometric properties in direct hydrogen peroxide detection. Graphene materials including mechanically exfoliated graphene, CVD graphene and rGO have been applied to reductive amperometric determination of hydrogen peroxide and their properties and utility in terms of fabrication of sensing devices have been compared.

Our results demonstrate that the quality of the graphene has an enormous impact on the amperometric performance and the use of graphene with less number of defects (CVDG) results in a significant improvement in signal compared to rGO. The H_2O_2 sensor based on CVDG yields a sensitivity of 173 mA $M^{-1}cm^{-2}$ (which is about 7 times better than that of rGO). It is concluded that the application of CVDG offers large perspectives in amperometric detection systems owing to its efficiency in better detection of hydrogen peroxide with higher sensitivity compared to rGO.

Although the sensitivity obtained from electrochemical sensor based on CVDG is slightly less than that of mechanically exfoliated graphene (202 mA $M^{-1}cm^{-2}$), CVDG is preferred as the material which suits commercial purposes and mass production. Compared to irregular shape, size and location of mechanically exfoliated graphene and its laborious production process, CVDG offers uniform large films with high quality, providing a superior candidate for functionalization and further fabrication of high sensitivity biosensors.

Furthermore we had the great possibility to develop a sample preparation technique, based on graphene-electrodeposited NiO nanoparticles, that provides an effective solution to sample stability issues encountered when immobilizing enzymes on graphene. By introducing the antidot lattices to graphene, we investigated the role of these circular holes on the NiO deposition and sensing performance of graphene for the nonenzymatic detection of glucose at room temperature.

Our results reveal that arrays of antidots selectively patterned on graphene by plasma etching, lead to higher density of electrodeposited NiO nanoparticles on graphene and further improvement of graphene's amperometric behavior.

Compared with plain CVDG, the graphene modified with antidot lattices was found to have higher sensitivity (54.47 µA $mM^{-1}mm^{-2}$) and wider linear range (0.1-12.8 mM) for the detection of glucose, which is attributed to the imposed array of antidots that provided more anchoring sites for the deposition of nanoparticles.

We also demonstrated that by tailoring the size and lattice constant of the controllable and reproducible nanopatterns on graphene surface, the electrochemical reactivity of graphene can

be optimized. When antidots were prepared with the hole diameter of 70 nm and lattice constant of 500 nm, the NiO nanoparticles deposited on the graphene film had the highest density (700 NPs per $100\mu m^2$), and the amperometric measurements showed the best current response toward glucose detection with the highest sensitivity (146.1 μA $mM^{-1}mm^{-2}$) and lowest detection limit (0.57 μM).

This fabrication procedure could be extended to the preparation of other metal (oxide) /graphene based electrochemical sensors with dedicated properties to achieve new applications in detection of other biological samples.

The discussion here can be considered as an outlook onto what future experiments could aim at. Being motivated by the significance of multianalyte sensor arrays in disease diagnosis, food safety and biological analysis, the demand for higher throughput testing, more rapid diagnoses, and a more efficient use of samples has been growing.

As perspective, the research presented here makes it conceivable to employ antidots to tailor the graphene electrode and design amperometric array-biosensors consisting of several transducer elements with different bioselective components for various substances and thereby detecting numerous target analytes simultaneously.

8. Appendix

8.1 Functionalization techniques for enzyme immobilization

The lifetime of an enzyme-based biosensor mainly depends on how long the biological activity of the loaded enzyme is retained, which in turn depends on the immobilization strategy for the enzyme. Immobilization of enzymes refers to the technique of confining/anchoring the enzymes in or on an inert support for their stability and functional reuse. By employing this technique, enzymes are made more efficient and cost-effective for their industrial use. As a result, the immobilization of enzymes is a decisive factor in construction of the biosensor and can greatly affect its performance [Put13] [Bar02].

To date, a variety of strategies for biomolecule immobilization [Sas12] [Dat13] have been proposed, including physical or chemical adsorption onto the electrode [Tsa09] [Toi14] [Tan04], entrapment within a membrane, gel or nanoporous polymer [Cos06] [Ivn08] [Rub05], cross-linking between molecules [Lee09] [She05], and covalent bonding to a surface [Hon08] [Bie06]. The adsorption of enzyme from a solution onto a solid surface or an electrode can be carried out by either physical or chemical interactions, including van der Waals forces, electrostatic attractions, hydrophobic interactions, or hydrogen bonding [Han09] [Gui06]. Irrespective of the method to be used, the immobilization should be simple to carry out, highly reproducible, and should be stable under extreme environmental conditions like pH, temperature, ionic strength, and chemical composition.

A suitable microenvironment for biomolecules immobilization and fast electron transfer between the immobilized biomolecules and electrode substrates is provided by functionalization. Graphene may also be functionalized in order to enhance its sensitivity, specificity and loading capacity.

Functionalization methods are divided into two general categories: covalent and noncovalent, which we discuss briefly in the next two subsections. For detailed chemistry, several previous articles on this topic may be referred to [Sin09] [Gor10] [Geo12].

8.1.1 Covalent methods

The covalent functionalization of graphene can take place at the edges of the sheets and/or on the basal plane of graphene and is associated with rehybridization of one or more sp^2 carbon atoms of the carbon network into the sp^3 configuration accompanied by simultaneous loss of electronic conjugation.

The coexistence of sp^3 carbons in the lattice is inherently classified as defects. The ratio between carbon atoms with sp^2 and sp^3 hybridization in the graphitic lattice is an indication of the degree of the covalent functionalization reaction. This ratio is estimated using Raman

spectroscopy as the I_D/I_G ratio, where I_D and I_G are the intensities of the peaks at ~1350 and 1580 cm^{-1}, which correspond to the number of sp^3 and sp^2 C atoms, respectively.

In contrast to noncovalent functionalization, covalent schemes change the electronic properties due to disruption of the crystallographic lattice. Chemical moieties, commonly carboxylic (–COOH) and hydroxyl (–OH) groups, can be covalently created on the graphene surface using strong acids and/or oxidants. The oxygen-containing chemical groups created on the graphene surface can serve as chemical handles to graft functional molecules (e.g., proteins, carbohydrates, polymers) through covalent bonding. For example, carboxylic groups can react with proteins, carbohydrates or other polymers via amide or ester linkages.

8.1.2 Noncovalent methods

Although covalent strategies can effectively, stably and specifically install functionalities, they unavoidably alter the native electronic structure and physical properties of graphene by converting sp^2 carbons to sp^3 ones, e.g., causing decrease in carrier mobility. In view of this problem, noncovalent modifications have been employed in order to preserve the intrinsic properties of the original graphene materials.

Noncovalent interactions are primarily based on van der Waals forces or π-π stacking of aromatic molecules on the graphene plane, leading to physical adsorption of various molecules onto graphene basal plane without the need of any coupling reagents. However, physical adsorption is non-specific. To deal with this issue, passivation molecules are often applied to block the unfunctionalized area (sites) in order to avoid non-specific adhesion of unwanted molecules [Liu12].

Graphene materials can be non-covalently decorated with metal nanoparticles (e.g., Au, Ag, Pt) through chemical reduction [Don11] [Gut12], electrospray [Hu14], or electrochemical deposition [Mor13]. These nanoparticles may serve as the catalysts to mediate signal transduction in graphene based sensors, or as the docking points to anchor sensing probes with high capacity. For instance, thiolated biomolecules (e.g., thiol-ssDNA) can be anchored onto gold nanoparticles via formation of a thio-gold bond [Jay12].

With this brief introduction, we will now provide an overview of the various strategies and experiments that have been performed throughout this work to functionalize graphene and immobilize the GOD enzyme for fabrication of a glucose biosensor.

The experimental procedures for graphene functionalization have been done by Eva-Maria Kirchner from the department of analytical chemistry, Regensburg University.

8.2 Crosslinker mediated biofunctionalization of graphene

Crosslinking is the process of chemically joining two or more molecules by a covalent bond. Among various crosslinker reactive groups for protein conjugation, carbodiimide compounds provide the most popular and versatile method for crosslinking to carboxylic acids.

Different literatures have previously reported the preparation of biosensors based on covalent linkage between the carboxylic acid groups on graphene oxide sheets and the amines of the enzyme in the presence of crosslinking reagents such as 1-ethyl-3-(3-dimethylaminoprophy) carbondiimide hydrochloride (EDC) and N-hydroxysuccinimide (NHS) [Put13] [Liu10] [Chi14]. NHS or its water-soluble analog (Sulfo-NHS) is often included in EDC coupling protocols to improve efficiency or create dry-stable (amine-reactive) intermediates that are considerably stable [The09].

In the present work, the amine groups of GOD were covalently attached to the edge and defect site carboxyl groups of perforated graphene surface via EDC-NHS amine coupling reaction, as schematically illustrated in Figure 8.1.
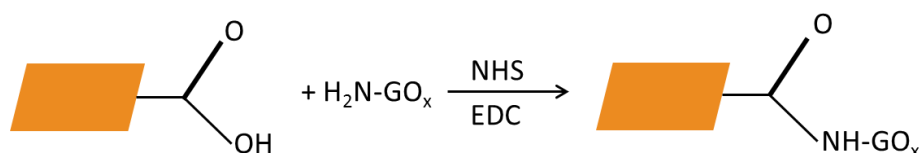
Figure 8.1. Schematic immobilization of GOD into GO sheets via peptide bonds between the amine groups of GOD and the carboxylic acid of GO

In the reaction, 2 mM EDC and 5 mM NHS were drop casted on the electrode and kept for 50 minutes to activate the COOH group of the perforated graphene. Then the electrodes were washed thoroughly with PBS. 10 µL of GOD in PBS at 5 mg/mL conc. was drop casted on the electrode and kept overnight at 4°C. Figure 8.2. shows the performance of the fabricated sensors investigated by CV and amperometry.

As can be observed, except for the first injection, the sensor shows no obvious changes of the peak currents after the addition of glucose, which represents failure in detecting glucose levels.
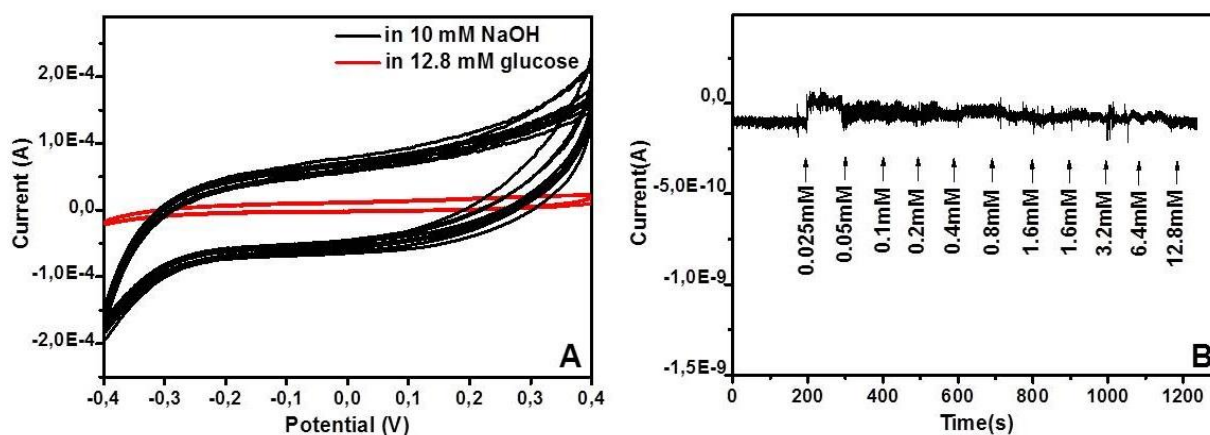
Figure 8.2. Sensing performance of GOD immobilized EDC/NHS/graphene to glucose. (A) CV of the graphene-based electrodes in the absence and presence of 12.8 mM glucose in 0.1 M NaOH solution (B)

Amperometric measurement under subsequent addition of glucose to cover a concentration range of 25 μM to 12.8 mM at a potential of 0.3 V

Since the use of EDC/NHS redox mediators was an unsuccessful method for immobilization of GOD on our graphene substrate, another immobilization protocol needs to be applied.

An entrapment in polymer membranes is a general method for enzyme immobilization that has been used for development of amperometric biosensors for glucose. In particular, Nafion has proved to be a good protective coating material and a support for immobilization of GOD on graphene [For92].

8.3 Nafion as a medium for glucose oxidase immobilization

Nafion encapsulation of enzyme is a common practice to prepare biosensors. Nafion is a sulfonated tetrafluorethylene copolymer that has been used extensively for the modification of electrode surfaces, offering great promise for oxidase-based amperometric biosensors. Having been applied as a binder/stabilizing agent in many different glucose sensor designs [Mou94] [Yan15], it has even proven to prolong the lifetime of the sensor in comparison to other binding agents [Tur90], and to act as an excellent matrix to protect GOD from thermal deactivation during glucose sensing, where the temperature can reach up to 68 °C and GOD would lose activity [Tse09].

Pioneering work by Zhou et.al. shows that GOD may interact with graphene sheets by the physical adsorption and since the GOD/graphene films are not stable, they can easily shed from the electrode. Therefore, it is necessary to use Nafion as a binder to hold the GOD stably kept on the electrode surface [Zho08].

However, a study by Lu et.al. shows that increasing Nafion concentration and adding an additional layer of Nafion on the graphene film leads to significant reduction of the sensitivity of the biosensor, because more Nafion could reduce the activity of enzyme and the additional layer of Nafion could block fast electron transfer [Lu07].

In the present work, we first modified the perforated CVD graphene electrodes with GOD, by drop casting the enzyme solution (500 U mL^{-1}). The enzyme modified electrodes were then dried and successively dipped in 10 mM phosphate buffer to remove excess unbound enzyme. After drying, 1 μL 0.1 wt% Nafion solution was spin coated onto the modified electrodes for 30 seconds at a speed of 3000 rpm. Amperometric measurements were performed under subsequent addition of glucose to the solution. Cyclic voltammograms were also obtained before and after the addition of 12.8mM glucose in the solution.

As illustrated in Figure 8.3, the Nafion/GOD/graphene electrode shows no redox peaks at the CV experiment and the Nafion coated graphene does not respond obviously to the glucose additions and is inapplicable for glucose detection.
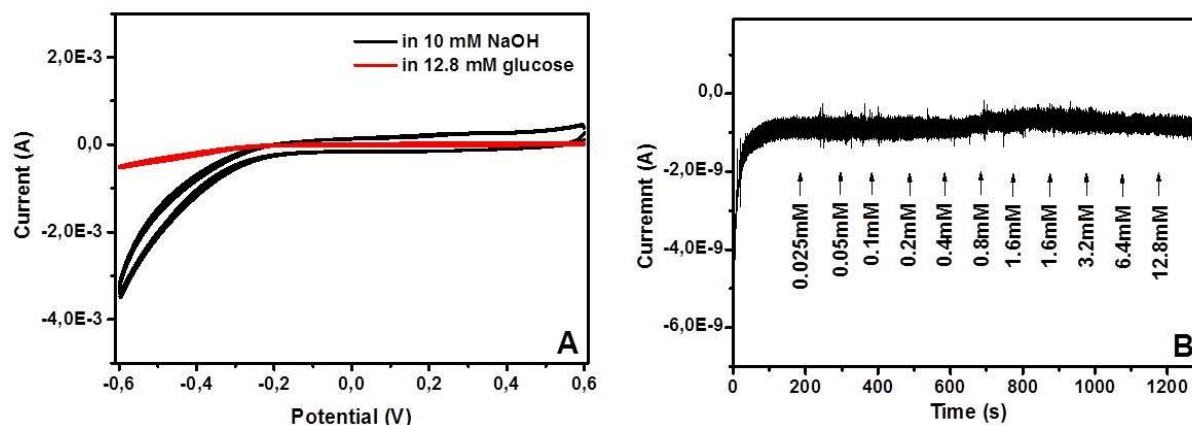
Figure 8.3. Sensing performance of GOD immobilized Nafion/graphene to glucose. (A) CV of the graphene-based electrodes in the absence and presence of glucose in 0.1 M NaOH solution, (B) Amperometric measurement under subsequent addition of glucose to cover a concentration range of 25 µM to 12.8 mM at a potential of 0.3 V.

According to the obtained results, it can be concluded that in our experiment, the Nafion film acts as a barrier to electron transfer and blocks the enzyme activity. Since this technique didn't lead to fabrication of a glucose biosensor either, another approach was employed as an alternative for graphene functionalization: surface modification by a spontaneous reaction between a diazonium salt and the graphene layer.

8.4 Covalent modification of graphene via diazonium salt chemistry

Another efficient method for the functionalization of graphene is based on the reaction of 4-nitrobenzene diazonium tetrafluoroborate (NBD) salts with graphene surface, widely employed for grafting aryl groups to the surface of sp^2-hybridized carbon materials.

The most common reaction mechanism of covalent functionalization with aryl diazonium salts is illustrated in Figure 8.4. The reaction intrinsically involves a spontaneous electron transfer from graphene to the aryl diazonium cation, which becomes an aryl radical after releasing a molecule of N_2. The aryl radical then forms a covalent bond with a carbon atom in the graphene lattice, changing its hybridization to sp^3 and displacing it out of the plane by ~0.7 Å [Jia06] [Pau13], finally leading to functionalization of the graphene with nitro groups.
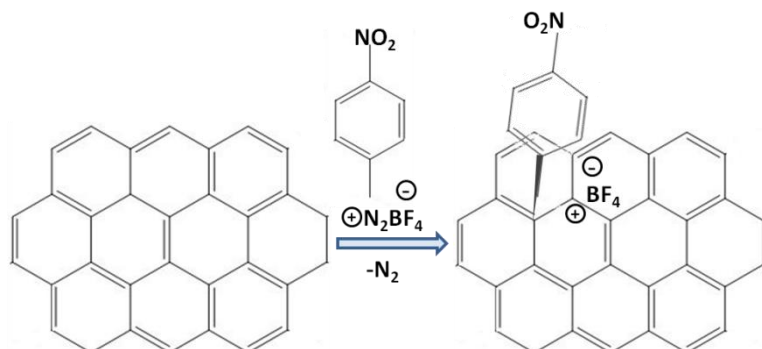
Figure 8.4. Schematic illustration of grafting a diazonium salt to a graphene sheet.

The electrochemical reduction of -NO$_2$ to -NH$_2$ is the key step in addressability, since the primary amine (-NH$_2$) groups produced by the electrochemical reduction are a ubiquitous starting point for covalently linking biomolecules such as enzymes, DNA, peptides, and antibodies to graphene surfaces as immobilization matrixes.

The diazonium coupling reaction of graphene is strongly dependent on graphene layers. Strano, et al., found that single GNS are almost 10 times more reactive than bi- or multilayers of graphene [Sha10b]. More interestingly, the reactivity of edges is at least two times higher than the reactivity of the bulk single GNS. This suggestion is supported by the research by Lim [Lim10] and Sinitskii, et al [Sin10].

In the present work, the functionalization was performed as follows: graphene was immersed in an aqueous solution of 20 mM 4-NBD for two hours at room temperature and afterwards rinsed with water. We should note that due to the photo instability of the diazonium salt, the reaction vials had to be kept in the dark.

To generate 4-carboxy diazonium compound, a mixture of 2 mM NaNO$_2$ in 2 mM p-aminobenzoic acid (PABA) in 5 mM HCl was stirred for 5 minutes and used as electrolyte in the three-electrode arrangement for the subsequent diazotization reaction.

CV measurements were performed in a potential window from -0.6 V to +0.6 V at a rate of 100 mVs^{-1}. The attachment of the NBD group to graphene surface can be readily investigated with Raman spectroscopy, where the conversion of sp^2 to sp^3 carbon atoms due to the reaction leads to distinct changes in the Raman spectra, emerging mainly as a prominent D-band. The Raman analyses (Figure 8.5) reveal a distinct D band after the reaction of the diazonium compound, indicating the rehybridization of C atoms from sp^2 to sp^3 as a result of successful binding of the diazonium compound to graphene surface.
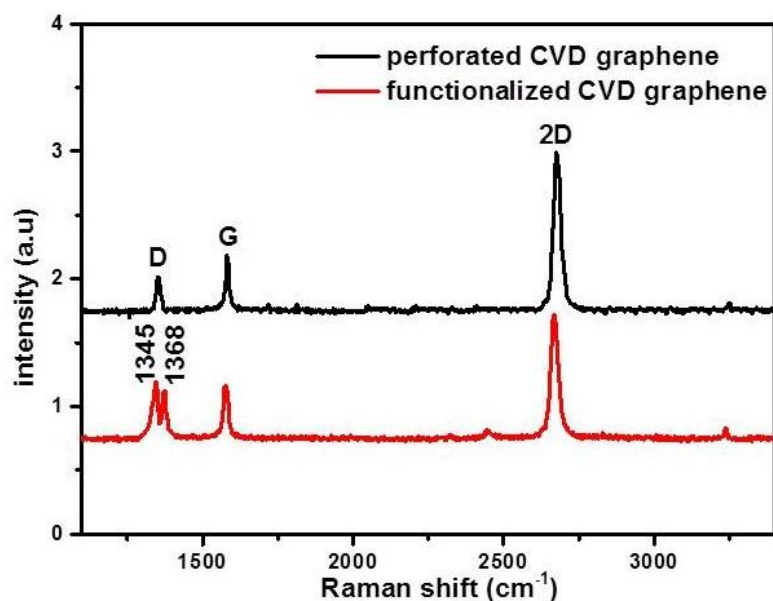
Figure 8.5. Changes in the Raman spectrum of graphene due to NBD-functionalization. The observation of two sharp D peaks at 1345 and 1368 cm^{-1} together with the decreased G and 2D bands is characteristic of the reduced periodicity of the π-bonds in NBD-functionalized graphene.

In order to immobilize GOD, 4-nitrobenzene modified graphene was reduced electrochemically to 4-aminobenzene modified graphene by doing CV in a potential range of -1.1 V to 0 V at a rate of 100 mV.s^{-1} for five cycles. The 4-aminobenzene modified graphene electrode was then activated by immersion in 1 mL of a solution of EDC (β = 50 mg mL^{-1}) in 140 mM NaCl. After rinsing the electrode with water, the electrode was immersed in a GOD solution (β = 250 U mL^{-1}) in 10 mM phosphate buffer containing 0.1 M KCl (pH 7.4). The electrodes were incubated in the enzyme solution overnight. Afterwards they were rinsed with water and stored at 4 °C when not in use.

The electrochemical performance of the resulted bioelectrode was tested through CV and amperometry as illustrated in Figure 8.6.
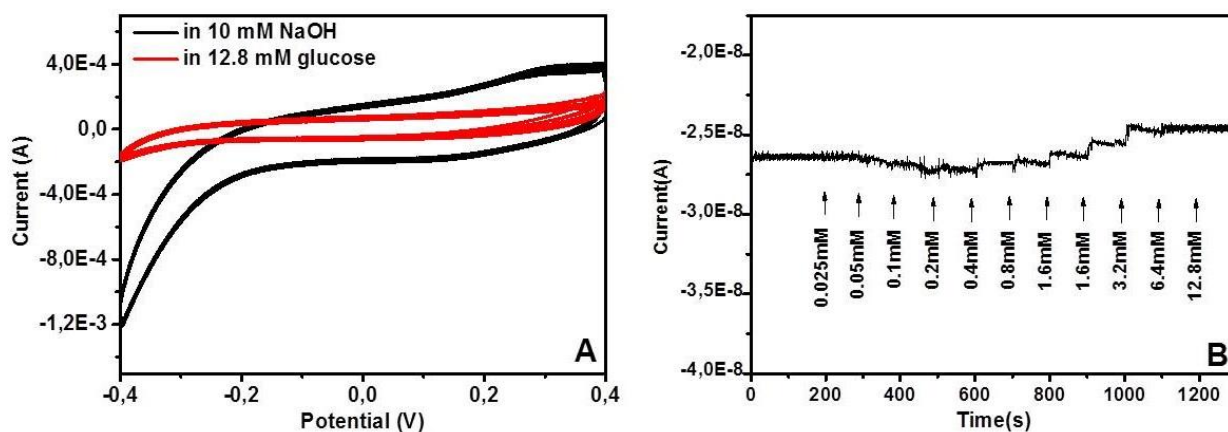
Figure 8.6. Sensing performance of GOD immobilized Nafion/graphene to glucose. (A) CV of the graphene-based electrodes in the absence and presence of glucose in 0.1 M NaOH solution, (B) Amperometric measurement under subsequent addition of glucose to cover a concentration range of 25 µM to 12.8 mM at a potential of 0.3 V.

According to the obtained results, the use of diazonium salt for graphene functionalization didn't satisfy our needs for fabrication of a sensitive and stable glucose biosensor with low detection limit. The current response of the fabricated biosensor toward glucose reduction appeared at a limited range of concentration (0.4-3.2 mM) and did not show stability after repeating the experiment under the same conditions. Once more, a new approach needs to be applied for graphene modification, in order to provide a reliable substrate for enzyme immobilization.

Bibliography

[Ali16]   M. Aliofkhazraei, N. Ali, W. I. Milne, C. S. Ozkan, S. Mitura and J. L. Gervasoni "Graphene science handbook: Mechanical and chemical properties" *CRC press* ISBN 9781466591318 (2016)

[Alk13]   R. C. Alkire, D. M. Kolb, J. Lipkowski and P. N. Ross "Bioelectrochemistry: Fundamentals, applications and recent developments" *John Wiley & Sons* ISBN: 978-3-527-32885-7 (2013)

[All09]   M. J. Allen, V. C. Tung, L. Gomez, Z. Xu, L. M. Chen, K. S. Nelson, C. W.Zhou, R. B. Kaner and Y. Yang "Soft transfer printing of chemically converted graphene" *Adv. Mat.* **21** 2098-2102 (2009)

[All10]   M. J. Allen, V. C. Tung and R. B. Kaner "Honeycomb carbon: A review of graphene" *Chem. Rev.* **110** 132-145 (2010)

[Alm10]   L. Al-Mashat, K. Shin, K. Kalantar-Zadeh, J. D. Plessis, S. H. Han, R. W. Kojima, R. B. Kaner, D. Li, X. L. Gou, S. J. Ippolito and W. Wlodarski "Graphene/polyaniline nanocomposite for hydrogen sensing" *J. Phys. Chem. C* **114** 16168–16173 (2010)

[Alw09]   S. Alwarappan, A. Erdem, C. Liu and C. Z. Li "Probing the electrochemical properties of graphene nanosheets for biosensing applications" *J. Phys. Chem.C* **113** 8853-8857 (2009)

[Amb10a]   A. Ambrosi and M. Pumera "Nanographite impurities dominate electrochemistry of carbon nanotubes" *Chem. Eur. J.* **16** 10946 –10949 (2010)

[Amb10b]   A. Ambrosia and M. Pumera "Stacked graphene nanofibers for electrochemical oxidation of DNA bases" *Phys. Chem. Chem. Phys.* **12** 8943–8947 (2010)

[Amb14]   A. Ambrosi, C. K. Chua , A. Bonanni and M. Pumera "Electrochemistry of graphene and related materials" *Chem. Rev.* **114** 7150-7188 (2014)

[Ans83]   F. C. Anson, R. A. Osteryoung "Chronocoulometry: a convenient, rapid and reliable technique for detection and determination of adsorbed reactants" *J. of Chem. Edu.* **60** 293-296 (1983)

[Ao08]   Z. M. Ao, J. Yang, S. Li and Q. Jiang "Enhancement of CO detection in Al doped graphene" *Chem. Phys. Lett.* **461** 276–279 (2008)

[Arc09]   L.G. De Arco, Y. Zhang, A. Kumar and C. Zhou "Synthesis, transfer, and devices of single and few-layer graphene by chemical vapor deposition" *IEEE Trans. Nanotechnol.* **8** 135–138 (2009)

[Bad14]   S. Badhulika, R. K. Paul, Rajesh, T. Terse and A. Mulchandani "Nonenzymatic glucose sensor based on platinum nanoflowers decorated multiwalled carbon nanotubes-graphene hybrid electrode" *Electroanal.* **26** 103–108 (2014)

[Bai13]   J. Bai and X. Jiang "A facile one-pot synthesis of copper sulfide-decorated reduced graphene oxide composites for enhanced detecting of H_2O_2 in biological environments" *Anal. Chem.* **85** 8095–8101 (2013)

[Bal08]   A. A. Balandin, S. Ghosh, W. Bao, I. Calizo, D. Teweldebrhan, F. Miao and C. Ning Lau "Superior thermal conductivity of single-layer graphene" *Nano Lett.* **8** 902-907 (2008)

[Ban05]   C. E. Banks and R. G. Compton "Exploring the electrocatalytic sites of carbon nanotubes for NADH detection: an edge plane pyrolytic graphite electrode study" *Analyst* **130** 1232–1239 (2005)

[Bao12]   Qiaoliang Bao and Kian Ping "Graphene photonics, plasmonics, and broad-band optoelectronic devices" *ACS Nano* **6** 3677–3694 (2012)

[Bar01]   A. J. Bard and L. R. Faulkner "Electrochemical methods: Fundamentals and applications" *John Wiley & Sons* Inc., New York, p. 833 (2001)

[Bar02]   A. J. Bard, M. Stratmann and G. S. Wilson "Encyclopedia of electrochemistry" Volume 9: Bioelectrochemistry, ISBN: 978-3-527-30401-1 67– 143 (2002)

[Bar05]   E. Barsoukov and J. R. Macdonald, "Impedance spectroscopy: Theory, experiment, and applications" ISBN: 978-0-471-64749-2 (2005)

[Bar09]   A. Barreiro, M. Lazzeri, J. Moser, F. Mauri and A. Bachtold "Transport properties of graphene in the high-current limit" *Phys. Rev. Lett.* **103** 076601 (2009)

[Bar14]   M. M. Barsana, K. P. Prathisha, X. Sunb and C. M.A. Brett "Nitrogen doped graphene and its derivatives as sensors and efficientdirect electron transfer platform for enzyme biosensors" *Sens. Actuat. B* **203** 579–587 (2014)

[Bee08]   C.W.J. Beenakker "Colloquium: Andreev reflection and Klein tunneling in graphene" *Rev. Mod. Phys.* **80** 1337-1354 (2008)

[Bie06]   A.T. Biegunski, A. Michota, J. Bukowska and K. Jackowska "Immobilization of tyrosinase on poly(indole-5-carboxylic acid) evidenced by electrochemical and spectroscopic methods" *Bioelectrochem.* **69** 41-48 (2006)

[Boa82]   J. Boardman, I. E. S. Edwards, N. G. L. Hammond and E. Sollberger "The Cambridge ancient history" 3, part1, ISBN: 9780521224963 31-33 (1982)

[Bon10]   F. Bonaccorso, Z. Sun, T. Hasan and A. C. Ferrari "Graphene photonics and optoelectronics" *Nat. Phot.* **4** 611-622 (2010)

[Bon11]   A. Bonanni and M. Pumera "Graphene platform for hairpin-DNA based impedimetric genosensing" *ACS Nano* **5** 2356–2361 (2011)

[Bor12]   S. Borgmann, A. Schulte, S. Neugebauer and W. Schuhmann "Amperometric Biosensors, in Advances in Electrochemical Science and Engineering: Bioelectrochemistry" *Wiley-VCH Verlag GmbH & Co. KGaA* **13** 1-83 (2012)

[Bri11]   W. H. Brito, R. Kagimura and R. H. Miwa "Hydrogenated grain boundaries in graphene" *Appl. Phys. Lett.* **98** 213107 (2011)

[Bro10]   D. A. C. Brownson and C. E. Banks "Graphene electrochemistry: an overview of potential applications" *Analyst* **135** 2768–2778 (2010)

[Bro11]   D. A.C. Brownson, D. K. Kampouris and C. E. Banks "An overview of graphene in energy production and storage applications" *J. of Power Sourc.* **196** 4873–4885 (2011)

[Bro12]   D.A. C. Brownson, D. K. Kampouris and C. E. Banks "Graphene electrochemistry: fundamental concepts through to prominent applications" *Chem. Soc. Rev.* **41** 6944–6976 (2012)

[Bro14]   D. A. C. Brownson and C. E. Banks, "The handbook of graphene electrochemistry" ISBN 978-1-4471-6428-9 (2014)

[Bun08]   J. S. Bunch "Mechanical and electrical properties of graphene sheets" Doctoral dissertation Cornell University (2008)

[Can04]   L.G. Cancado, M. A. Pimenta,1 B. R. A. Neves,1 G. Medeiros-Ribeiro, T. Enoki, Y. Kobayashi, K. Takai, K. Fukui, M. S. Dresselhaus, R. Saito and A. Jorio "Influence of the atomic structure on the Raman spectra of graphite edges" *Phys. Rev. Lett.* **93** 47403 (2004)

[Cas09]   A. H. Castro Neto, F. Guinea, N. M. R. Peres, K. S. Novoselov, and A. K. Geim "The electronic properties of graphene" *Revs. Mod. Phys.* **81** 109-162 (2009)

[Cel13]   K. Celebi "Chemical vapor deposition of graphene on copper" Doctoral dissertation, university of ETH Zurich (2013)

[Cha02]   A. Chaubey and B. D. Malhotra "Mediated biosensors" *Biosen. & Bioelec.* **17** 441-456 (2002)

[Che10]   H. Chen, W. Zhu and Z. Zhang "Contrasting behavior of carbon nucleation in the initial stages of graphene epitaxial growth on stepped metal surfaces" *Phys. Rev. Lett.* **104** 186101 (2010)

[Chi14]   N. F. Chiu, T.Y. Huang, H.C. Lai and Kou-Chen Liu "Graphene oxide-based SPR biosensor chip for immunoassay applications" *Nan. Res. Lett.* **9** 445-452 (2014)

[Chu12]   M. G. Chung, D.H. Kim, D. K. Seo, T. Kim, H. U. Im, H. M. Lee, J.B. Yoo, S.H. Hong, T. Kang and Y. H. Kim "Flexible hydrogen sensors using graphene with palladium nanoparticle decoration" *Sens. and Act.* B **169** 387– 392 (2012)

[Chu14]   C. K. Chua and M. Pumera "Chemical reduction of graphene oxide: a synthetic chemistry viewpoint" *Chem. Soc. Rev.* **43** 291-312 (2014)

[Cla62]   L.C. Clark and C. Lyons "Electrode systems for continuous monitoring cardiovascular surgery" *Ann.NY Acad. Sci.* **102** 29-45 (1962)

[Col00]   P. G. Collins, K. Bradley, M. Ishigami and A. Zettl "Extreme oxygen sensitivity of electronic properties of carbon nanotubes" *Science* **287** 1801-1804 (2000)

[Cos06]   S. Cosnier, C. Mousty, C. Gondran, A. Lepellec "Entrapment of enzyme within organic and inorganic materials for biosensor applications: Comparative study" *Mater. Sci. Eng. C* **26** 442-447 (2006)

[Cus15]   G.W. Cushing, V. Johánek, J. K. Navin, and I. Harrison, "Graphene growth on Pt(111) by ethylene chemical vapor deposition at surface temperatures near 1000 K" *J. Phys. Chem. C* **119** 4759-4768 (2015)

[Dat13]   S. Datta, L. R. Christena, Y. Rani and S. Rajaram "Enzyme immobilization: an overview on techniques and support materials" *Biotech.* **3** 1–9 (2013)

[Deg89]   Y. Degani and A. Heller "Electrical Communication between redox centers of glucose oxidase and electrodes via electrostatically and covalently bound redox polymers" *J. Am. Chem. Soc.* **111** 2358-2361 (1989)

[Dha14]   K. Dharaa, J. Stanley, R. Ta, B. G. Nair and S. Babu "Pt-CuO nanoparticles decorated reduced graphene oxide for the fabrication of highly sensitive non-enzymatic disposable glucose sensor" *Sens. and Actuat. B* **195** 197–205 (2014)

[Don11]   X. Dong, W. Huang and P. Chen "In situ synthesis of reduced graphene oxide and gold nanocomposites for nanoelectronics and biosensing" *Nanoscale Res. Lett.* **6** 60-65 (2011)

[Dor03]   P. D'Orazio "Biosensors in clinical chemistry" *Clinica Chimica Acta* **334** 41-69 (2003)

[Dre05]   M.S. Dresselhaus, G. Dresselhaus, R. Saito and A. Jorio "Raman spectroscopy of carbon nanotubes" *Phys. Rep.* **409** 47-99 (2005)

[Dre11]   D. R. Dreyer, H. Jia, A. D. Todd, J. Geng and C. W. Bielawski "Graphite oxide: a selective and highly efficient oxidant of thiols and sulfides" *Org. Biomol. Chem.* **9** 7292–7295 (2011)

[Eck13]   A. Eckmann, A. Felten, I. Verzhbitskiy, R. Davey and C. Casiraghi "Raman study on defective graphene: Effect of the excitation energy, type, and amount of defects" *Phys. Rev. B* **88** 035426 (2013)

[Eda08]   G. Eda, G. Fanchini, and M. Chhowalla "Large-area ultrathin films of reduced graphene oxide as a transparent and flexible electronic material" *Nat. Nano* **3** 270–274 (2008)

[Egg02]   B. Eggins "Chemical sensors and biosensors" Analytical Techniques in the Sciences. John Wiley & Sons, West Sussex, (2002)

[Eiz79]   M. Eizenberg and J. M. Blakely "Carbon monolayer phase condensation on Ni(111) Surface" *Science* **82** 228-236 (1979)

[Ens13]   A. A. Ensafi, M. Jafari Asl and B. Rezaei "A novel enzyme-free amperometric sensor for hydrogen peroxide based on Nafion/exfoliated graphene oxide-Co_3O_4 nanocomposite" Talanta **103** 322-329 (2013)

[Fer06]   A.C. Ferrari, J.C. Meyer, V. Scardaci, C. Casiraghi, M. Lazzeri, M. Mauri, S. Piscanec, Da Jiang, K.S. Novoselov, S. Roth and A.K. Geim "Raman spectrum of graphene and graphene layers" *Phys. Rev. Lett.* **97** 187401 (2006)

[Fer07]   A. C. Ferrari "Raman spectroscopy of graphene and graphite: Disorder, electron–phonon coupling, doping and nonadiabatic effects" *Solid State Commun.* **143** 47-57 (2007)

[Fer13]   A. C. Ferrari and D. M. Basko "Raman spectroscopy as a versatile tool for studying the properties of graphene" *Nat. Nanotech.* **8** 235-246 (2013)

[For92]   G. Fortie, M. Vaillancourt and D. Belanger "Evaluation of nafion as media for glucose oxidase immobilization for the development of an amperometric glucose biosensor" *Eleclroanal.* **4** 275-283 (1992)

[Fow09]   J. D. Fowler, M. J. Allen, V. C. Tung, Y. Yang, R. B. Kaner and B. H. Weiller "Practical chemical sensors from chemically derived graphene" *ACS Nano* **3** 301-306 (2009)

[Fue14]   J. La Fuente, "Electrochemical reduction of graphene oxide for industrial applications" 2014 www.graphenea.com/pages/reduced-graphene-oxide

[Fu15]   L. Fu, G. Lai, B. Jia and A. Yu "Preparation and electrocatalytic properties of polydopamine functionalized reduced graphene oxide-silver nanocomposites" *Electrocatalys.* **6** 72–76 (2015)

[Fuh10]   M.S. Fuhrer, C.N. Lau and A.H. Macdonald "Graphene: Materially better carbon" *MRS Bullet.* **35** 289-295 (2010)

[Gal15]   A.L. Galant, R.C. Kaufman and J.D. Wilson "Glucose: Detection and analysis" *Food Chem.* **188** 149-160 (2015)

[Gan11]   T. Gan and S. Hu "Electrochemical sensors based on graphene materials" *Microchim Acta* **175** 1–19 (2011)

[Gao09]   W. Gao, L. B. Alemany, L. Ci and P. M. Ajayan "New insights into the structure and reduction of graphite oxide" *Nature Chemistry* **1** 403- 408 (2009)

[Gao14]   W. Gao, W.W. Tjiu , J. Wei and T. Liu "Highly sensitive nonenzymatic glucose and H_2O_2 sensor based on $Ni(OH)_2$/electroreduced graphene oxideMultiwalled carbon nanotube film modified glass carbon electrode" *Talant.* **120** 484–490 (2014)

[Gei07]   A. K. Geim, K. S. Novoselov "The rise of graphene" *Nat. Mat.* **6** 183-191

[Geo12]   V. Georgakilas, M. Otyepka, A. B. Bourlinos, V. Chandra, N. Kim, K. C. Kemp, P. Hobza, R. Zboril and K.S. Kim "Functionalization of graphene: covalent and non-covalent approaches, derivatives and applications" *Chem. Rev* **112** 6156–6214 (2012)

[Gor10]   B. K. Gorityala, J. M. Ma, X. Wang, P. Chen and X. W. Liu, "Carbohydrate functionalized carbon nanotubes and their applications" *Chem. Soc. Rev.* 39, 2925–2934 (2010)

[Gra07]   D. Graf, F. Molitor, K. Ensslin, C. Stampfer, A. Jungen, C. Hierold and L. Wirtz "Spatially resolved Raman spectroscopy of single- and few-layer graphene" *Nano Lett.* **7** 238–242 (2007)

[Gri08]   D. Grieshaber, R. MacKenzie, J. Vörös and E. Reimhult "Electrochemical biosensors-sensor principles and architectures" *Sensors* **8** 1400-1458 (2008)

[Gui06]   J. M. Guisan (Ed) "Immobilization of enzymes and cells" Second edition 2006 ISBN 978-1-58829-290-2 15-30

[Guo12]   S. Guo, M. Ghazinejad, X. Qin, H. Sun, W. Wang, F. Zaera, C. S. Ozkan and M. Ozkan "Tuning of electron transport in graphene based field effect devices using block co-polymers" *Small* **8** 1073-1080 (2012)

[Gut12]   A. Gutés, C. Carraro and R. Maboudian "Single-layer CVD-grown graphene decorated with metal nanoparticles as a promising biosensing platform" Biosensors and Bioelectronics **33** 56– 59 (2012)

[Don12]   X. Dong, H. Xu, X.Wang, Y. Huang, M. B. Chan-Park, H. Zhang, L.H. Wang, W. Huang and P. Chen "3D graphene/cobalt oxide electrode for high-performance supercapacitor and enzymeless glucose detection" *ACS Nano* **6** 3206–3213 (2012)

[Han05]   K. Han, Z. Wu, J. Lee, I. Ahn, J. W. Park, B. R. Min and K. Lee "Activity of glucose oxidase entrapped in mesoporous gels" *Biochem. Eng. J.* **22** 161-166 (2005)

[Han09]   U. Hanefeld, L. Gardossib and E. Magner "Understanding enzyme immobilization" *Chem. Soc. Rev.* **38** 453-468 (2009)

[Hel08]   A. Heller and B. Feldman "Electrochemical glucose sensors and their applications in diabetes management" *Chem. Rev.* **108** 2482–2505 (2008)

[Hel08]   A. Heller and B. Feldman "Electrochemistry in diabetes management" *Acc. Chem. Res*. **43** 963–973 (2010)

[Her13]   G. T. Hermanson "Bioconjugate Techniques" (Third Edition) ISBN: 978-0-12-382239-0

[Hey10]   S. Heydrich, M. Hirmer, C. Preis, T. Korn, J. Eroms, D. Weiss and C. Schüller "Scanning Raman spectroscopy of graphene antidot lattices: Evidence for systematic p-type doping" *Appl. Phys. Lett.* **97** 043113 (2010)

[Hey14]   S. Heydrich "Raman spectroscopy of nanopatterned graphene "Doctoral dissertation" university of Regensburg February (2013)

[Hir08]   B. Hirschorn, I. Ibrahim, M. E. Orazem, H. Takenouti and B. Tribollet "Effect of large perturbation amplitudes on the impedance response of an electrochemical system" *ECS Transactions* **13** 81-100 (2008)

[Hol11]   J. T. Holland, C. Lau, S. Brozik, P. Atanassov and S. Banta "Engineering of glucose oxidase for direct electron transfer via site-specific gold nanoparticle conjugation" *J. Am. Chem. Soc.* **133** 19262–19265 (2011)

[Hon08]   J. Hong, D. Xu, P. Gong, J.Yu, H. Ma and S. Yao "Covalent-bonded immobilization of enzyme on hydrophilic polymer covering magnetic nanogels" *Microporous and Mesoporous Materials* **109** 470-477 (2008)

[Hu12]   B. Hu, H. Ago, Y. Ito, K. Kawahara, M. Tsuji, E. Magome, K. Sumitani, N. Mizuta, K. Ikeda and S. Mizuno "Epitaxial growth of large-area single-layer graphene over Cu(111)/sapphire by atmospheric pressure CVD" *Carbon* **50** 57-65 (2012)

[Hu14]   T. Hu, G. Xin, H. Sun, X. Sun, M. Yu, C. Liua and J. Lian "Electrospray deposition of a Co_3O_4 nanoparticles–graphene composite for a binder-free lithium ion battery electrode" *RSC Adv.* **4** 1521-1525 (2014)

[Hua08]   B. Huang, Z. Y. Li, Z. R. Liu, G. Zhou, S. G. Hao, J. Wu, B. L. Gu and W. H. Duan "Adsorption of gas molecules on graphene nanoribbons and its implication for nanoscale molecule sensor" *J. Phys. Chem. C* **112** 13442–13446 (2008)

[Hum58]   W. S. Hummers Jr and R. E. Offeman "Preparation of graphitic oxide" *J. Am. Chem. Soc.* **80** 1339–1339 (1958)

[Ike91]   T. Ikeda, F. Matsushita and M. Senda "Amperometric fructose sensor based on direct bioelectrocatalysis" *Biosens. and Bioelectron.* **6** 299-304 (1991)

[Ivn08]   D. Ivnitski, K. Artyushkova, R.A. Rincon, P. Atanassov, H. R. Luckarift, and G. R. Johnson "Entrapment of enzymes and carbon nanotubes in biologically synthesized silica: glucose oxidase- catalyzed direct electron transfer" *small* **4** 357-364 (2008)

[Jaf09]   M. Jafarian, F. Forouzandeh, I. Danaee, F. Gobal and M. G. Mahjani "Electrocatalytic oxidation of glucose on Ni and NiCu alloy modified glassy carbon electrode" *J. Solid State Electrochem.* **13** 1171–1179 (2009)

[Jan13]   J. I. Jang (Ed) "New Developments in photon and materials research" ISBN 978-1-62618-384-1 Ch.19 'Raman spectroscopy of graphene and related materials' (2013)

[Jay12]   K. Jayakumara, R. Rajeshb, V. Dharumana, R. Venkatasanb, J.H. Hahnc and S. Karutha Pandian "Gold nano particle decorated graphene core first generation PAMAM dendrimer for label free electrochemical DNA hybridization sensing" *Biosensors and Bioelectronics* **31** 406– 412 (2012)

[Jia06]   D. Jiang, B. G. Sumpter and S. Dai "How do aryl groups attach to a graphene sheet?" *J. Phys. Chem. B* **110** 23628-23632 (2006)

[Jia11]   Z. X. Jiang, J. J. Wang, L. H. Meng, Y. D. Huang and L. Liu "A highly efficient chemical sensor material for ethanol: Al2O3/Graphene nanocomposites fabricated from graphene oxide"

[Jin10]   E. Jin, X. Lu, L. Cui, D. Chao and C. Wang "Fabrication of graphene/prussian blue composite nanosheets and their electrocatalytic reduction of H_2O_2" *Electrochim. Acta* **55** 7230–7234. (2010)

[Joh14]   J. E. Johns, J. M. P. Alaboson, S. Patwardhan, C. R. Ryder, G. C. Schatz and M. C. Hersam "Metal oxide nanoparticle growth on graphene via chemical activation with atomic oxygen" *J. Am. Chem. Soc.* **135** 18121-18125 (2014)

[Kan09]   X. H. Kang, J. Wang, H. Wu, I. A. Aksay, J. Liu and Y. H. Lin "Glucose oxidase-graphene-chitosan modified electrode for direct electrochemistry and glucose sensing" *Biosens. Bioelectron.* **25** 901–905 (2009)

[Kat03]   E. Katz and I.Willner "Probing biomolecular interactions at conductive and semiconductive surfaces by impedance spectroscopy: Routes to impedimetric immunosensors, dna-sensors, and enzyme biosensors" *Electroanalysis* **15** 913–947 (2003)

[Kat14]   S. Kataria, S. Wagner, J. Ruhkopf, A. Gahoi, H. Pandey, R. Bornemann, S. Vaziri, A. D. Smith, M. Ostling and M. C. Lemme "Chemical vapor deposited graphene: From synthesis to applications" *Phys. Status Solidi A* **211** 2439–2449 (2014)

[Kim09]   K. S. Kim, Y, Zhao, H. Jang, S. Y. Lee, J. M. Kim, J. H. Ahn, P. Kim, J. Y. Choi and B. H. Hong "Large-scale pattern growth of graphene films for stretchable transparent electrodes" *Nature* **457** 706-710 (2009)

[Kim12]   M. Kim, N. S. Safron, E. Han, M. S. Arnold and P. Gopalan "Electronic transport and raman scattering in size-controlled nanoperforated graphene" *ACS Nano* **6** 9846–9854 (2012)

[Kim14]   K. Kim, H.B.R. Lee, R.W. Johnson, J. T. Tanskanen, N. Liu, C. Pang, C. Ahn, S. F. Bent and Z. Bao "Selective metal deposition at graphene line defects by atomic layer deposition" *Nat. Commun.* **5** 4781 (2014)

[Kin97]   K. T. Kinnear and H. G. Monbouquette "An amperometric fructose biosensor based on fructose dehydrogenase immobilized in a membrane mimetic layer on gold" *Anal. Chem.* **69** 1771-1775 (1997)

[Koc12]   S. Kochmann, T. Hirsch and O. S. Wolfbeis "Graphenes in chemical sensors and biosensors" *Analytical Trends in Chemistry* **39** 87-113 (2012)

[Koc13]   S. Kochmann "Graphene as a sensor material" Doctoral dissertation, university of Regensburg March (2013)

[Kui12]   T. Kuila, S. Bose, A. Kumar Mishra, P. Khanra, N. H. Kim and J. Hee Lee "Chemical functionalization of graphene and its applications" Prog. in Mat. Science **57** 1061–1105 (2012)

[Kum13]   B. Kumar, K. Min, M. Bashirzadeh, A. Barati Farimani, M. H. Bae, D. Estrada, Y. D. Kim, P. Yasaei, Y. D. Park, E. Pop, N. R. Aluru and A. Salehi-Khojin "The role of external defects in chemical sensing of graphene field-effect transistors" *Nano Lett.* **13** 1962−1968 (2013)

[Kum15a]   V. Kumar "Synthesis and characterization of high quality large area graphene oxide" *Int. J. Sci., Tech. & Man.* **4** 86-91 (2015)

[Kum15b]   N. A. Kumar, M. A. Dar, R. Gul and J. B. Baek "Graphene and molybdenum disulfide hybrids: synthesis and applications" *Mat. Today* **18** (2015)

[Lan11]   U. Lange, T. Hirsch, V. M. Mirsky and O. S. Wolfbeis "Hydrogen sensor based on a graphene - palladium nanocomposite" *Electrochim. Acta* **56** 3707–3712 (2011)

[Lee09]   J. Lee, H. Bin Na, B. C. Kim, J. H. Lee, B. Lee, J. H. Kwak , J. Park, M. B. Gu, J.Kim, J. Joo, C.Shin, J. W. Grate, T. Hyeon and J. Kim "Magnetically-separable and highly-stable enzyme system based on crosslinked enzyme aggregates shipped in magnetite-coated mesoporous silica" *J. Mater. Chem.* **19** 7864-7870 (2009)

[Leo14]   S. G. Leonardi, D. Aloisio, N. Donato, P. A. Russo, M. C. Ferro, N. Pinna and G. Neri "Amperometric sensing of H_2O_2 using Pt–TiO2/rGO nanocomposite" *Chem. Electro. Chem.* **1** 617-624 (2014)

[Ler98]   A. Lerf, H. He, M. Forster, J. Klinowski, "Structure of graphite oxide revisited" *J. Phys. Chem. B* **102** 4477–82 (1998)

[Ler13]   M. B. Lerner, N. Kybert, R. Mendoza, R. Villechenon, M. A. B. Lopez and A. T. C. Johnson "Scalable, non-invasive glucose sensor based on boronic acid functionalized carbon nanotube transistors" *Appl. Phys. Lett.* **102** 183113 (2013)

[Li07]   J. Li, X. Lin "Glucose biosensor based on immobilization of glucose oxidase in poly(*o*-aminophenol) film on polypyrrole-Pt nanocomposite modified glassy carbon electrode" *Biosens. and Bioelectron.* **22** 2898–2905 (2007)

[Li08]   D. Li, M. B. Müller, S. Gilje, R. B. Kaner and G. G. Wallace "Processable aqueous dispersions of graphene nanosheets" *Nat. Nanotech.* **3** 101-105 (2008)

[Li09]   X. Li, W. Cai, L. Colombo and R. S. Ruoff "Evolution of graphene growth on Ni and Cu by carbon isotope labeling*" Nano Lett.* **9** 4268-4272 (2009)

[Li10]   W. Li, M. Zhao, X. Zhao, Y. Xiab and Y. Mu "Hydrogen saturation stabilizes vacancy-induced ferromagnetic ordering in graphene" *Phys. Chem. Chem. Phys.* **12** 13699–13706 (2010)

[Li13]   G. Li, P. Miao "Electrochemical analysis of proteins and cells" *Springer* ISBN 978-3-642-34251-6 (2013)

[Li14a]   S. J. Li, J. M. Du, J. P. Zhang, M. J. Zhang and J. Chen "A glassy carbon electrode modified with a film composed of cobalt oxide nanoparticles and graphene for electrochemical sensing of H_2O_2" *Microchim Acta* **181** 631–638 (2014)

[Li14b]   M. Li, X. Bo, Z. Mu, Y. Zhang and L. Guo "Electrodeposition of nickel oxide and platinum nanoparticles on electrochemically reduced graphene oxide film as a nonenzymatic glucose sensor" *Sens. and Actuat. B* **192** 261–268 (2014)

[Li14c]   S. J. Li, N. Xia, X.L. Lv, M. M. Zhao, B. Q. Yuan and H. Pang "A facile one-step electrochemical synthesis of graphene/NiO nanocomposites as efficient electrocatalyst for glucose and methanol" *Sens.and Actuat. B* **190** 809 (2014)

[Lim10]   H. Lim, J. S. Lee, H. J. Shin, H. S. Shin and H. C. Choi "Spatially resolved spontaneous reactivity of diazonium salt on edge and basal plane of graphene without surfactant and its doping effect" *Langmuir* **26** 12278–12284 (2010)

[Lin11]   K. Y. Lin "Characterizing the role of defects on the sensing performance of carbon nanotube and graphene based gas sensors" Doctoral dissertation, University of Illinois at Urbana-Champaign (2011)

[Liu10]   Y. Liu, D. Yu, C. Zeng, Z. Miao and L. Dai "Biocompatible graphene oxide-based glucose biosensors" *Langmuir* **26**, 6158–6160 (2010)

[Liu12]   Y. Liu, X. Dong and P. Chen "Biological and chemical sensors based on graphene materials" *Chem. Soc. Rev.* **41** 2283–2307 (2012)

[Log09]   E Loginova, N C Bartelt, P J Feibelman and K F McCarty "Factors influencing graphene growth on metal surfaces" *New J. Phys.* **11** 063046 (2009)

[Lor75]   W. Lorenz and K. D. Schulze "Application of transform-impedance spectrometry" *J. Elec. Chem.* **65** 141–153 (1975)

[Lu07]   J. Lu, L.T. Drzal, R. M. Worden and I. Lee "Simple fabrication of a highly sensitive glucose biosensor using enzymes immobilized in exfoliated graphite nanoplatelets nafion membrane" *Chem. Mater.* 19 6240–6246 (2007)

[Luo11]   Z. Luo, Y. Lu, D. W. Singer, M. E. Berck, L. A. Somers, B. R. Goldsmith and A. T. C. Johnson "Effect of substrate roughness and feedstock concentration on growth of wafer-scale graphene at atmospheric pressure" *Chem. Mater.* **23** 1441-1447 (2011)

[Mah14]   M. R. Mahmoudian, Y. Aliasa, W.J. Basiruna, P, M, Woia and M. Sookhakian "Facile preparation of MnO_2nanotubes/reduced graphene oxidenanocomposite for electrochemical sensing of hydrogen peroxide" *Sens. and Actuat.B* **201** 526–534 (2014)

[Mal09]   L. M. Malard, M. A. Pimenta, G. Dresselhaus and M. S. Dresselhaus "Raman spectroscopy in graphene" *Phys. Rep.* **473** 51-87 (2009)

[Maj08]   K. Majer-Baranyi, N. Adanyi and M. Varadi "Investigation of a multienzyme based amperometric biosensor for determination of sucrose in fruit juices" *Eur. Food. Res. Technol.* **228** 139–144 (2008)

[Maj14]   S. K. Maji, S. Sreejith, A. K. Mandal, X. Ma and Y. Zhao "Immobilizing gold nanoparticles in mesoporous silica covered reduced graphene oxide: a hybrid material for cancer cell detection through hydrogen peroxide sensing" *ACS Appl Mater Interfaces* **6** 13648–13656 (2014)

[Mar11]   P. R. Martins, M. A. Rocha, L. Angnes, H. E. Toma and K. Araki "Highly sensitive amperometric glucose sensors based on nanostructured α-Ni(OH)$_2$ electrodes" *Electroanal.* **23** 2541 – 2548 (2011)

[Mat11]   C. Mattevi, H. Kima and M. Chhowalla "A review of chemical vapor deposition of graphene on copper" *J. Mater. Chem.* **21** 3324-3334 (2011)

[Mca07]   M. J. McAllister, J. L. Li, D.H. Adamson, H. C. Schniepp, A. A. Abdala, M. Herrera-Alonso, D. L. Milius, R. Car, R. K. Prud'homme and I. A. Aksay "Single sheet functionalized graphene by oxidation and thermal expansion of graphite" *Chem. Mater.* **19** 4396-404 (2007)

[Mcc08]   R. L. Mc Creery "Advanced carbon electrode materials for molecular electrochemistry" *Chemical Reviews* **108** 2647-2686 (2008)

[Mer68]   N. D. Mermin "Crystalline order in two dimensions" *Phys. Rev.* **176** 250–254 (1968)

[Mer08]   I. Meric, M. Y. Han. A. F. Young, B.Ozyilmaz, P.Kim and K. L. Shepard "Current saturation in zero-bandgap, topgated graphene field-effect transistors" *Nat. Nanotech.* **3** 654-659 (2008)

[Mia11]   S. Mikhailov (Ed.) "Physics and applications of graphene-experiments, Chapter 3: Chemical vapor deposition of graphene" ISBN: 978-953-307-217-3 (2011)

[Mia14]   Y. Miao, L. Ouyang, S. Zhou, L. Xu, Z. Yang and M. Xiao "Electrocatalysis and electroanalysis of nickel, its oxides, hydroxides and oxyhydroxides toward small molecules" *Biosens. and Bioelec.* **53** 428–439 (2014)

[Mis11]   A. K. Mishra and S. Ramaprabhu "Functionalized graphene-based nanocomposites for supercapacitor application" *J. Phys. Chem. C* **115** 14006–14013 (2011)

[Moh05]   H. Mohammadi, A. Amine, S. Cosnier and C. Mousty "Mercury–enzyme inhibition assays with an amperometric sucrose biosensor based on a trienzymatic-clay matrix" *Analytica. Chimica. Acta.* **543** 143–149 (2005)

[Mor13]   A. Moradi Golsheikh , N.M. Huang, H.N. Lim, R. Zakaria and C.Y. Yin "One-step electrodeposition synthesis of silver-nanoparticle-decorated graphene on indium-tin-oxide for enzymeless hydrogen peroxide detection" *Carbon* **62** 405-412 (2013)

[Mou94]   F. Moussyt, S. Jakeway, D. J. Harrlson and R. V. Rajotte "In vitro and in vivo performance and lifetime of perfluorinated ionomer-coated glucose sensors after high-temperature curing" *Anal. Chem.* **66** 3882-3888 (1994)

[Nai08]   R.R. Nair, P. Blake, A.N. Grigorenko, K.S. Novoselov, T.J. Booth, T. Stauber, N. M. R Peters and A. K. Geim "Fine structure constant defines visual transparency of graphene" *Science* **320** 1308 (2008)

[Nav07]   C. Gomez-Navarro, R. T. Weitz, A. M. Bittner, M. Scolari, A. Mews, M. Burghard, and K. Kern "Electronic transport properties of individual chemically reduced graphene oxide sheets" *Nano Lett.* **7** 3499-3503 (2007)

[Nem77]   R.J. Nemanich and S.A. Solin "Observation of an anomolously sharp feature in the 2nd order Raman spectrum of graphite" *Solid State Commun.* **23** 417-420 (1977)

[Nen10]   R. Nenkova, D. Ivanova, J. Vladimirova and T. Godjevargova "New amperometric glucose biosensor based on cross-linking of glucose oxidase on silica gel/multiwalled carbon nanotubes/polyacrylonitrile nanocomposite film" *Sens.and Actuat. B* **148** 59–65 (2010)

[Nov04]   K. S. Novoselov, A. K. Geim, S. V. Morozov, D. Jiang, Y. Zhang, S. V. Dubonos, I. V. Grigorieva and A. A. Firsov "Electric field effect in atomically thin carbon films" *Science* **306** 666-669 (2004)

[Nov07]   K.S. Novoselov, Z. Jiang, Y. Zhang, S.V. Morozov, H. L. Stormer, U. Zeitler, J. C. Maan, G. S. Boebinger, P. Kim and A. K. Geim "Room-temperature quantum Hall effect in graphene" *Science* **315** 1379 (2007)

[Nov12]   K. S. Novoselov, V. I. Falko, L. Colombo, P. R. Gellert, M. G. Schwab and K. Kim "A roadmap for graphene" *Nature* **490** 192-200 (2012)

[Pal15]   S. Palanisamy, H. F. Lee, S. M. Chen and B. Thirumalraj "An electrochemical facile fabrication of platinum nanoparticle decorated reduced graphene oxide; application for enhanced electrochemical sensing of H_2O_2" *RSC Adv.* **5** 105567-105574 (2015)

[Pan07]   P. Pandey, S. P. Singh, S. K. Arya, V. Gupta, M. Datta, S. Singh and B. D. Malhotra "Application of thiolated gold nanoparticles for the enhancement of glucose oxidase activity" *Langmuir* **23** 3333-3337 (2007)

[Par15]   C. M. Parnell, F. Watanabe, U. B. Nasini, B. C. Berry, Travis Mitchell, A. U. Shaikh and A. Ghosh "Electrochemical sensing of hydrogen peroxide using a cobalt(III) complex supported on carbonaceous nanomaterials" *J. of Electroanal. Chem.* **740** 37–44 (2015)

[Pei35]   R. E. Peierls "Quelques proprietes typiques des corpses solides" *Ann. I. H. Poincare* **5** 177–222 (1935)

[Pim07]   M. A. Pimenta, G. Dresselhaus, M. S. Dresselhaus, L. G. Cancado, A. Jorioa and R. Saito "Studying disorder in graphite-based systems by Raman spectroscopy" *Phys. Chem. Chem. Phys.* **9** 1276-1291 (2007)

[Pat99]   F. Patolsky, M. Zayats, E. Katz and I. Willner "Precipitation of an insoluble product on enzyme monolayer electrodes for biosensor applications: Characterization by faradaic impedance spectroscopy, cyclic voltammetry, and microgravimetric quartz crystal microbalance analyses" *Anal. Chem.* **71** 3171–3180 (1999)

[Pau13]   G. L. C. Paulus, Q. H.Wang and M. S. Strano "Covalent electron transfer chemistry of graphene with diazonium salts" *Acc. Chem. Res.* **46** 160–170 (2013)

[Pol15]   E. S. Polsen, D. Q. McNerny, B. Viswanath, S. W. Pattinson and A. J. Hart "High-speed roll-to-roll manufacturing of graphene using a concentric tube CVD reactor" *Sci. Rep.* **5** 10257 (2015)

[Pri03]   C. P. Price "Point-of-care testing in diabetes mellitus" *Clin. Chem. Lab. Med.* 41 1213–1219 (2003)

[Pum09]   M. Pumera "Electrochemistry of graphene: New horizons for sensing and energy storage" *The Chemical Record* **9** 211-223 (2009)

[Pum10]   M. Pumera "Graphene-based nanomaterials and their electrochemistry" *Chem. Soc. Rev.* **39** 4146-4157 (2010)

[Pum11]   M. Pumera "Graphene in biosensing Materials" *Today* **14** 308-315 (2011)

[Put13]   W. Putzbach and N. J. Ronkainen "Immobilization techniques in the fabrication of nanomaterial-based electrochemical biosensors: A review" *Sensors* **13** 4811-4840 (2013)

[Qia12]   N. Qiao and J. Zheng "Nonenzymatic glucose sensor based on glassy carbon electrode modified with a nanocomposite composed of nickel hydroxide and graphene" *Microchim. Acta* **177** 103-109 (2012)

[Rac15]   R. Raccichini, A.Varzi, S. Passerini and B. Scrosati "The role of graphene for electrochemical energy storage" *Nat. Mat.* **14** 271-279 (2015)

[Ran13]   E. P. Randviir and C. E. Banks "Electrochemical impedance spectroscopy: an overview of bioanalytical applications" *Anal. Methods* **5** 1098-1115 (2013)

[Rei04]   S. Reich and C. Thomsen "Raman spectroscopy of graphite" *Philos. Trans. R. Soc.* **362** 2271-2288 (2004)

[Rei08]   E. Reitz, W. Jia, M. Gentile, Y. Wang and Y. Lei "CuO nanospheres based nonenzymatic glucose sensor" *Electroanal.* **20** 2482-2486 (2008)

[Rei09]   A. Reina, X. T. Jia, J. Ho, D. Nezich, H. B. Son, V. Bulovic, M. S. Dresselhaus and J. Kong "Large area, few-layer graphene films on arbitrary substrates by chemical vapor deposition" *Nano Lett.* **9** 30-35 (2009)

[Rie10]   C. Riedl, C. Coletti and U. Starke "Structural and electronic properties of epitaxial graphene on SiC(0001): A review of growth, characterization, transfer doping and hydrogen intercalation" *J. Phys. D: Appl. Phys.* **43** 374009 (2010)

[Rob12]   T. R. Robinson "On Klein tunneling in graphene" *Am. J. Phys.* **80** 141-147 (2012)

[Ron10]   N. J. Ronkainen, H. B. Halsall and W. R. Heineman "Electrochemical biosensors" *Chem. Soc. Rev.* **39** 1747-1763 (2010)

[Rub05]   J. Rubio-Retama, E. López-Cabarcos and B. López-Ruiz "High stability amperometric biosensor based on enzyme entrapment in microgels" *Talanta* **68** 99-107 (2005)

[Saf09]   A. Safavi, N. Maleki and E. Farjami "Fabrication of a glucose sensor based on a novel nanocomposite electrode" *Biosens. Bioelec.* **24** 1655–1660 (2009)

[Sas12]   A. Sassolas, L. J. Blum and B. D. Leca-Bouvier "Immobilization strategies to develop enzymatic biosensors" *Biotechnology Advances* **30** 489-511 (2012)

[Say15]   S. Sayed, A. Abd El-Moneim, A. M. Fath El-Bab and K. Nakamura "High performance carbon monoxide gas sensor based on graphene" *Int. J. of Eng. Res. & Technol.* **4** 518-523 (2015)

[Sca09]   F. Scarpa, S. Adhikari and A. Srikantha Phani "Effective elastic mechanical properties of single layer graphene sheets" *Nanotechnology* **20** 065709 (2009)

[Sch02]   M. J. Schöning and A. Poghossian "Recent advances in biologically sensitive field-effect transistors (biofets)" *Analyst* **127** 1137-1151 (2002)

[Sch06]   H. C. Schniepp, J. L. Li, M. J. McAllister, H. Sai, M. Herrera-Alonso, D. H. Adamson, R. K. Prud'homme, R. Car, D. A. Saville and I. A. Aksay "Functionalized single graphene sheets derived from splitting graphite oxide" *J. Phys. Chem.* **B** 110 8535–8539 (2006)

[Sch07]   F. Schedin, A. K. Geim, S. V. Morozov, E. W. Hill, P. Blake, M. I. Katsnelson and K. S. Novoselov "Detection of individual gas molecules adsorbed on graphene" *Nat. Mater.* **6** 652-655 (2007)

[Sea14]   C. M. Seah, S. P. Chai and A. R. Mohamed "Mechanisms of graphene growth by chemical vapor deposition on transition metals" Carbon **70** 1-21 (2014)

[Sha09]   C. S. Shan, H. F. Yang, J. F. Song, D. X. Han, A. Ivaska and L. Niu "Direct electrochemistry of glucose oxidase and biosensing for glucose based on graphene" *Anal. Chem.* **81** 2378-2382 (2009)

[Sha10a]   Y. Y. Shao, J. Wang, H. Wu, J. Liu, I. A. Aksay and Y. H. Lin "Graphene based electrochemical sensors and biosensors: A review" *Electroanalysis* **22** 1027 (2010)

[Sha10b]   R. Sharma, J. H. Baik, C. J. Perera and M. S. Strano "Anomalously large reactivity of single graphene layers and edges toward electron transfer chemistries" *Nano Lett.* **10** 398-405 (2010)

[Sha10c]   Y. Shao, J. Wang, M. Engelhard, C. Wang and Y. Lin "Facile and controllable electrochemical reduction of graphene oxide and its applications" *J. Mater. Chem.* **20** 743-748 (2010)

[She05]   R. A. Sheldon, R. Schoevaart and L. M. Van Langen "Cross-linked enzyme aggregates (CLEAs): A novel and versatile method for enzyme immobilization (a review)" *Biocatalys. and Biotransform.* **23** 141-147 (2005)

[Shi15]   D. H. Shin, J. S. Lee, J. Jun, J. H. An, S. G. Kim, K. H. Cho and J. Jang "Flower-like palladium nanoclusters decorated graphene electrodes for ultrasensitive and flexible hydrogen gas sensing" *Sci. Rep.* **5** 12294 (2015)

[Sin09]   P. Singh, S. Campidelli, S. Giordani, D. Bonifazi, A. Bianco and M. Prato "Organic functionalisation and characterisation of single-walled carbon nanotubes" *Chem. Soc. Rev.* **38** 2214–2230 (2009)

[Sin10]   A. Sinitskii, A. Dimiev, D. A. Corley, A. A. Fursina, D. V. Kosynkin and J. M. Tour "Kinetics of diazonium functionalization of chemically converted graphene nanoribbons" *ACS Nano* **4** 1949–1954 (2010)

[Sko07]   D. A. Skoog, F. J. Holler and S. R. Crouch "Principles of instrumental analysis" Brooks/Cole USA (2007)

[Sta06]   S. Stankovich, R.D. Piner, X. Chen, N. Wu, S.T. Nguyen and R.S. Ruoff "Stable aqueous dispersions of graphitic nanoplatelets via the reduction of exfoliated graphite oxide in the presence of poly(sodium 4-styrenesulfonate)" *J. Mater. Chem.* **16** 155–158 (2006)

[Sta07]   S. Stankovich, D.A. Dikin, R.D. Piner, K.A. Kohlhaas, A. Kleinhammes, Y. Jia, Y. Wu, S. T. Nguyen and R. S. Ruoff "Synthesis of graphene-based nanosheets via chemical reduction of exfoliated graphite oxide" *Carbon* **45** 1558–1565 (2007)

[Sto08]   M. D. Stoller, S. Park, Y. Zhu, J. An and R. S. Ruoff "Graphene-based ultracapacitors" *Nano Lett.* **8** 3498-3502 (2008)

[Str15]   A. J. Strudwick, N. E. Weber, M. G. Schwab, M. Kettner, R. T. Weitz, Josef R. Wünsch, K. Müllen and H. Sachdev "Chemical vapor deposition of high quality graphene films from carbon dioxide atmospheres" *ACS Nano* **9** 31–42 (2015)

[Su16]   Y. Su, B. Luo and J. Z. Zhang "Controllable cobalt oxide/Au hierarchically nanostructured electrode for nonenzymatic glucose sensing" *Anal. Chem* **88** 1617–1624 (2016)

[Sub14]   P. Subramanian, J. Niedziolka-Jonsson, A. Lesniewski, Q. Wang, M. Li, R. Boukherroub and S. Szunerits "Preparation of reduced graphene oxide–Ni(OH)$_2$ composites by electrophoretic deposition: application for non-enzymatic glucose sensing" *J. Mater. Chem. A* **2**, 5525-5533 (2014)

[Suk11]   J. W. Suk, A. Kitt, C.W. Magnuson, Y. Hao, S. Ahmed, J. An, A. K. Swan, B. B. Goldberg and R. S. Ruoff "Transfer of CVD-grown monolayer graphene onto arbitrary substrates*" ACS Nano* **5** 6916–6924 (2011)

[Sun15]   Y. Sun, H. Yang, X. Yu, H. Menga and X. Xu "A novel non-enzymatic amperometric glucose sensor based on a hollow Pt–Ni alloy nanotube array electrode with enhanced sensitivity" *RSC Adv.* **5** 70387-70394 (2015)

[Sut08]   P. W. Sutter, J. I. Flege and E. A. Sutter "Epitaxial graphene on ruthenium" *Nat. Mater.* **7** 406-411 (2008)

[Tab14]   M. A. Tabrizi and J. N. Varkani "Green synthesis of reduced graphene oxide decorated with gold nanoparticles and its glucose sensing application" *Sens. and Actuat. B* **202** 475–482 (2014)

[Tan04]   H. Tang, J. Chen, S. Yao, L. Nie, G. Deng and Y. Kuang "Amperometric glucose biosensor based on adsorption of glucose oxidase at platinum nanoparticle-modiWed carbon nanotube electrode" *Analytical Biochemistry* **331** 89–97 (2004)

[Tas11]   F. Tasca, M. N. Zafar, W. Harreither, G. Nöll, R. Ludwigb and L. Gortona "A third generation glucose biosensor based on cellobiose dehydrogenase from Corynascus thermophilus and single-walled carbon nanotubes" *Analyst***136** 2033-2036 (2011)

[Teh15]   F. Tehrani L. Reiner and B. Bavarian "Rapid prototyping of a high sensitivity graphene based glucose sensor strip" *PLOS One* **10** 145036 (2015)

[The09]   Thermo Fisher Scientific "Thermo scientific pierce crosslinking technical handbook" (2009)

[Tli06]   A. Tlili, A. Abdelghani, S. Ameur, N. Jaffrezic-Renault "Impedance spectroscopy and affinity measurement of specific antibody-antigen interaction" *Mat.Sci.& Eng. C* **26** 546–550 (2006)

[Tog10]   K. E. Toghill and R. G. Compton "Electrochemical non-enzymatic glucose sensors: A perspective and an evaluation" *Int. J. Electrochem. Sci.* **5** 1246-1301 (2010)

[Toi14]   H. Toit, M. Di Lorenzo "Glucose oxidase directly immobilized onto highly porous gold electrodes for sensing and fuel cell applications" *Electrochimica Acta* **138** 86–92 (2014)

[Tom05]   I. N. Tomita, A. Manzoli, F. L. Fertonani and H. Yamanaka "Amperometric biosensor for ascorbic acid" Ecl. Quim. **30** 37- 43 (2005)

[Tsa09]   T. Tsai, G. Heckert, L. F. Neves, Y. Tan, D. Kao, R. G. Harrison, D. E. Resasco and D. W. Schmidtke, "Adsorption of glucose oxidase onto single-walled carbon nanotubes and its application in layer-by-layer biosensors" *Anal. Chem.* **81** 7917-7925 (2009)

[Tse09]   T. Tseng, Y.Yang, M. Chuang, S.L. Lou, M. Galik, G.U. Flechsig and J. Wang "Thermally stable improved first-generation glucose biosensors based on Nafion/glucose-oxidase modified heated electrodes" *Electrochem. Commun.* **11** 1819–1822 (2009)

[Tur90]   R. F. B. Turner, D. J. Harrison, R.V. Rajotte and H. P. Balets "A biocompatible enzyme electrode for continuous in vivo glucose monitoring in whole blood" *Sens. and Actuat. B* **l** 561-564 (1990)

[Urb15]   S. Urban, T. Unmüssig, P. Daubinger, J. Kieninger and G. Urban "Stability of non-enzymatic glucose sensor based on platinum micro-/nanostructures" *Proc. Eng.* **120** 1145–1148 (2015)

[Vam06]   V. Vamvakaki, K. Tsagaraki, and N. Chaniotakis "Carbon nanofiber-based glucose biosensor" *Anal. Chem.* **78** 5538-5542 (2006)

[Via09]   L. Vial and P. Dumy "Artificial enzyme-based biosensors" *New J. Chem.* **33**, 939–946 (2009)

[Xio14]   G. Xiong, C. Meng, R. G. Reifenberger, P. P. Irazoqui and T. S. Fisher "A review of graphene-based electrochemical microsupercapacitors" *Electroanalysis* **26** 30-51 (2014)

[Wal47]   P. R. Wallace, "The band theory of graphite" Phys. Rev. 71 622–634 (1947)

[Wan03]   J. Wang, M. Musameh and Y. Lin "Solubilization of carbon nanotubes by nafion toward the preparation of amperometric biosensors" *J. Am. Chem. Soc.* **125** 2408-2409 (2003)

[Wan08]   J. Wang "Electrochemical glucose biosensors" *Chem. Rev.* **108** 814-825 (2008)

[Wan10]   C. Wang, L. Yin, L. Zhang, and R. Gao "Ti/TiO2 nanotube array/Ni composite electrodes for nonenzymatic amperometric glucose sensing" *J. Phys. Chem. C* **114** 4408-4413 (2010)

[Wan11]   Y. Wang, Z. Li, J. Wang, J. Li and Y. Lin "Graphene and graphene oxide: biofunctionalization and applications in biotechnology" *Trends in Biotechnology* **29** 205-212 (2011)

[Wan13]   B. Wang, Y. S. Puzyrev and S. T. Pantelides "Enhanced chemical reactions of oxygen at grain boundaries in polycrystalline graphene" *Polyhedron* **64** 158-162 (2013)

[Wan14]   X. Wang, E.Liu and X. Zhang "Non-enzymatic glucose biosensor based on copper oxide-reduced graphene oxide nanocomposites synthesized from water-isopropanol solution" *Electrochim. Act.* **130** 253–260 (2014)

[War13]   J. H. Warner, F. Schäffel, A. Bachmatiuk and M. H. Rümmeli "Graphene: Fundamentals and emergent applications" Ch. 4 Elsevier (2013)

[Wil09]   G.S. Wilson and Y.B. Hu "Enzyme-based biosensors for in vivo measurements" *Chem. Rev.* **100** 2693-2704 (2009)

[Wil05]   I. Willner and E. E. Katz "Bioelectronics-from theory to applications" *Wiley-VCH* ISBN: 3-527-30690-0 (2005)

[Wir14]   C. Wirtz, K. Lee, T. Hallam and G. S. Duesberg "Growth optimisation of high quality graphene from ethene at low temperatures" *Chem. Phys. Let.* **595** 192–196 (2014)

[Woo14]   M. Wooten, S. Karra, M. Zhang and W. Gorski "On the direct electron transfer, sensing, and enzyme activity in the glucose oxidase/carbon nanotubes system" *Anal. Chem.* **86** 752−757 (2014)

[Woo15]   J. D Wood, G. P. Doidge, E. A. Carrion, J. C Koepke, J. A. Kaitz, I. Datye, A. Behnam, J. Hewaparakrama, B.Aruin, Y. Chen, H. Dong, R. T. Haasch, J. W Lyding and E. Pop "Annealing free, clean graphene transfer using alternative polymer scaffolds" *Nanotechnology* **26** 055302 (2015)

[Xia15]   ] H. Xian, T. Peng, H. Sun and J. Wang "The Effect of thermal exfoliation temperature on the structure and supercapacitive performance of graphene nanosheets" *Nano-Micro Lett.* **7** 17-26 (2015)

[Yan10]   W. Yang, K. R. Ratinac, S. P. Ringer, P. Thordarson, J. J. Gooding, and F. Braet "Carbon nanomaterials in biosensors: Should you use nanotubes or graphene?" *Angew.Chem.Int.Ed.* **49** 2114 – 2138 (2010)

[Yan15]   L. Yang, B. Wang, H. Qi, Q. Gao, C.Li, and C. Zhang "Highly sensitive electrochemical sensor for the determination of 8-hydroxy-2-deoxyguanosine incorporating SWCNTs-nafion composite film" *J. of Sens.* **2015** 504869(2015)

[Yu15]   C. Yu, L. Wang, W. Li, C. Zhu, N. Bao, H. Gu "Detection of cellular H_2O_2 in living cells based on horseradish peroxidase at the interface of Au nanoparticles decorated graphene oxide" *Sens. and Actuat. B: Chemical* **211** 17–24 (2015)

[Zha05]   Y. Zhang, Y.-W. Tan, H.L. Stormer, P. Kim "Experimental observation of the quantum Hall effect and Berry's phase in graphene" *Nature* **438** 201-204 (2005)

[Zha10]   Zhao J, Pei S, Ren W, Gao L, Cheng H-M. "Efficient preparation of large-area graphene oxide sheets for transparent conductive films" *ACS Nano* **4** 5245–5252 (2010)

[Zha13a]   Y. Zhang, L. Zhang and C. Zhou, "Review of chemical vapor deposition of graphene and related applications" *Acc. of Chem. Res.* **46** 2329–2339 (2013)

[Zha13b]   Y. Zhang, X. Xiao, Y. Sun, Y. Shi, H. Dai, P. Ni, J. Hu, Z. Li, Y. Song, L. Wang "Electrochemical deposition of nickel nanoparticles on reduced graphene oxide film for nonenzymatic glucose sensing" *Electroanal.* **25** 959 – 966 (2013)

[Zho07]   S. Zhou " Dirac Fermions in graphene and graphite---a view from angle-resolved photoemission spectroscopy" Doctoral dissertation" university of California, Berkeley (2007)

[Zho08]   M. Zhou, L. Shang, B. Li, L. Huang and S. Dong "Highly ordered mesoporous carbons as electrode material for the construction of electrochemical dehydrogenase- and oxidase-based biosensors" *Biosens. and Bioelectron.* **24** 442–447 (2008)

[Zöp16]   A. Zöpfl, M. Sisakthi, J. Eroms F.M. Matysik, C. Strunk and T. Hirsch "Signal enhancement in amperometric peroxide detection by using graphene materials with low number of defects" *Microchim. Acta* **183** 83–90 (2016)

Acknowledgements

I would first like to thank God for his mercy and guidance that helped me in conducting this study and in the preparation of this thesis.

I would like to express my deep gratitude to my official advisor, Prof. Dr. Christoph Strunk for entrusting me and giving me the opportunity to work on this thesis. I would also like to thank him for the generosity with his time, critical thinking and ideas.

Special thanks to my colleagues at the chemistry department, Dr. Thomas Hirsch, for his guidance and for the useful discussions we had together, which extended my view towards the world of chemistry, to Dr. Alexander Zöpfl and Eva-Maria Kirchner, who helped me with the experiments and understanding the concept behind them.

My sincere thanks go to Dr. Jonathan Eroms. Despite his extremely busy schedule, he would always make himself available for help and advice.

I would like to extend my great appreciation to Prof. Dr. Dieter Weiss, the head of the chair at which this work was performed, for the excellent equipment of the clean room and all other facilities.

My gratitude also extends to the DFG Research Training Group 1570 and the Chancengleichheit & Familienservice of the University of Regensburg for funding the research included in this dissertation. In particular, Dr. Tobias Korn and Dr. Andrea Donarini, the representatives of the Chancengleichheit and Familienservice in Physics department who helped and supported me to get the financial support from this organization in the last year of my research.

At the very end of this thesis I would like to acknowledge the invaluable role of my family who stood by to support me during my PhD journey. Especially my husband really deserves this appreciation. I want to thank:

Ali for so many things that it is hard to even get started. I find it difficult to express my appreciation because it is so boundless. It is probably easiest to thank you for simply being in my life, for giving up so much to make my career a priority in our lives, for being supportive and encouraging. Without you, I would have never been able to thrive in my doctoral program or balance my research with my personal life. Thank you for everything, I owe you a lot.

My parents for their constant support. It is hard to value your care and unconditional love high enough. There are no words to convey how much I love you and how appreciated I am that you two raised me to be who I am today. I hope I will ever get the chance to even start paying you back what I owe you!

My parents-in-law for taking care of my baby when I was working on my project. Without your willingness to be Daniel's primary caregiver this dissertation would have taken even longer to complete.

My brother, Amin, who though younger than me, taught me a lot, and despite being far away from me, was always with me and showed me how to stay strong, positive and faithful in difficulties. Thank you for being an absolute symbol of inner freedom, and endless source of hope and kindness.

Daniel, my son, my delight and the most important result of Ph.D. time. You mean the world to me and your laughters are the absolute renewable source of energy and joy in my life. You carry me to the infinite horizons of prosperity with your little hands. If this work has sometimes prevented us from sharing important moments of life, know that I never stopped thinking about you.